HUMBOLDT BAY INDEPENDENT SPENT FUEL STORAGE INSTALLATION (ISFSI) UPDATED TSUNAMI ASSESSMENT

25 November 2024

TABLE OF CONTENTS

Page

APPENDICES

LIST OF FIGURES

Page

Page

LIST OF TABLES

LIST OF ACRONYMS AND ABBREVIATIONS

ADCP	Acoustic Doppler Current Profilers
ARP/ARPs	Annual Return Probability / Annual Return Probabilities
ASCE	American Society of Civil Engineers
B.P.	Before present; in radiocarbon dating, it indicates years before the year 1950
CCC	California Coastal Conservancy
C.E.	Common era (equivalent to A.D.)
CGS	California Geological Survey
cm	centimeter(s)
CRESCENT	Cascadia Region Earthquake Science Center
CSZ	Cascadia subduction zone
DEM	Digital elevation model
DF	Deformation front
DOGAMI	Oregon Department of Geology and Mineral Resources
DOT	Department of Transportation
ETS	Episodic tremor and slip
FOP	Friends of the Pleistocene
ft	feet
GNSS	Global Navigational Satellite System
GPS	Global positioning system
in	inch(es)
InSAR	Interferometric synthetic aperture radar
IPCC	Intergovernmental Panel on Climate Change
ISFSI	Independent Spent Fuel Storage Installation
ka	thousand years old
ky	thousand year(s)
LCI	Lettis Consultants International, Inc.
LiDAR (lidar)	Light detection and ranging
LSF	Little Salmon fault
LTSP	Long-Term Seismic Program
m	Meter(s)
M	Magnitude (of earthquake)
mi	mile(s)
mm	millimeters
M_w	Moment magnitude
MCS	Multichannel seismic
MHHW	Mean higher high sea level
MLLW	Mean lower low sea level

MRF	Mad River fault
MSL	Mean sea level
MTJ	Mendocino Triple Junction
MWH	Mean high water
NOAA	National Oceanic and Atmospheric Administration
NRC	Nuclear Regulatory Commission
NSHM	National Seismic Hazard Model
OAH	Outer arc high
OPC	Ocean Protection Council
OSL	Optically stimulated luminescence
PG&E	Pacific Gas and Electric Company
PHILLS	Portable Hyperspectral Imager for Low Light Spectroscopy
PORTS	Physical Oceanographic Real-time System
PTHA	Probabilistic tsunami hazard assessment
RCTWG	Redwood Coast Tsunami Work Group
RSL	Relative sea level
SLRT	Sea-level Rise Leadership Team
SRL	Sea level rise
Topobathy	Topography + bathymetry
USGS	U.S. Geological Survey
VML	Vertical land motion or vertical land movement
WCC	Woodward-Clyde Consultants
yr	year(s)

EXECUTIVE SUMMARY

This report, prepared by the Pacific Gas & Electric Company (PG&E) Geosciences Department, presents the results from an updated tsunami assessment for the Humboldt Bay Independent Spent Fuel Storage Installation (ISFSI) located along the east margin of Humboldt Bay on a graded pad near the top of Buhne Hill at an elevation of 13.4 m (44 ft.) NAVD88 datum. Previous tsunami studies have been performed for the ISFSI, the decommissioned former nuclear power plant that was the source of the spent fuel, and the nearby operating PG&E Humboldt Bay Natural Gas Plant. These studies integrated the best state-of-knowledge and modeling approaches at the time, and adapted conservative assumptions to capture uncertainties to support design, licensing, and hazard evaluations. The Humboldt Bay ISFSI original license expires in 2025, and this updated tsunami assessment supports a 20-year license extension to the year 2045.

The tsunami update review shows that the ISFSI is safe, with a significant margin, from potential tsunami inundation as informed by recent research findings and updated modeling. The safety margin (freeboard elevation above estimated highest tsunami levels) reasonably accommodates current uncertainties in tsunami sources and modeling. Additionally, the ISFSI was designed as a below ground vault to provide safe containment of the spent fuel casks even in the event that tsunami inundation would rise to the grade level of the facility, providing conservative defense-in-depth protection.

New information incorporated in the update focused on potential tsunami sources and modeling approaches, including the following specific items:

- New bathymetry and geophysical data along the offshore southern Cascadia and the Humboldt Bay
- Updated characterization of Cascadia tsunami sources, which is an area of active research, with many recent publications encompassing a diverse and extensive range of topics and research groups
- New information and ongoing research on interseismic and coseismic vertical land changes in the Humboldt Bay
- Climate-change-driven sea level rise
- Recent local geologic and fault investigations
- Advances in tsunami modeling approaches and tsunami inundation maps

This updated tsunami assessment was performed by a multi-disciplinary team consisting of Geosciences Department Project Manager Dr. Ozgur Kozaci, and technical reviewers Dr. William Page and Mr. Jeff Bachhuber. External expert support was provided by Dr. Mark Hemphill-Haley (tsunami sources, sea level rise, and tectonic land level changes) and Dr. Hong Kie Thio (tsunami model). The external experts are significantly involved in, or leading, research and application of tsunami source and hydrodynamic models in their areas or expertise, including research on the Cascadia subduction zone (CSZ) and the local tectonics, and model inputs and hydrodynamic analyses used for the State of California tsunami mapping program. Mr. Jearl Strickland, PG&E internal consultant and spent fuel installation expert, and Dr. Stu Nishenko, expert subcontractor consultant, provided technical review of the document.

As a first step, this updated tsunami study reviewed information and results from past studies that are summarized in the last comprehensive tsunami report prepared by PG&E (Page and

Nishenko, 2015). The 2015 study included evaluation of tsunami sources, historic events, tectonic land level changes, long-term sea level rise estimates, and scenario-based tsunami inundation levels at the ISFSI. The 2015 study also included results from a URS (2007) deterministic tsunami hydrodynamic analysis that included a large CSZ event scenario similar to the commonly accepted 1700 C.E. **M** 9 earthquake on the main subduction zone interface with additional movement on the crustal faults in the area, such as the Little Salmon and the Mad River faults. Model results showed significant inundation in the Humboldt Bay with a runup elevation ranging between 23.8 feet and 33.6 feet (MHW), but with locally elevated areas like Buhne Point and the ISFSI site remaining dry. The 2015 study concluded that the Humboldt Bay ISFSI is at a sufficiently high elevation, well above the estimated inundation levels, and thus safe from a tsunami hazard.

The next step for the 2024 tsunami update included evaluation of new information since the 2015 PG&E study, focusing on key input parameters used for tsunami hydrodynamic modeling. This included an evaluation of new offshore and near-shore elevation surveys, CSZ ruptures and recurrence models, sea level rise, and land level changes (vertical land movements) as a result of tectonics and other processes.

Since the 2015 study, additional bathymetric and land elevation data have been collected and evaluated. Important new survey data include near-shore topography combined with offshore bathymetry collected by the California Coastal Conservancy (CCC) between 2009 and 2013, a detailed digital elevation model by the National Oceanic and Atmospheric Administration (NOAA) in 2019, and a compilation of seismic reflection data with 10- to 40-m (33- to ~130-ft.) resolution reported by Hill et. al. in 2020.

Studies to improve models of the CSZ rupture and recurrence are part of a broad area of ongoing active research by numerous researchers, supported in part by the Cascadia Regional Earthquake Science Center (CRESCENT), which was founded in 2023. Cascadia rupture models have benefitted from new survey and science-driven data and consider both a complete (end-to-end) and segmented rupture of the subduction zone. This work includes continued data and evaluation on the last large CSZ earthquake that is increasingly confirmed to have occurred in 1700 C.E. with a magnitude of **M** 9+, and which was used as a scenario event for the previous 2015 PG&E ISFSI tsunami study. New data continues to refine the recurrence intervals for large Cascadia events that is currently estimated at between about 390 and 540 years. The impact of a segmented rupture along the southern CSZ and interactions with onshore connecting faults was evaluated for this 2024 HBISFSI tsunami update.

The previous 2015 Humboldt Bay ISFSI study incorporated projected long-term sea level rise (SLR) impacts on estimated tsunami inundation levels. SLR research has been conducted since 2015 and is ongoing, with the new available data evaluated for this update. This includes SLR estimates by LCI (2020), IPCC (2022) and SLRT/OPC (2024). For an extended timeframe out to the years 2100 and 2150, the new data suggest minor differences from the Page and Nishenko (2015) study, with estimated maximum SLR values ranging between about 0.5 and 0.6 m (1.6 and 2.0 ft.) by the year 2100, and 1.9 to 2.2 m (6.2 to 7.2 ft.) by 2150. SLR in the Humboldt Bay through the year 2045, when the renewed license for the ISFSI is expected to expire, is estimated at between 3 and 27.4 cm (0.1 and 0.9 ft.). SLR is already exacerbating shoreline retreat along the California coast, and local historical imagery shows that significant shoreline retreat causing erosion of Buhne Hill bluff occurred previously, indicating that the native deposits are erodible.

However, the Buhne Hill shoreline is currently protected by a seaward-sloping riprap berm that was installed in the 1950s and upgraded in the 1980s (PG&E, 2005).

New tsunami hazard modeling since Page and Nishenko (2015) includes an American Society of Civil Engineers (ASCE) study to develop offshore tsunami hazard maps (ASCE 7-16, 2017) that covered the entire U.S. west coast and Hawaii. These maps are based on subduction zone sources around the Pacific Basin, which are capable of producing the largest earthquakes in the world. In Humboldt Bay, the ASCE-modeled tsunami hazard is driven primarily by sources in Alaska for short return periods (< 800 yr), whereas for longer return periods, the CSZ is the most significant source. Due to the geometry of the CSZ curving landward at its southern terminus, the Humboldt Bay area is situated on the seaward side of the hinge line that separates uplift from subsidence during megathrust earthquakes. The probability of subsidence at the ISFSI is therefore small compared to that farther north along the Oregon and Washington coastlines. Additionally, ISFSI is sited on Buhne Hill, a local fault-bounded topographic high capped by an 80-ka marine terrace that has been correlated with flights of marine terraces to the east and northeast, on Humboldt Hill and in Eureka. This suggests that intraseismic regional subsidence in the Humboldt Bay area may not apply to Buhne Hill, or that the net tectonic motion over several intraseismic and coseismic events adds up to uplift. Most recently, a California-wide tsunami Probabilistic Tsunami Hazard Assessment (PTHA) produced tsunami inundation maps using a high-resolution control grid (10-m [33-ft.]) published by the California Geological Survey (CGS, 2021). The CGS effort incorporated previous models by Thio (2019) and developed estimated tsunami runup maps for several scenarios ranging between a 72- and a 3000-year Annual Return Probability (ARP). The 2475-year ARP is a reasonable return period to consider for the 20-year license extension for the facility, and results in a conservative (~5 m [~17 ft]) amount of freeboard at the ISFSI site above the 2475-yr ARP model runup estimate (Figure ES-1). The previous 2015 estimates represent a deterministic scenario that was used for the ISFSI design, and are equal to or higher than the newer probabilistic estimates that incorporate the current best research and understanding of tsunami sources and modeling approaches.

Historical imagery attests to the erodibility of Buhne Hill bluff, especially since the construction of the Humboldt Bay jetties in the 19th century (Figure 1-4). Currently, the shoreline near the ISFSI is protected by a seaward-sloping riprap berm that has protected Buhne Hill from coastal erosion since it was installed in the 1950s and upgraded in the 1980s (PG&E, 2005). The horizontal distance between the ISFSI pad and the top of the shoreward cliff provides a buffer zone against potential slope erosion related to a large tsunami event with multiple pulses of high energy waves. PG&E performs periodic inspection and maintenance of the riprap berm, and this is an important ongoing effort to protect against rising sea level and provide some defense against tsunami scour.

In conclusion, this 2024 tsunami update review shows that the Humboldt Bay ISFSI is safe, with a margin, from potential tsunami inundation as informed by recent research findings and updated modeling. The safety margin (freeboard elevation above estimated tsunami levels) reasonably accommodates current uncertainties in SLR, tectonic land level changes, tsunami sources and modeling. PG&E will continue to evaluate new information as part of its due diligence under its Long-Term Seismic Program (LTSP).

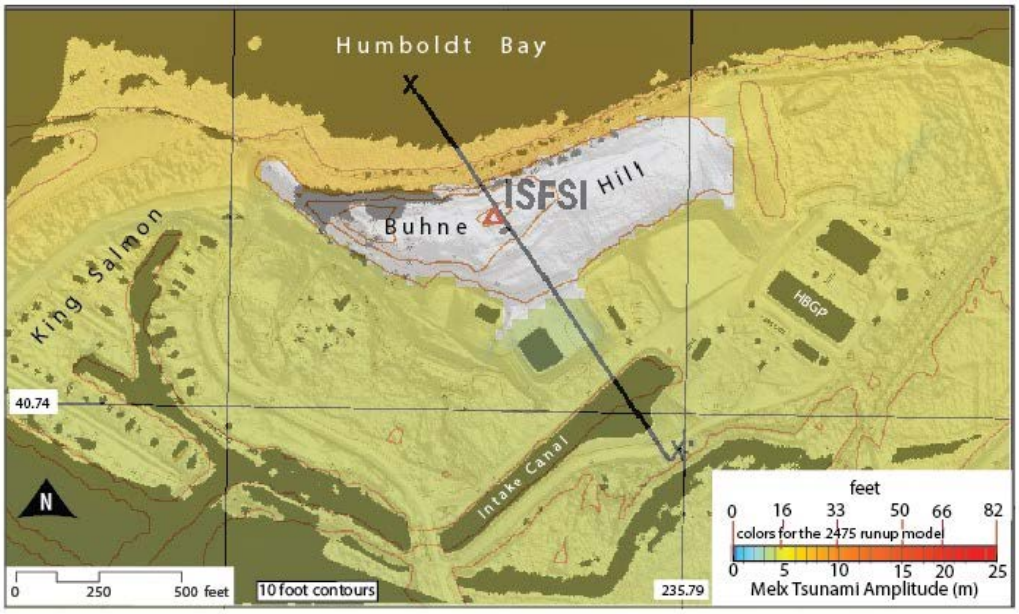

DEM of Buhne Hill Showing the 2475 Year Tsunami Inundation Levels

EXPLANATION

Qc	Colluvium
Qpm	Intertidal marsh, silt and peat
Qt	Marine terrace, Pleistocene 80 ka
Qh	Hookton Fm, Pleistocene marine siltstone

NOTES :

Two separate surveys are merged at the Buhne Hill coast line. NAVD88 is the reference datum for the onshore elevations at Buhne Hill. Sea levels, MSL, MLLW, MHW, measured at Fields Landing (Figure 1-5) are the data used for marine sea level data. In the Fields Landing data set NAVD88 is located 3.5 feet below MSL. To merge the two, NAVD88 is 3.5 feet below MSL . Therefore, 3.5 feet is added to the tsunami runup.

The Cross section shows the point tsunami elevation on the Buhne Hill bluff and on the leaward side west of the Intake Canal

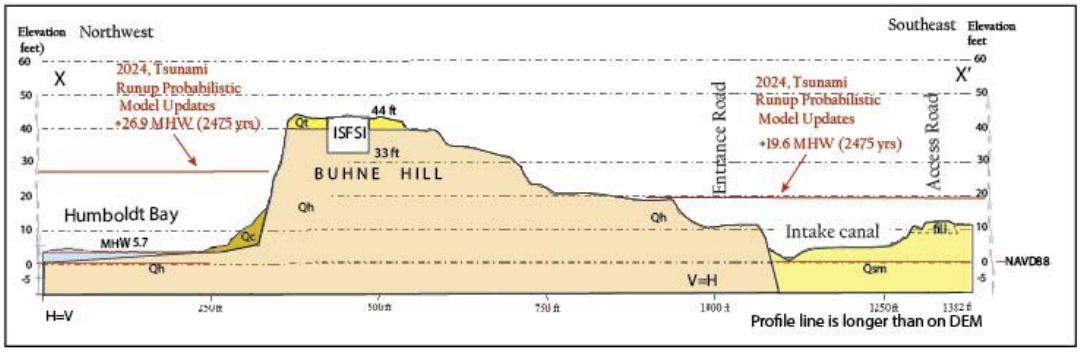

Figure ES-1. Schematic cross-section across Buhne Hill showing the 2024 model runup heights based on CGS (2021) at MHW.

1.0 INTRODUCTION

Pacific Gas and Electric (PG&E) has prepared this report as part of its continued assessment of the safety of the Humboldt Bay Independent Spent Fuel Storage Installation (ISFSI). In 2021, the State of California published tsunami runup models for the California coast; this prompted PG&E to reevaluate the tsunami hazard to the ISFSI site by assessing the most recent research on this subject relevant to the site since PG&E's last evaluation in 2020. Previous assessments were completed in 2003 and 2015. The goals of this updated assessment and report are two-fold, as follows:

1. Summarize the findings of new research on the Cascadia subduction zone (CSZ), subsidence in Humboldt Bay, sea level change, and the geology of the Humboldt Bay region.
2. Adopt the most-recent tsunami hazard model developed by the State with an emphasis on the estimated tsunami runup at Buhne Hill and the ISFSI.

The project team for this tsunami update evaluation consisted of the following individuals:

- Ozgur Kozaci, PhD, PG
- William D. Page, PhD, CEG
- Mark Hemphill-Haley, PhD
- Hong Kie Thio, PhD
- Jeffrey Bachhuber, MS, CEG
- Jearl Strickland, BSCE, MBA, PE

As discussed in detail in this report, the tsunami hazard and erosion potential at Buhne Hill and at the ISFSI are a function of the site's coastal setting. This area could be exposed to tsunamis generated by both distant and regional sources (e.g., Japan trench subduction zone, Alaska and Cascadia subduction zones), with the tsunami-induced inundation potentially influenced by local complexities resulting from tectonic uplift and/or subsidence at Buhne Hill related to an earthquake on the CSZ, the Little Salmon fault (LSF) and other nearby faults and offshore landslides; and exacerbation of inundation levels by storm surges, high tides and global-warming-driven sea level rise. In this report, we summarize the findings of various recent investigations that have a bearing on the potential tsunami hazard at ISFSI, including advances in the tectonic understanding of the CSZ and local faults (e.g., the LSF), evolving estimates of sea level rise, and newly developed modeling approaches for tsunami inundation estimation. Previous PG&E reports, as well as peer-reviewed scientific and public reports, are cited so the reader can refer to them for additional information and details.

1.1 Background

1.1.1 Site History and Location

In 1952, PG&E acquired Buhne Hill and the surrounding area along the east margin of Humboldt Bay for the purposes of building two fossil-fuel powered plants (Units 1 and 2) and a small nuclear power plant (Unit 3, 62 Mw). All three plants were constructed by 1962. Fuel loading and operations at the nuclear power plant started in 1963 and ceased in 1973. The decision to decommission the plant was made in 1983, with the spent fuel being stored in the plant under a

"Safe Store" condition. In 2005, PG&E obtained a license from the Nuclear Regulatory Commission (NRC) to store the spent fuel onsite in an Independent Spent Fuel Storage Installation (ISFSI) that was constructed at the top of Buhne Hill. In 2008, the spent fuel generated during the approximately ten years of operation was transferred from wet storage in spent fuel pools to dry storage in the ISFSI. Power plant decommissioning was completed in 2021 when the NRC approved termination of the plant's operating license. During the decommission, Greater-than-Class-C radioactive waste generated during the plant removal was added to the ISFSI. Storage in the ISFSI of spent nuclear fuel will continue until the Department of Energy is able to remove and store or reprocess the material.

Buhne Hill is an isolated hill separated from Humboldt Hill by a low-lying swampy area (Figure 1-1). Erosion of the west side of Buhne Hill was extensive following the 1889 construction of the jetties and dredging of the entrance to the bay (Figure 1-2). Continued erosion of the hill was mitigated when PG&E constructed a boulder berm at the base of Buhne Hill in 1952; this berm was reinforced in 1989. As will be discussed further in this report, Humboldt Bay is exposed to tsunamis coming through the channel but somewhat protected by the North and South spits.

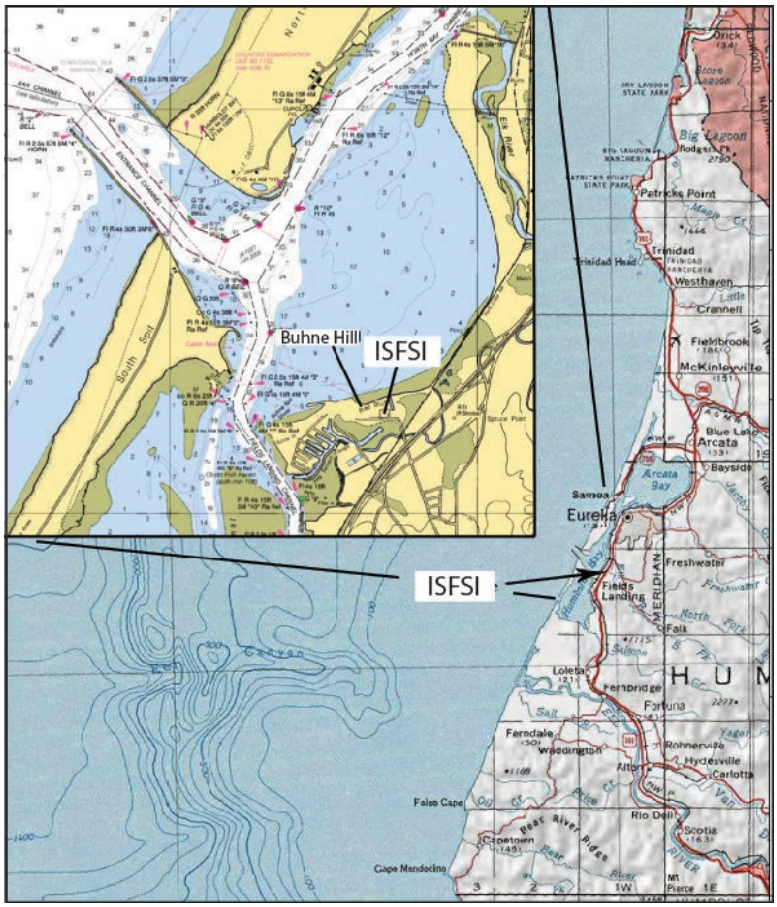

Figure 1-1. Location of Buhne Hill and the ISFSI

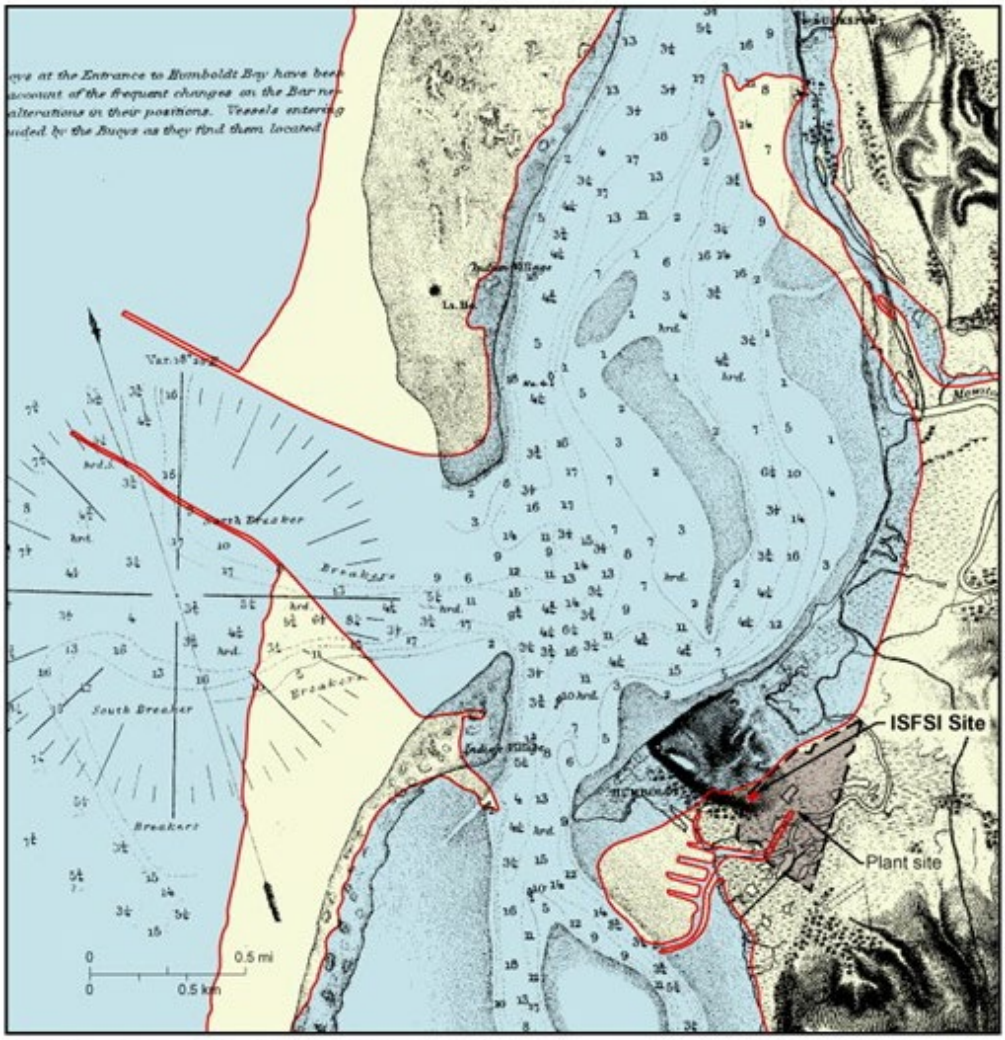

Preliminary Survey of Humboldt Bay, California, U.S. Coast Survey, 1858 (edition of 1879), (original scale 1:30,000) (aids to navigation corrected to 1885). Depths are in feet below mean lower low water to lowest dotted line, then in fathoms. Red line delineates present shoreline and jetties from USGS Fields Landing 7.5 minute Quadrangle (1989). Brown area is plant site.

Figure 1-2. Entrance to Humboldt Bay showing the historical erosional retreat of Buhne Hill (Red Bluff), with the coastline as of 1858 and 1879 shown in gray, and 1989 shoreline features shown in color. ISFSI shown in brown.

1.1.2 Terminology

A tsunami (pronounced (t)soo-NAH-mee, a Japanese composite word meaning “harbor wave”) is a series of sea waves caused by a sudden displacement of the ocean water. Tsunamis are characterized by their length, speed, low period, and low observable amplitude: the waves can be up to 125 miles (200 km) long from one crest to the next, they travel in the deep ocean at speeds of typically about 950 km/hr (600 mi/hr), and have periods of between 5 minutes and up to a few hours (with most tsunami periods ranging between 10 and 60 minutes). The wave height in the open ocean is very small, a few meters at most. However, as a tsunami approaches a coastline and enters shallow water, its speed decreases to about 30 to 50 km/hr (20 to 30 mi/hr), and the height of the waves increases as the water piles up, with the potential to reach heights of 30 m

(100 ft.) or more. The effect of these waves can be amplified where a bay, harbor or lagoon funnels the waves as they move inland.

Terminology related to observations or measurements of the impact of a tsunami on normally dry land include “water or wave height,” “runup, wave runup, or uprush,” and “inundation.” Wave height is the maximum elevation, typically in meters, of the wave above a reference sea level datum such as Mean Sea Level (MSL). Runup is the maximum elevation, also typically reported in meters, of ground wetted by the tsunami. Inundation is the result of a tsunami traveling inland and is the horizontal measurement of the path of the tsunami. A tsunami wave may first arrive at a coast as a trough, with water receding and exposing the sea floor over a much larger area than it is typical during extremely low tide. The receding water will rush back in, generally in a few minutes, typically as a bore, with the fast-rising flood potentially causing significant damage. Figure 1-3 illustrates the terms wave height, runup and inundation.

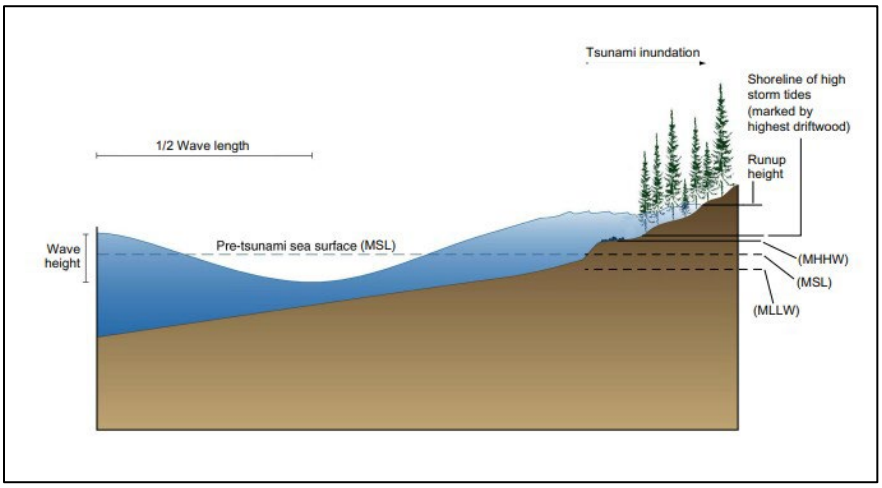

Figure 1-3. Terms used for tsunami studies, including wavelength, wave height, runup, and inundation. Wave height and runup (or runup height) are vertical distances measured relative to a sea level datum such as mean sea level (MSL), mean lower low sea level (MLLW) or mean higher high sea level (MHHW). Inundation is the distance the tsunami travels across the landscape.

The most frequent causes of tsunamis are underwater earthquakes and submarine landslides that cause a sudden disturbance or displacement of the sea floor and the column of water above. The earthquakes that often generate tsunamis typically, although not always, occur along subducting plate boundaries where one tectonic plate is being subducted under another. The margins of nearly the entire Pacific Ocean basin, with the exception of the coastline along Canada, central and southern California, and Baja California, are defined by subducting plates. Humboldt Bay and the ISFSI could be impacted by tsunamis generated anywhere along the Pacific Ocean basin, including Japan, Alaska, and the local CSZ. An earthquake on the CSZ could induce coseismic deformation (i.e., subsidence or uplift) at Buhne Hill, with this in turn affecting the reach and impact of a tsunami at the ISFSI. This is illustrated on Figure 1-4.

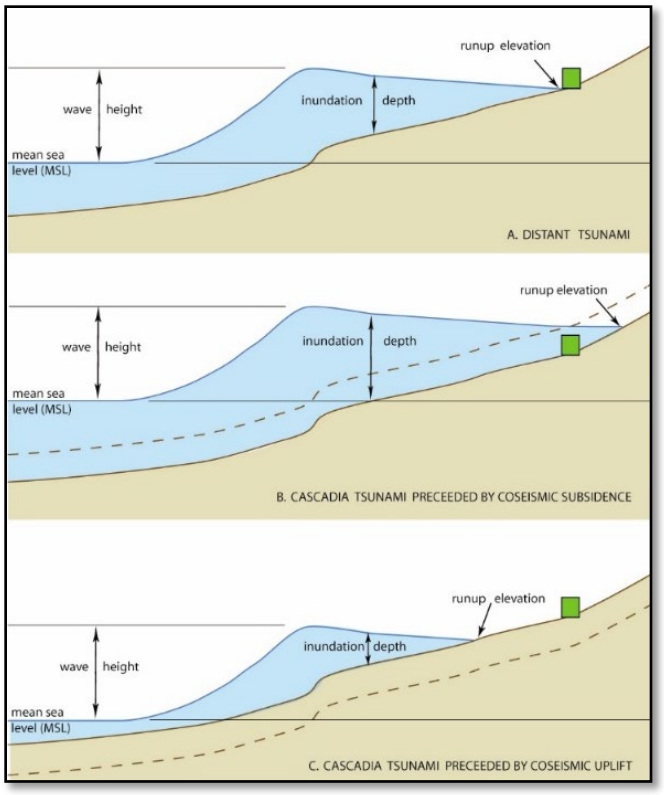

Figure 1-4. Comparison of tsunami parameters for different scenarios of coseismic deformation, including from a distant tsunami source (upper panel), and subsidence (middle panel), or uplift (lower panel) associated with an earthquake on the CSZ

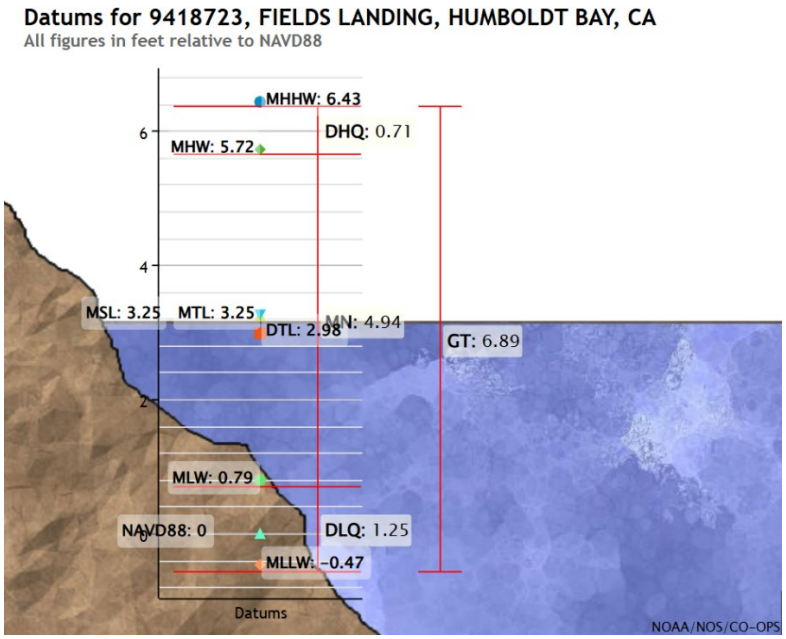

Figure 1-5. Tide Levels and Water-Level Datums for Fields Landing

1.2 Earliest Tsunami Hazard Evaluations

Over the years, PG&E has performed various tsunami hazard evaluations for the former nuclear plant site and ISFSI, with the studies implementing the most up-to-date advances in the understanding of tsunami sources and modeling. The first of these tsunami evaluations was conducted in 1965 by Dr. R. Wiegel, a Professor at UC Berkeley, who was retained to perform the study following the tsunami from the 27 March 1964 **M** 9.2 Alaska earthquake that devastated Crescent City. He estimated a potential runup at Buhne Hill of up to 7.92 m (26 ft.) resulting from a distant tsunami (Wiegel, 1965).

Note that all reports prior to and including the PG&E 2003 report for the ISFSI (Section 1.3) refer to water levels and tsunami runups based on the Mean Lower Low Water (MLLW) as the reference level, a datum traditionally used in bathymetric charts for ship navigation (Figure 1-5). The models in the 2008 tsunami assessment update utilized Mean Sea Level (MSL), which is 1.13 m (3.72 ft.) above MLLW.

The Weigel (1965) estimated runup of 7.92 m (26 ft.) relative to MLLW (7.78 m [25.53 ft.] relative to NAVD88) was considered at the time to be a conservative estimate, as this level of runup was observed in Alaska near the Alaska earthquake epicentral zone. However, documentation of tsunami heights and effects from the 1964 Alaska earthquake in Humboldt Bay varies. Observation at HBPP Intake for 1964 event was 2.9 m (9.6 ft) (presumably NAVD88), in a note from G. E. Altman, PG&E at 1:30 PM, 28 March 1964. The National Oceanic and Atmospheric Administration (NOAA, 2023) estimates that the 1964 tsunami waves reached heights of around 1 to 2 m (3.3 to 6.6 ft.) relative to MSL [2 to 3m (6.55 to 9.85 ft.) relative to NAVD88] in Humboldt Bay near King Salmon-Fields Landing, and a University of Southern California (USC) evaluation group estimated runup heights of around 4.27 m (14 ft.) relative to MSL [5.26 m (17.25ft.) relative to NAVD88] in Humboldt Bay.

The 1964 tsunami sparked a whole new field of study, with researchers evaluating the long-term worldwide historical data on tsunamis, combining that information with mathematical models to estimate distantly generated, 100-year and 500-year probability teletsunami runup elevations for the west coast of the United States (Houston and Garcia, 1974, 1978; Garcia and Houston, 1975; Houston et al., 1975). Then, in 1986, Brian Atwater identified a submerged forest in Washington and this discovery sparked research that confirmed the previously unknown activity of the CSZ with the potential for very large subduction earthquakes and tsunamis (Atwater, 1987). After the discovery of the 1700 C.E. earthquake and tsunami, oral histories from the Orick (now referred to as Yurok) Tribe in the Eureka area (Carver, 1998, personal communication with W.D. Page), and other tribes in Washington and British Colombia were found that described events that are interpreted to have been from Cascadia earthquakes and tsunamis.

PG&E stayed abreast of these studies and findings, funding several in-depth investigations of paleotsunamis along the northern coast of California, and evaluations of tsunami potential at the ISFSI site, including runup estimates at Buhne Hill by experts in the field. Thus, in 1985, PG&E reported estimated MLLW runups at the site of 4.9 m (16.1 ft) at the Bay Entrance based on studies by Brandsma et al. (1979), and 6.3 m (20.7 ft) based on studies by Houston and Garcia (PG&E, 1985). In the 1990s, PG&E considered runups at ISFSI of 3 m (10 ft) based on the work by Bernard et al. (1994), 12.4 m (12.4 ft) based on the investigation by Lamberson et al. (1998), and 9.1 m (30 ft) offshore based on the work by Myers et al. (1999). For actual runup at Buhne

Hill these MLLW need to be reduced by 0.1 m (0.47 ft) to agree with NAVD88 elevations. Information from these investigations and tsunami assessments was the basis for the ISFSI siting considerations, with these data incorporated into the ISFSI tsunami report submitted to the NRC (PG&E, 2003) that is described further in the section below.

1.3 2003 Seismic Hazard Assessment for the Humboldt Bay ISFSI

In 2003, PG&E issued to the NRC a comprehensive report entitled “Seismic Hazard Assessment for the Humboldt Bay ISFSI Project” in support of its license request for construction and operation of an ISFSI to be developed at Buhne Hill (PG&E, 2003). The report included the findings of several extensive investigations that had updated the tectonic setting of the Humboldt Bay region and reevaluated the seismic and tsunami hazards at the ISFSI site.

1.3.1 Tectonics

Investigations for the ISFSI addressed earthquake sources and potential for surface faulting focused on the CSZ and LSF. The CSZ extends offshore from British Columbia to Cape Mendocino and is recognized as the source of the **M** 9 1700 C.E. earthquake and tsunami (Figure 1-6). The southern end of the subduction zone appears to swing east and trend onshore in the Humboldt Bay area. The LSF zone follows the base of Humboldt Hill and extends offshore south of Buhne Hill (Figure 1-7). In the area of Buhne Hill there is a series of secondary and antithetic faults along the northeast margin of the LSF that include the Bay Entrance and Buhne Point faults (secondary faults), and the antithetic Discharge fault (Figure 1-8). During earthquakes on the LSF, Buhne Hill is uplifted as a block between these faults (Figure 1-9). Extensive trenching has shown that the ISFSI footprint and the adjacent area are not underlain by any faults that offset the ~80,000-year-old terrace that caps Buhne Hill (PG&E, 2003). This supports the absence of a significant surface fault rupture hazard at the facility, but nearby faults could result in localized uplift or subsidence of the hill.

Figure 1-6. Generalized tectonic setting of the western United States and ISFSI (after PG&E, 2003, Figure 2-1). Black arrows show fault motion; red arrows indicate general plate motion.

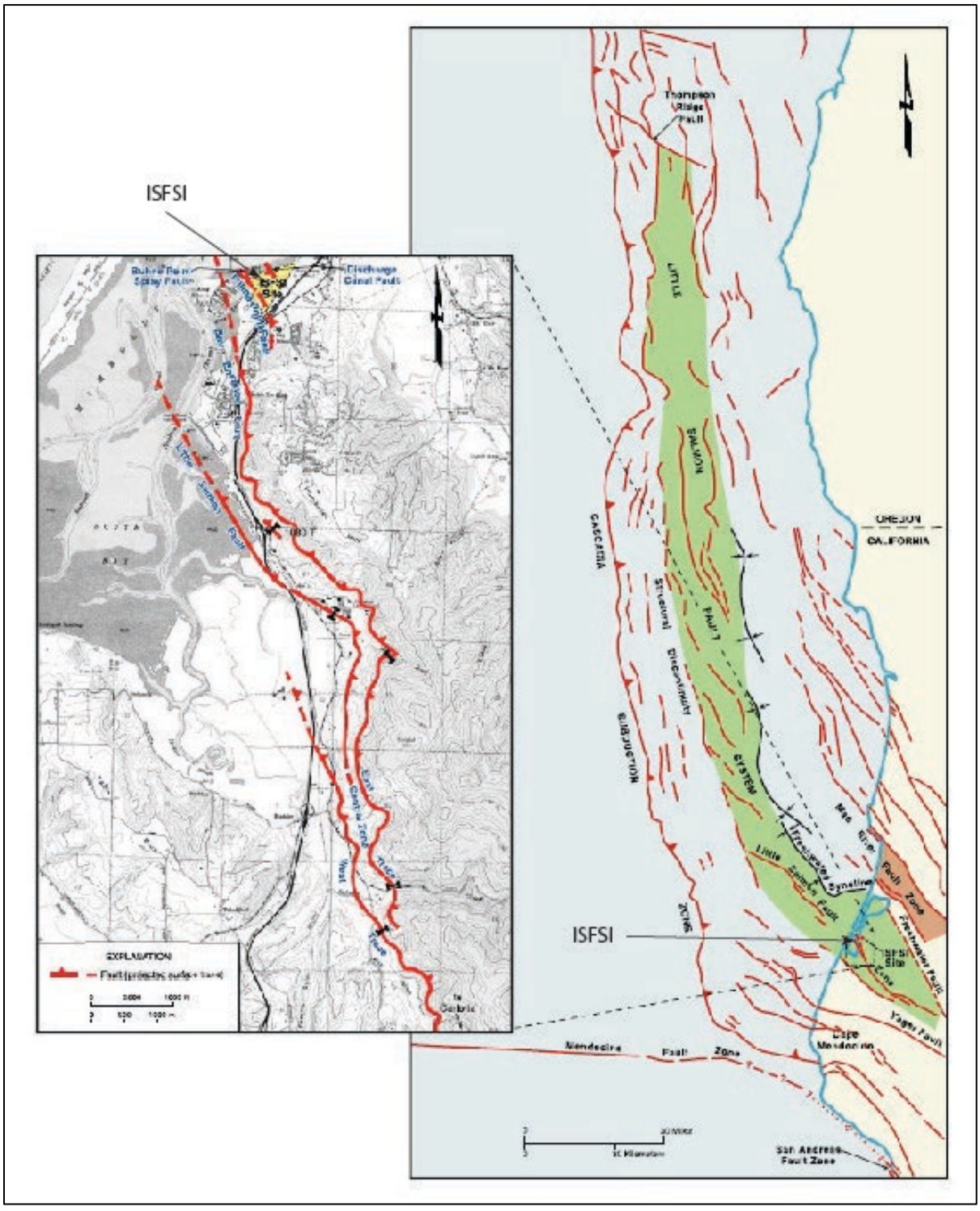

Figure 1-7. Cascadia subduction zone (CSZ) showing where the subduction zone trends onshore (modified from PG&E, 2003, Figure 2-5).

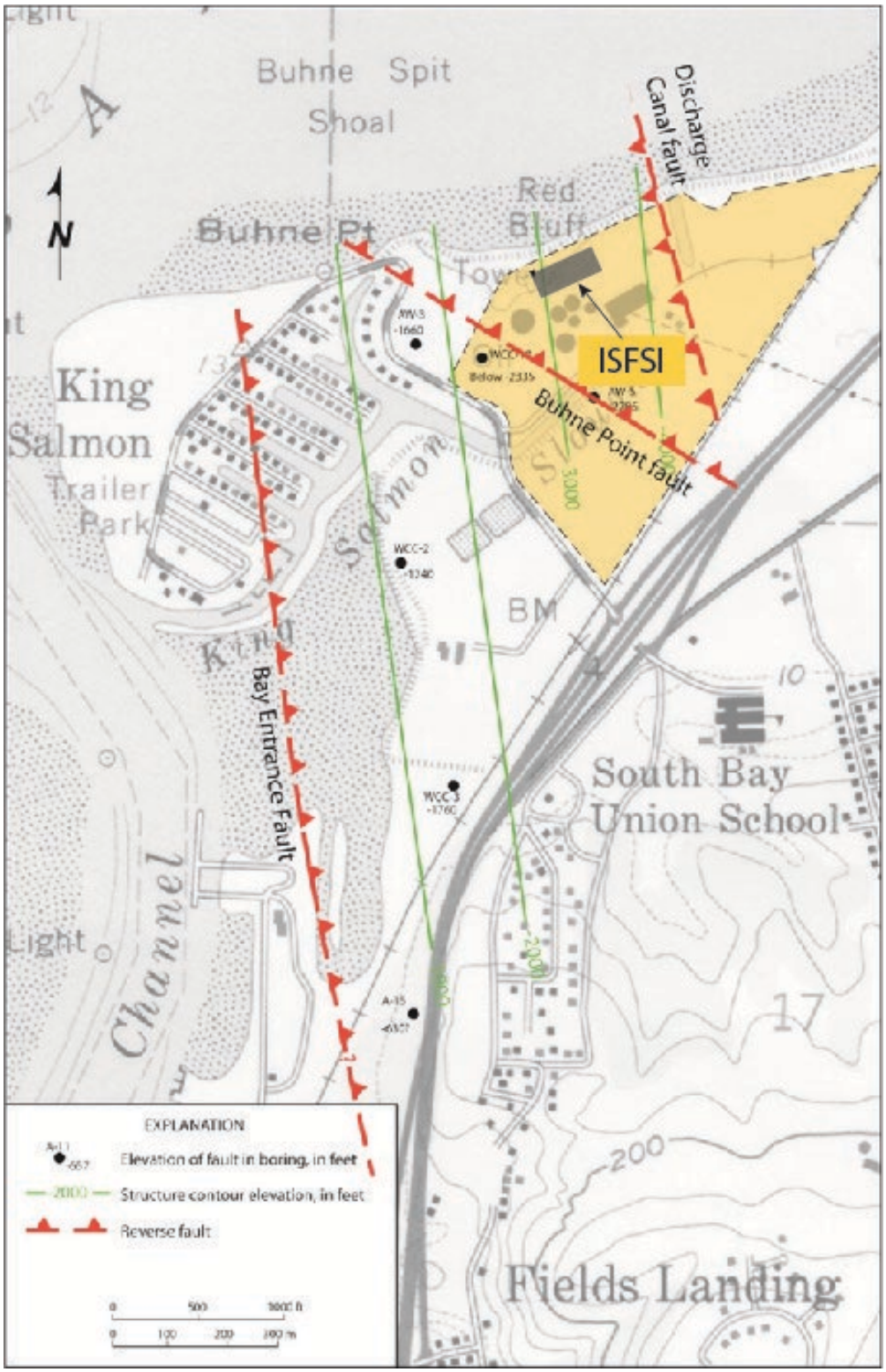

Figure 1-8. Splays of the Little Salmon fault zone at Buhne Hill
(after PG&E, 2003, Figure 4-13). The Bay Entrance fault is the northern extension of the east splay of the Little Salmon fault. The Buhne Point and Discharge Canal faults are secondary faults.

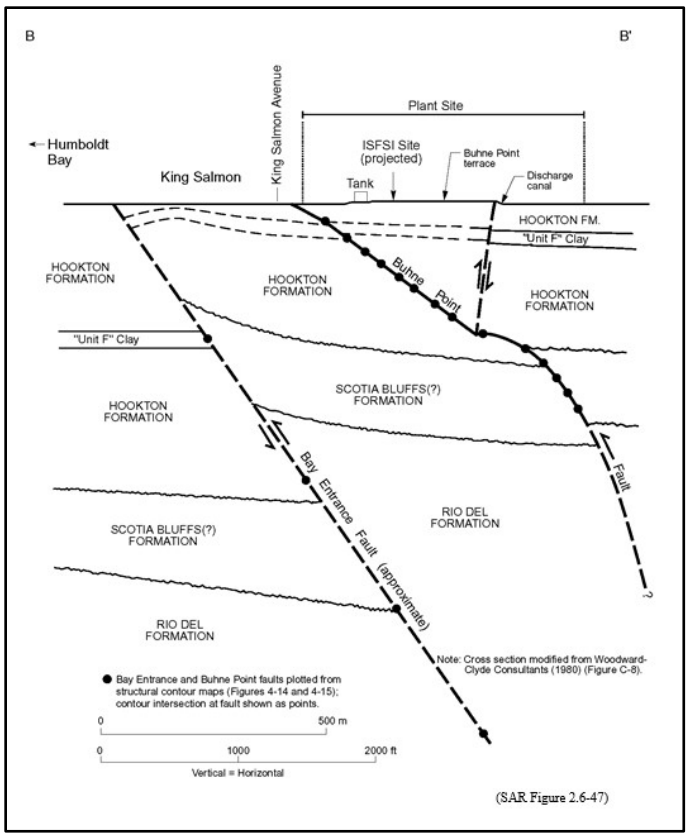

Figure 1-9. Cross section showing the Little Salmon Fault zone at Buhne Hill. The Bay Entrance fault is mapped at the surface south of King Salmon. The Buhne Point and Discharge Canal faults offset the 80-ka terrace but the area between is not faulted.

1.3.2 Paleotsunamis

Section 9 of the PG&E (2003) ISFSI report summarized the recent tsunami history of Humboldt Bay and presented the results of several geologic studies of prehistoric tsunamis (paleotsunamis) along the northern California coast, including Humboldt Bay. The results of the paleotsunami investigations are summarized below because they provide physical evidence to compare with model simulations.

Dr. Gary Carver and his students at Humboldt State University (now Cal Poly Humboldt) conducted paleotsunami investigations at 16 sites (Carver et al. 1998, Appendix in PG&E, 2003). Results from the analysis of these sites provided data on the 1700 C.E. tsunami and previous events (Figures 1-10 and 1-11), as follows:

- Four salt marsh sites, namely Crescent City, Lagoon Creek, Humboldt Bay South Spit, and Hookton Slough, documented evidence for four separate paleotsunamis in the past 2,000 years, the same sequence as found in Oregon and Washington by Atwater (1987).
- The Humboldt Bay North Spit site documented a paleotsunami that crossed the coastal sand dunes at the south end of the higher dunes north of Samoa. Samoa is 4.4 miles, and the paleotsunami site is about 5.5 miles from the bay entrance channel.).
- Two inundated sites from the 1700 C.E. event were reported by the Orick (now referred to as the Yurok) Tribe at Redwood Creek.

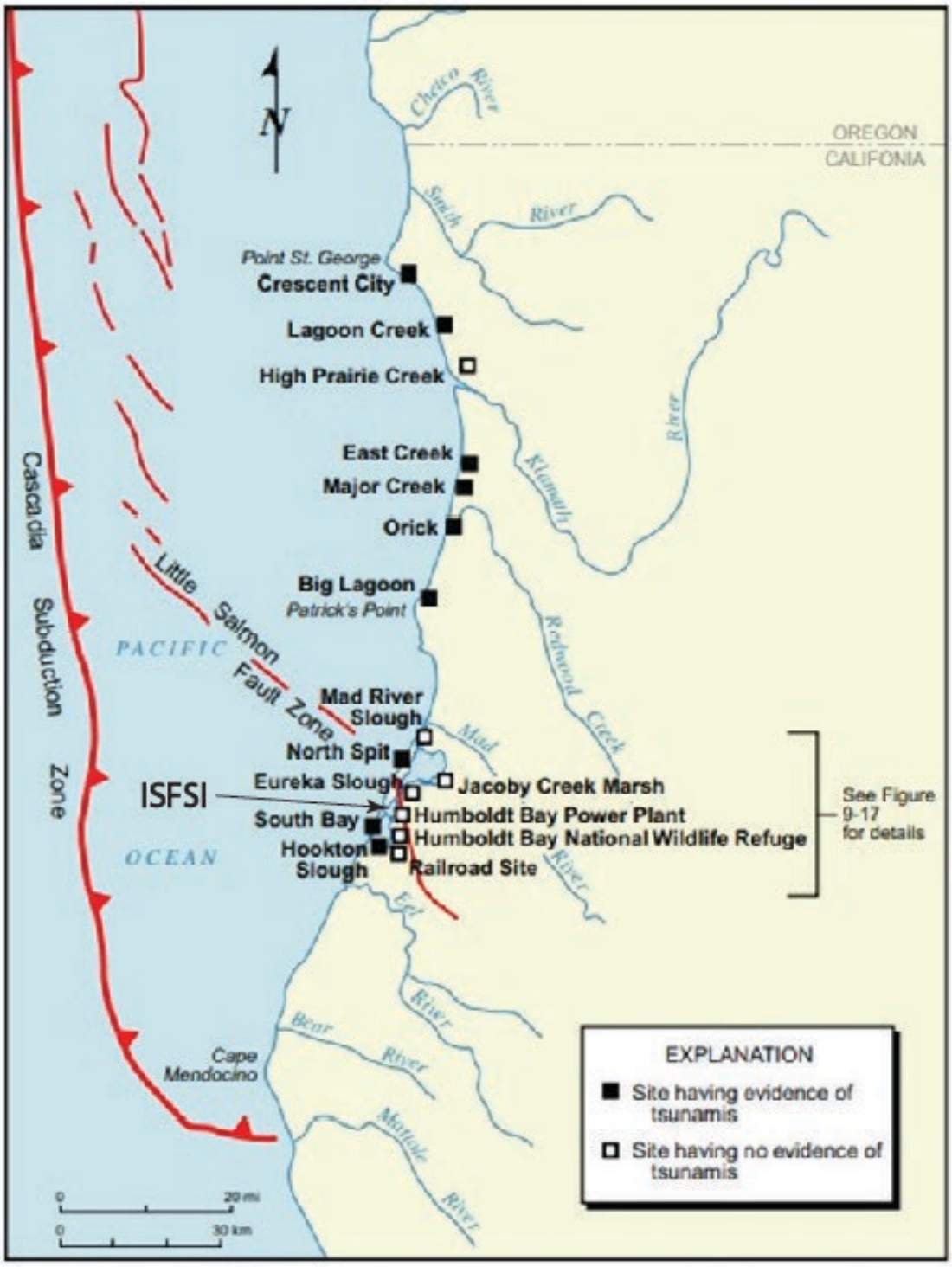

Figure 1-10. Coastal sites investigated for evidence of paleotsunami

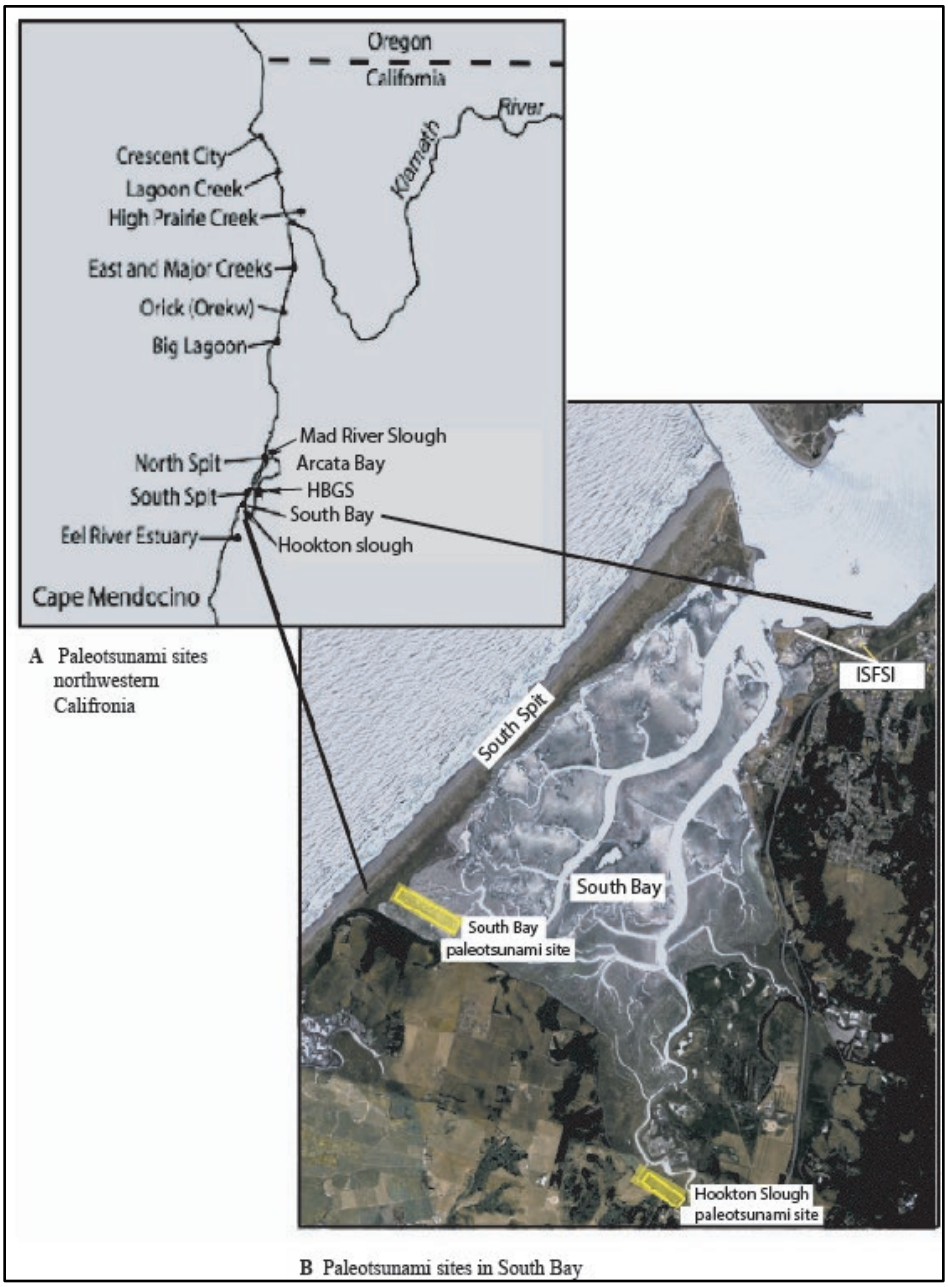

Figure 1-11. Paleotsunami sites in northwestern California (A), and paleotsunami sites in South Bay (B). Low tide image of the South Bay shows the Hookton Slough site is about 6 km (3.7 mi) inland from the ocean. The 1700 C.E. Cascadia tsunami may have arrived during low tide when the bay was drained, as in this image, and deposited a sand layer in Hookton Slough.

Table 1-1. Open Coast Runup Estimates from Paleotsunami Sites along the Northern California Coast Compared to Worldwide Data (from PG&E, 2003, Table 9-7**).**

Site	Estimated Runup Height at Coast (feet above MLLW)	Comments
Crescent City	Higher than 28 to 31 feet	Comparison of paleotsunami deposits with deposits in Kodiak Island from the 1964 Alaska earthquake.
Lagoon Creek	18 to 52 feet Most likely 26 to 33 feet	Table 9-6 – values calculated using particle size and settlement velocities for "Y", "W", "U", and "S" events. Most likely runup is judged to be 26 to 33 feet.
Orick	66 to 69 feet	From Native American oral history; high elevation may be anomalous local runup.
North Spit	A) Somewhat higher than 38 feet; less than 50 feet estimate 35 to 40 feet B) Less than 53 to 72 feet	A) Pebble layer at elevation of 38 ft. in dunes provides minimum estimate. Adding 12 feet depth to transport pebbles gives possible 50 feet B) Height of dunes provides maximum estimate.
South Spit	A) Higher than 18 to 23 feet B) Less than 20-40 feet	A) Height of dunes B) Height of marsh plus estimated depth of 13 to 33 ft. based on comparison with event "Y" at Lagoon Creek.
World Wide Data (Appendix 9A)	A) 35 feet B) 30 to 40 feet	Figure 9-19 Empirical relationship for a tectonic runup vs. magnitude. Runup for MLLW adds 3.7 feet to MSL. A) For a 8.8 Cascadia event runup is 31 feet MSL B) For magnitude range 8.5 to 9.2 runup is 26 to 36 feet MSL

As part of the ISFSI investigations, Dr. George Plafker (2002a, 2002b) of the United States Geological Survey (USGS) explored the relationship between earthquake magnitude and runup heights from a compilation of worldwide data. He was able to separate large runups generated by offshore landslides triggered by earthquakes from runups from direct subsea fault ruptures (Figure 1-12).

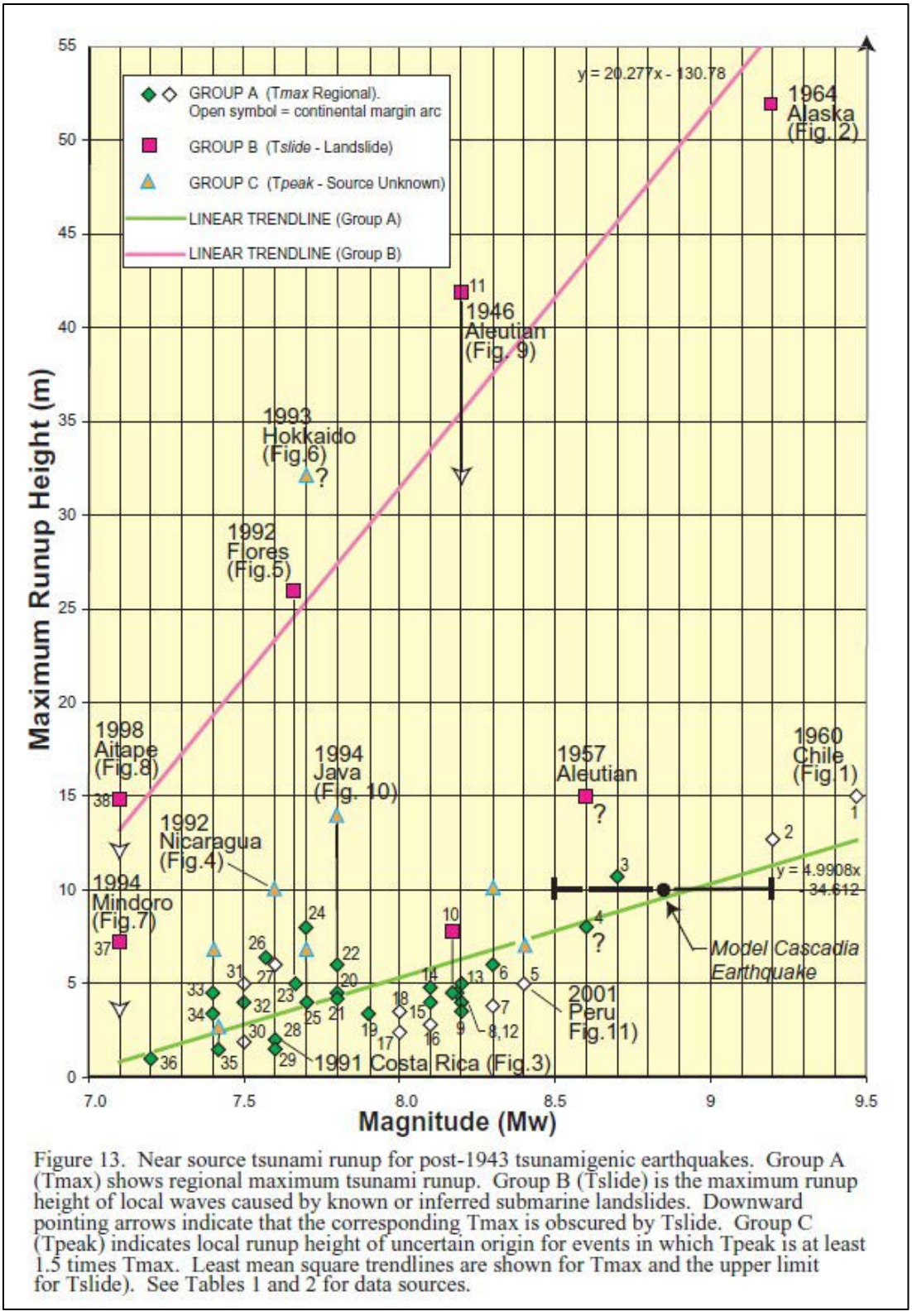

Figure 13. Near source tsunami runup for post-1943 tsunamigenic earthquakes. Group A (Tmax) shows regional maximum tsunami runup. Group B (Tslide) is the maximum runup height of local waves caused by known or inferred submarine landslides. Downward pointing arrows indicate that the corresponding Tmax is obscured by Tslide. Group C (Tpeak) indicates local runup height of uncertain origin for events in which Tpeak is at least 1.5 times Tmax. Least mean square trendlines are shown for Tmax and the upper limit for Tslide). See Tables 1 and 2 for data sources.

Figure 1-12. Runup heights compared to earthquake magnitude from worldwide data (from Plafker, 2002b, Appendix 9A in PG&E, 2003, his figure 13).

1.3.2.1 Tsunami Runup at Buhne Hill

Several factors control the onshore runup and inundation at Buhne Hill. These include:

- the bathymetry offshore and in Humboldt Bay,
- the jetties and depth at the entrance to Humboldt Bay,
- the tide level at the time of arrival of the tsunami, and
- the elevation of Buhne Hill and of the North and South spits at the time of the tsunami, which could change by coseismic uplift or subsidence immediately prior to the arrival of the tsunami waves.

Figure 1-13 is a simplified cross-section across Humboldt Bay, from the Pacific Ocean to Buhne Hill, that summarizes the various estimates of tsunami runup (and inundation) at Buhne Hill developed since the first tsunami assessment study in 1965. These estimates are based on various analytic models and the geologic estimates obtained from studies of paleotsunami runups. Where appropriate, the results of a given study are presented as a vertical bar that captures the tidal range or the estimated runup values. The upper panel in Figure 1-13 shows the location and lateral extent of the cross-section presented in the lower panel.

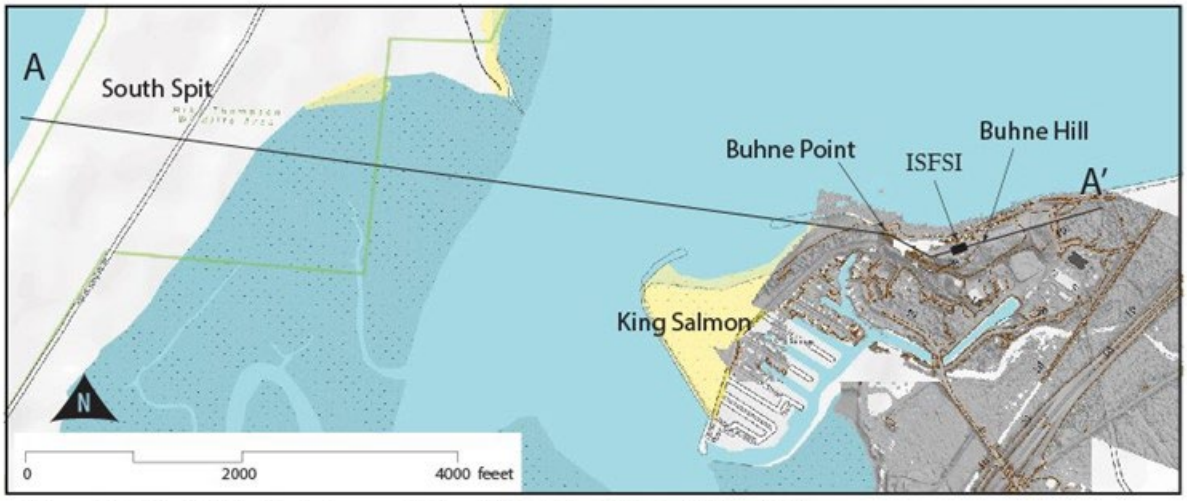

Map of Profile A A' South Spit across Buhne Hill to Marsh East of Buhne Hill

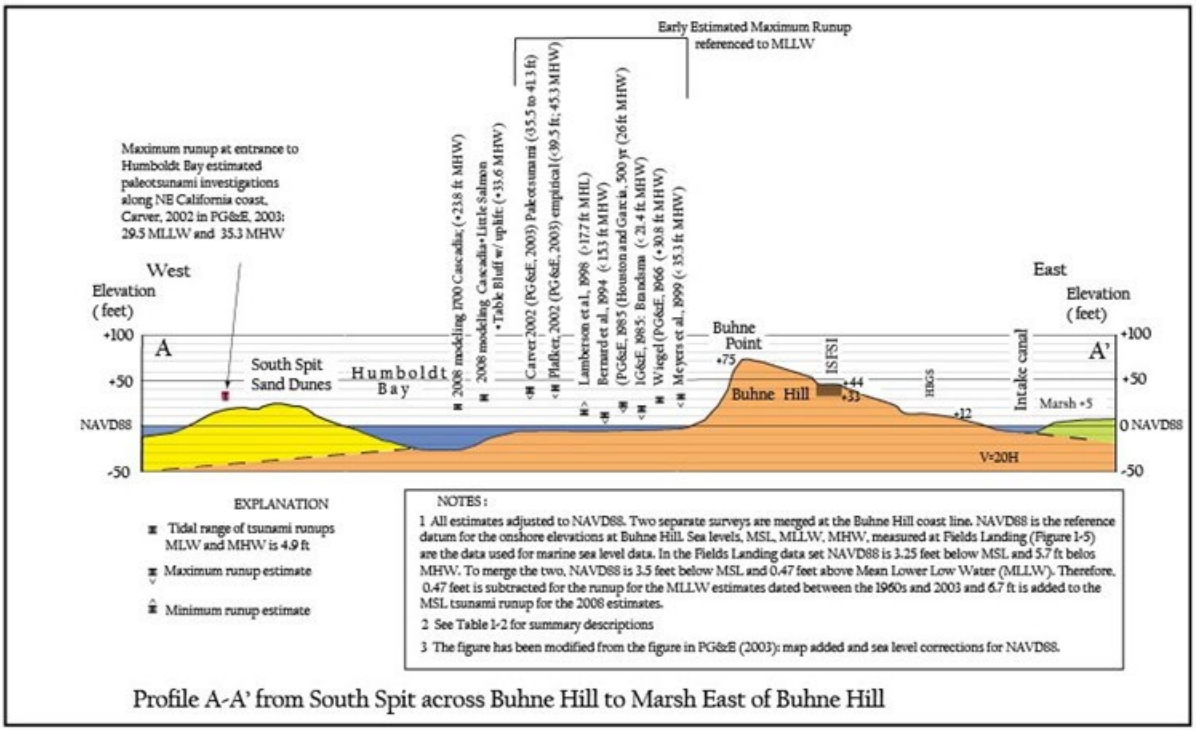

Profile A-A' from South Spit across Buhne Hill to Marsh East of Buhne Hill

Figure 1-13. Schematic diagram showing previously estimated runup at the Humboldt Bay ISFSI (modified from PG&E, 2003, Figure 9-20)

1.4 2005 Long-Term Analysis of Global-Warming-Induced Sea Level Rise and Tectonic Deformation at Buhne Hill

Following the 26 December 2004 **M** 9.0 Indian Ocean Tsunami, PG&E's Geosciences Department completed an assessment of the long-term global-warming-induced sea level rise and tectonic deformation at Buhne Hill (PG&E, 2005) at the request of the California Coastal Commission. The findings confirmed the earlier conclusion (PG&E, 2003) that the ~80-ka

marine terrace that caps Buhne Hill has recorded the long-term uplift on the hanging wall of the Little Salmon fault zone (Figures 1-8, 1-9 and 1-14).

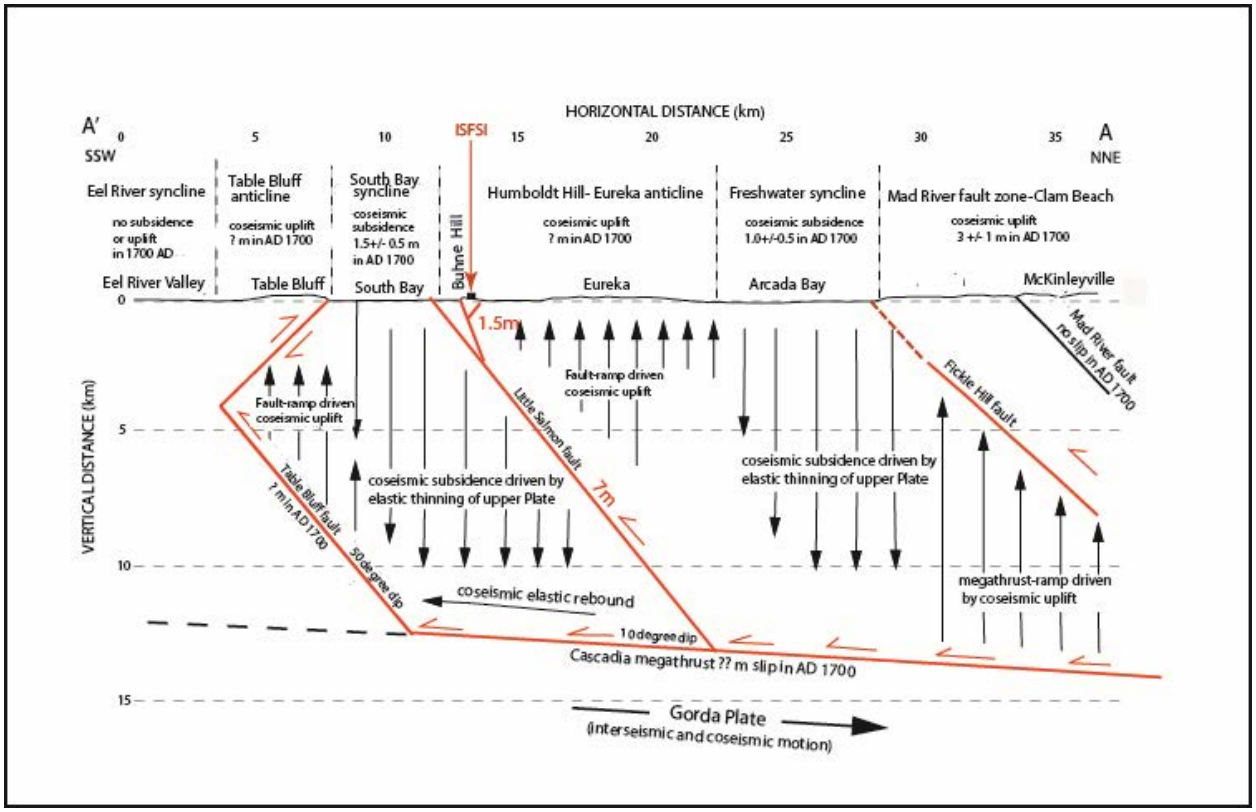

Figure 1-14. Cross section A-A' for the Cascadia-Little Salmon model at Humboldt Bay (from PG&E, 2005). Faults shown are schematic.

The 2005 analysis considered the most recent information available at the time regarding climate-change-induced sea level rise and changes in sea level resulting from ice accumulation from the predicted shift from the current interglacial period to a glacial period.

The short-term 100-year forecast showed that the relative change in sea level at Buhne Hill (IPCC, 2001) when combined with the tectonic land level change predicted over the next 100 years, global sea level may rise at rates between 0.8 and 12.5 mm/yr (0.26 and 4.1 feet per century). Simultaneously, local land level elevations at Buhne Hill likely will increase at a short-term rate of about 4 ± 1 mm/yr (1.3 ± 0.3 ft./century). The resulting relative sea level curve predicts Buhne Hill to be at an elevation of about 13.4 ± 0.18 m (44 ± 0.6 ft.) above mean sea level in the year 2050, and about 13.35 ± 0.49 m (43.8 ± 1.6 ft.) in the year 2100 (Figure 1-15). The report noted that if a Cascadia and/or LSF earthquake occurs in the next 100 years, as it may, Buhne Hill may be subjected to sudden coseismic subsidence of about 1.8 m (6 ft.). The town of King Salmon that is on the footwall of the LSF may experience additional subsidence of several more feet. An independent earthquake on the Little Salmon fault zone could result in coseismic uplift of Buhne Hill of several feet. Since coseismic uplift or subsidence of Buhne Hill is equivocal, this represents an uncertainty that can be checked against estimated tsunami model runup results to assess if adequate freeboard remains relative to the elevation of the ISFSI.

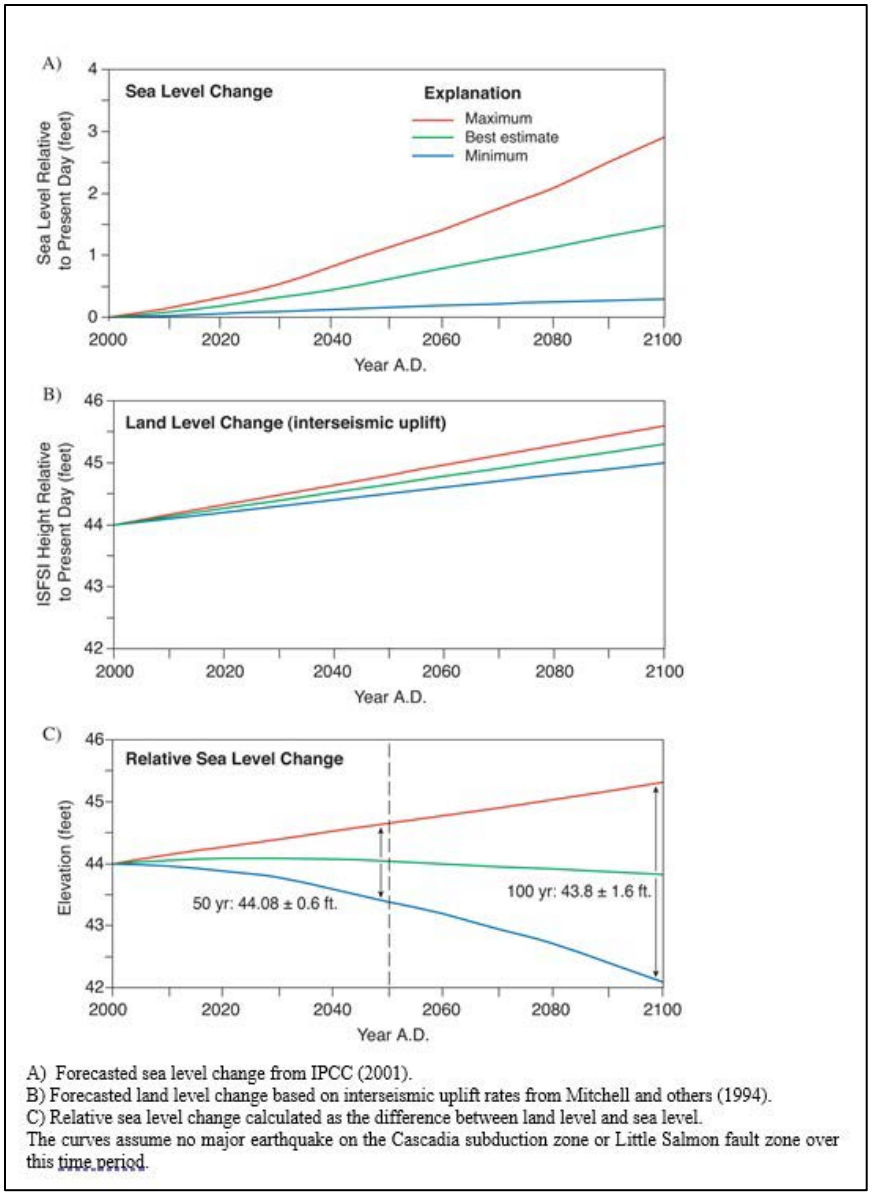

A) Forecasted sea level change from IPCC (2001).
B) Forecasted land level change based on interseismic uplift rates from Mitchell and others (1994).
C) Relative sea level change calculated as the difference between land level and sea level.
The curves assume no major earthquake on the Cascadia subduction zone or Little Salmon fault zone over this time period.

Figure 1-15. Forecasted changes in relative sea level at Buhne Hill over the next 100 years

1.5 2008 To 2015 Assessments of Potential Tsunami Runup at the Humboldt Bay Generating Station

In 2015, PG&E's Geosciences Department completed a report started in 2008 estimating the potential for tsunami runup at the Humboldt Bay Generation Station (HBGS), a natural gas-fueled plant constructed north of the former nuclear plant site and northeast of the Humboldt Bay ISFSI. The HBGS plant grade is at an elevation of 3.66 m (12 ft)(NAVD88) and 9.75 m (32 ft.) lower than the ISFSI pad at 13.4 m (44 ft.). The HBGS assessment built upon the tsunami hazard studies that had been previously conducted for the region and for the nuclear plant and ISFSI. This was the most comprehensive review to date of previous work. The 2015 report incorporated

for the first-time hydraulic modeling of tsunami runups in Humboldt Bay. The discussion below summarizes the approach followed and the conclusions from this past study.

Significantly, at the time there were no engineering guidelines or governmental regulations requiring that the potential tsunami hazard be considered during the design and construction of similar power plants. Nevertheless, PG&E's Geosciences Department assessed the potential wave height resulting from a tsunami likely to impact the proposed HBGS site. The report updated earlier estimates of potential tsunami runup conducted for the ISFSI (PG&E, 2003) (discussed above) and compared the results to analyses by Patton and Dengler (2006), Uslu (2008), and Thio et al. (2010). The analysis also incorporated new information on the stratigraphy from groundwater studies conducted at the HBGS site (Kleinfelder, Inc., 2006; Gregg In Situ, Inc., 2006). In addition, the lessons learned from the numerical simulations of tsunami runup and inundation for the PG&E Diablo Canyon Power Plant were evaluated for comparison to other areas in Humboldt Bay (PG&E, 2008).

1.5.1 Geologic-Tectonic Setting of Buhne Hill and the HBGS site

While the tectonics of the CSZ and the LSF were investigated extensively in the PG&E (2003) study, the potential for coseismic uplift or subsidence was not considered in the tsunami evaluation for Buhne Hill and the ISFSI. However, the site's position relative to the CSZ and the LSF is an important factor in understanding and predicting potential runup heights.

As discussed in the ISFSI section, the CSZ lies offshore and extends from north of Cape Mendocino to British Columbia (Figure 1-6). In northern California, the Cascadia "hinge line" that separates the areas experiencing coseismic subsidence from those experiencing uplift, intersects the coast near the mouth of the Klamath River (Gary Carver, 2007, oral communication, as reported in Page and Nishenko, 2015). Coseismic coastal subsidence predominates offshore north of the Klamath River, whereas coastal uplift occurs to the south and trends inland 20 to 30 kilometers (12.4 to 18.6 mi) east of Humboldt Bay. The zone of coseismic uplift onshore follows the Mad River and Little Salmon fault zones where the southern end of the CSZ approaches the Mendocino triple junction (Figure 1-7). In this area, the edge of the overriding plate is broken into several crustal pieces separated by reverse faults that effectively partition the strain. In the Humboldt Bay area, coseismic subsidence is modified by uplift on the Mad River, Little Salmon and Table Bluff faults during Cascadia events or in separate LSF events. Arcata and South Bays have experienced subsidence from both elastic rebound and elastic thinning or stretching of the crust. The South Bay syncline lies between the Table Bluff and Little Salmon faults, and the Freshwater syncline that underlies Arcata Bay is between the Fickle Hill and Mad River faults (Figure 1-14).

The National Research Council Committee on Sea Level Rise (NRC, 2012) found that north of Cape Mendocino, land is generally rising at a rate of between 1.5 and 3.0 mm/yr (0.06 to 0.12 in/yr) as the ocean plates descend below the North American plate along the CSZ. However, Humboldt Bay has not experienced regional uplift but instead has the highest subsidence rate recorded for the California coast (Patton et al., 2015), making the area particularly susceptible to the effects of sea level rise (California Coastal Commission, 2015).

The hills east of Humboldt Bay have a flight of marine terraces attesting to long-term uplift (Figure 1-16). In contrast, Arcata, Humboldt and South bays all record long-term subsidence. Buhne Hill is an uplifted outlier east of the west end of Humboldt Hill with a low area of alluvial

fill and tidal marsh in between.

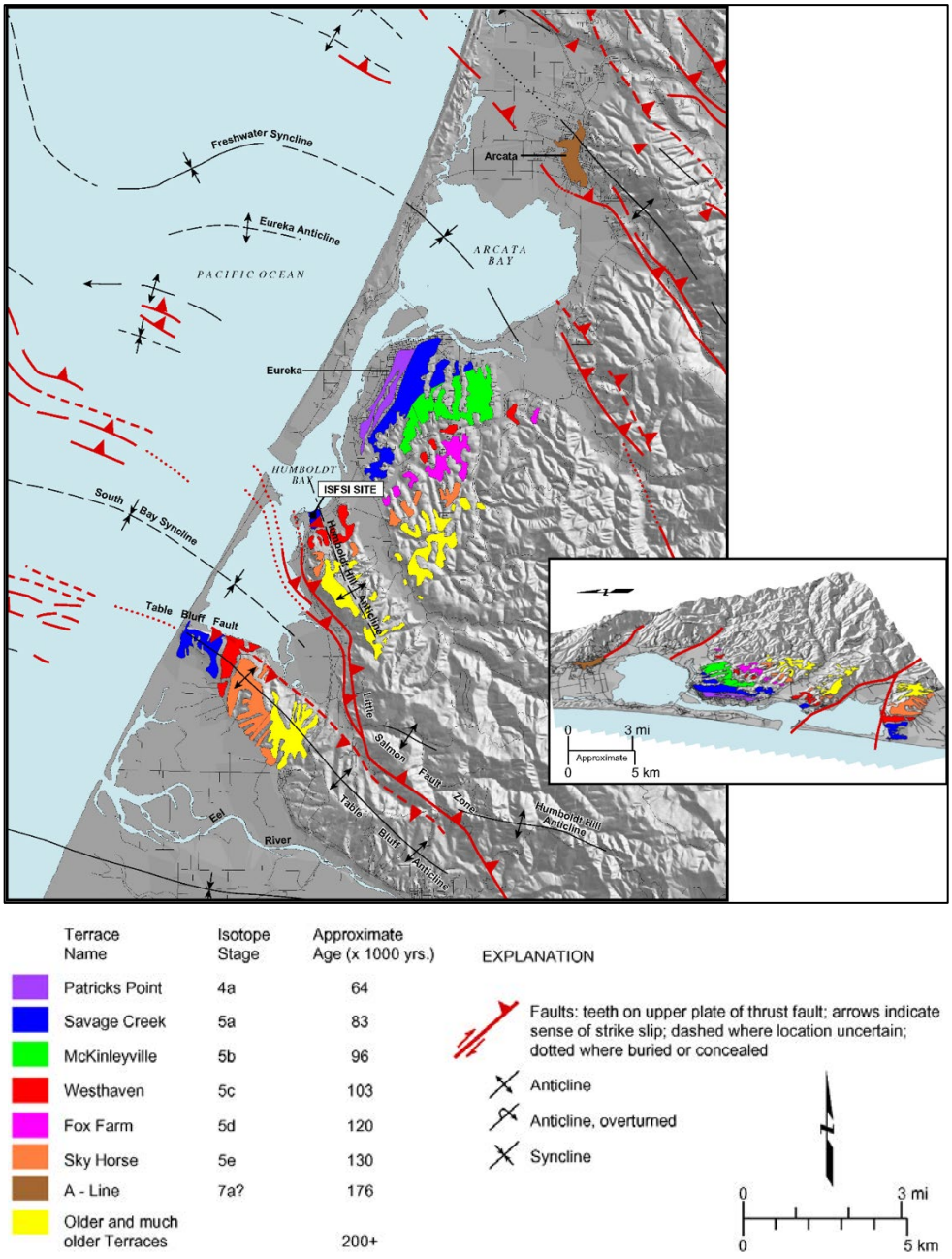

Figure 1-16. Marine terraces south and east of Humboldt Bay
(from Swan et al., 2002, their figure 3-6). The terraces record progressive uplift of anticlinal folds that are presumed to be growing coseismically in response to movement on various thrust faults that extend across the area.

1.5.2 Tsunami Model Simulations

PG&E selected several earthquake and tsunami scenarios to model the range of potential runup and inundation in Humboldt Bay and Buhne Hill. The scenarios included both far-field, circum-Pacific tsunamis and tsunamis originating from the CSZ, the subduction zone with the LSF, and a

hypothetical offshore submarine landslide in Eel River Canyon. Individual scenarios were calibrated using eyewitness observations, tide gauge records, and geologic evidence of paleotsunamis.

The general hydrodynamic model used in this study was based on Satake (1995) with new bathymetry and topography data compiled by the Center for Integrative Coastal Observation, Research and Education (CICORE) for the entire Humboldt Bay area (Figure 1-17) that was sampled at 6 m (~ 1/5 arc-second). This new elevation dataset significantly improved the earlier 10-m-sampling data used for the 2008 and 2011 tsunami modeling of the North and South spits, based on a comparison with paleotsunami data. Other adjustments to the modeling results of tsunami runups included consideration of a 1.07-m (3.5-ft.) increase in water level resulting from a combined 0.49-m (1.6-ft.) storm surge and 0.58-m (1.9-ft.) rise in sea level to the year 2120 due to climate change.

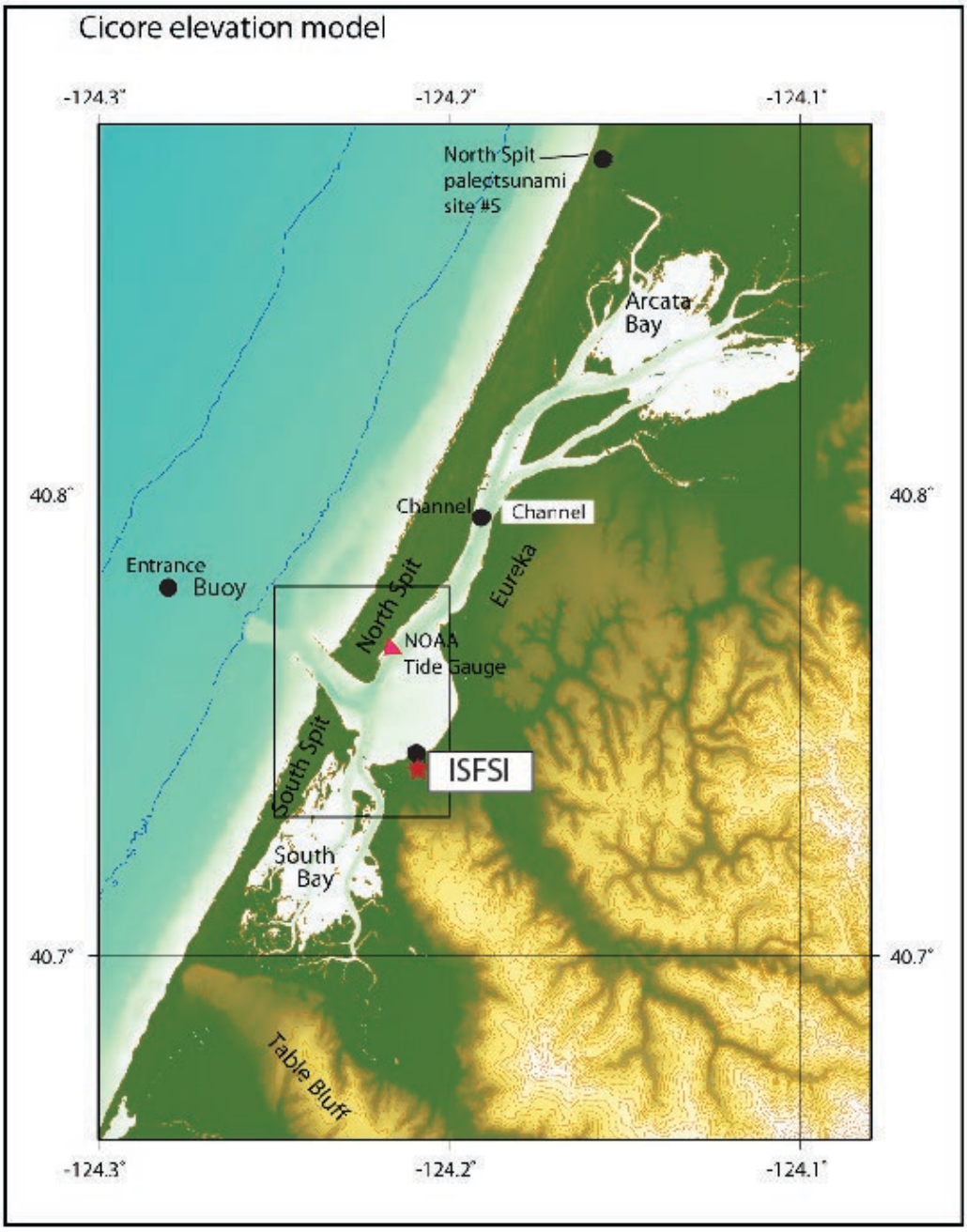

Figure 1-17. CICORE 6-m grid Digital elevation model (DEM) for Humboldt Bay.
Black circles are locations of sites discussed in the text.

The model results for a distant tsunami scenario closely match the tide gauge records from recent Pacific Ocean tsunamis, showing that the modeling can be used with a high degree of confidence in areas where the bathymetry and topography are sufficiently accurate and where the tsunami source characterization is well defined. Figure 1-18 shows as an example a comparison between the water levels from a simulated distant tsunami scenario and the actual tide gauge readings measured during the 15 November 2006 M_w 8.3 Kuril tsunami at both Crescent City and Humboldt Bay.

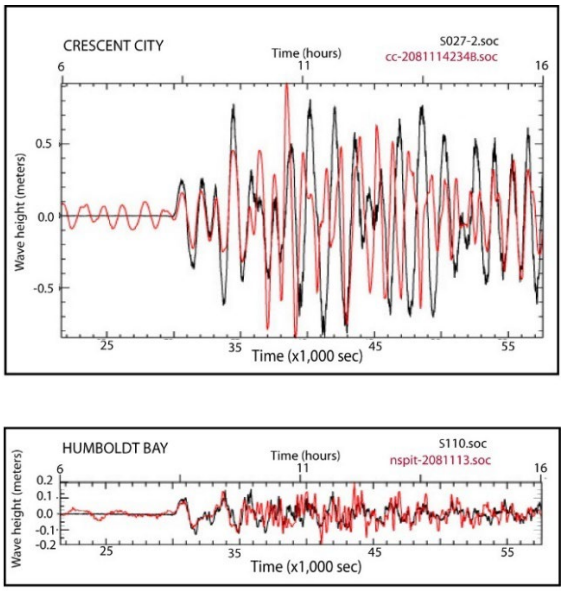

Figure 1-18. Comparison of simulation (black) to marigrams (red) for the 15 November 2006 M_w 8.3 Kuril tsunami at Crescent City (top) and Humboldt Bay North Spit (bottom) tide gauge stations.

Two additional scenarios were selected to illustrate the earthquake and model results: the offshore 1700 C.E. scenario and the Cascadia-Little Salmon fault scenario. These are described further in the following sub-sections.

1.5.2.1 1700 C.E. Cascadia Scenario

A hypothetical M_w 9.3 Cascadia subduction event was modeled to extend from Vancouver Island to Cape Mendocino (Figure 1-19); this scenario is herein referred to as the 1700 C.E. model. Figure 1-20 shows the modeled results from this scenario for Crescent City and compares the results to the inundation levels observed during the 1964 Alaska tsunami. The modeled tsunami inundation at Buhne Hill from this hypothetical scenario (the 1700 C.E. model) (Figure 1-21) shows that the ISFSI is located above the estimated runup level and would thus not be impacted (Table 1-2).

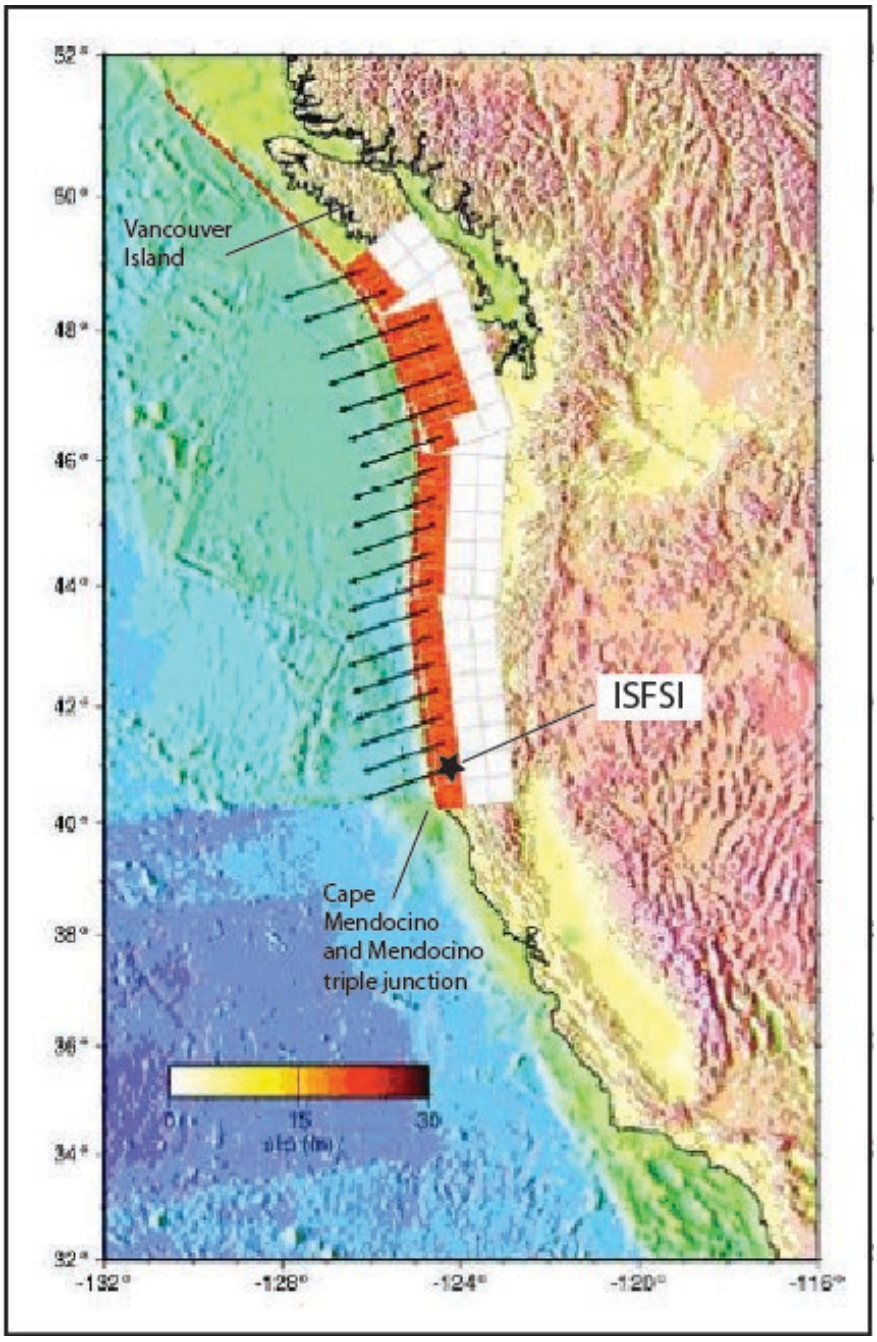

Figure 1-19. Source model for the 1700 C.E. Cascadia earthquake. The dashed red line is the surface trace of the Cascadia subduction zone. The squares represent the grid used to model the earthquake rupture area and are colored coded by the amount of fault displacement. The arrows show the rake or direction of fault motion that is parallel to the relative plate motion. In this relatively simple model, the southern end of the CSZ terminates at the Mendocino triple junction at Cape Mendocino (after Satake et al., 2003).

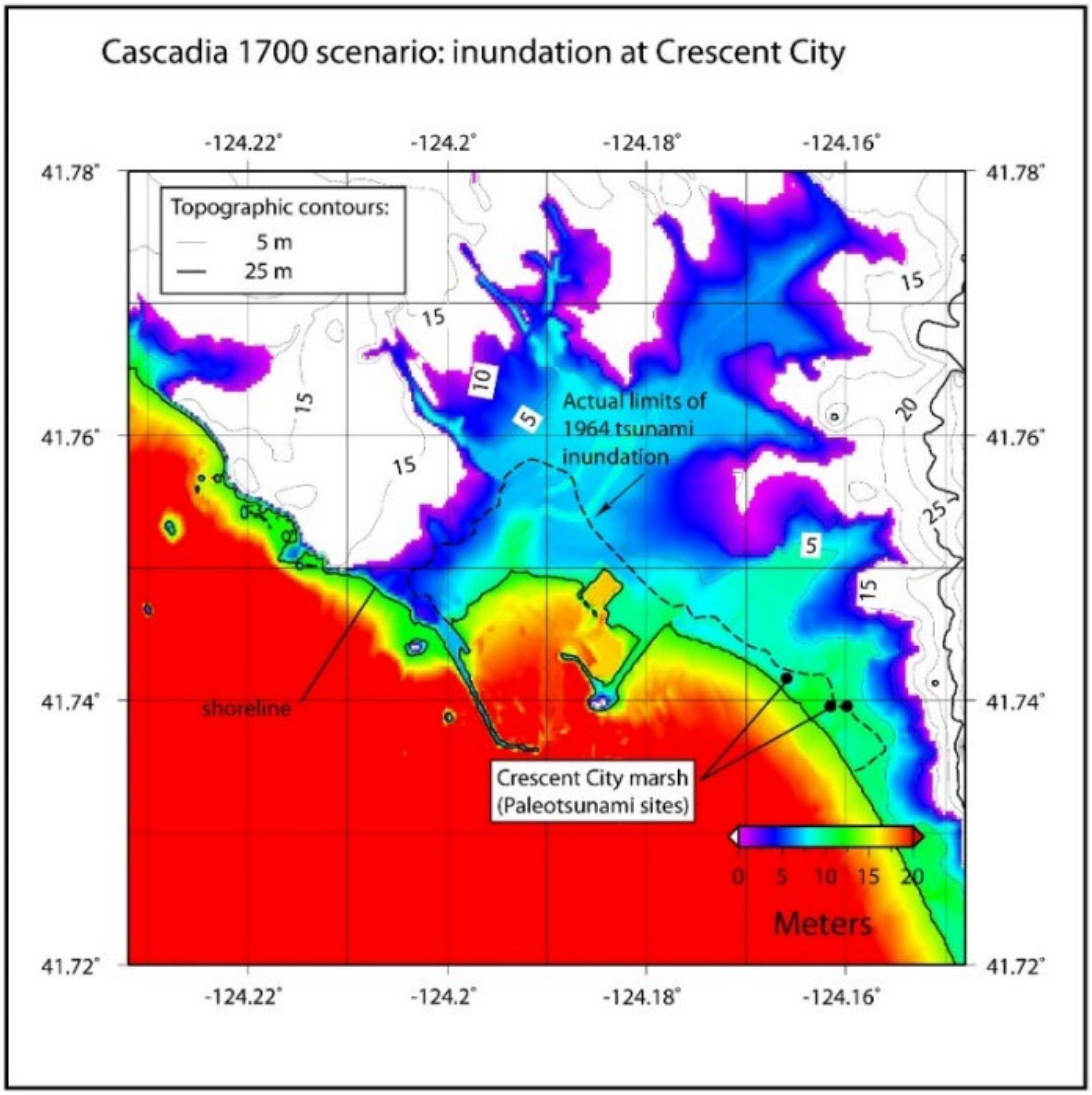

Figure 1-20. Calculated maximum tsunami inundation (colored area) and water depths from the Cascadia 1700 C.E. scenario at Crescent City. In this scenario the coast at Crescent City subsides coseismically 3.5 to 4 meters. Simulations are based on 90-m DEM. Dashed line shows observed inundation from the 1964 Alaska tsunami.

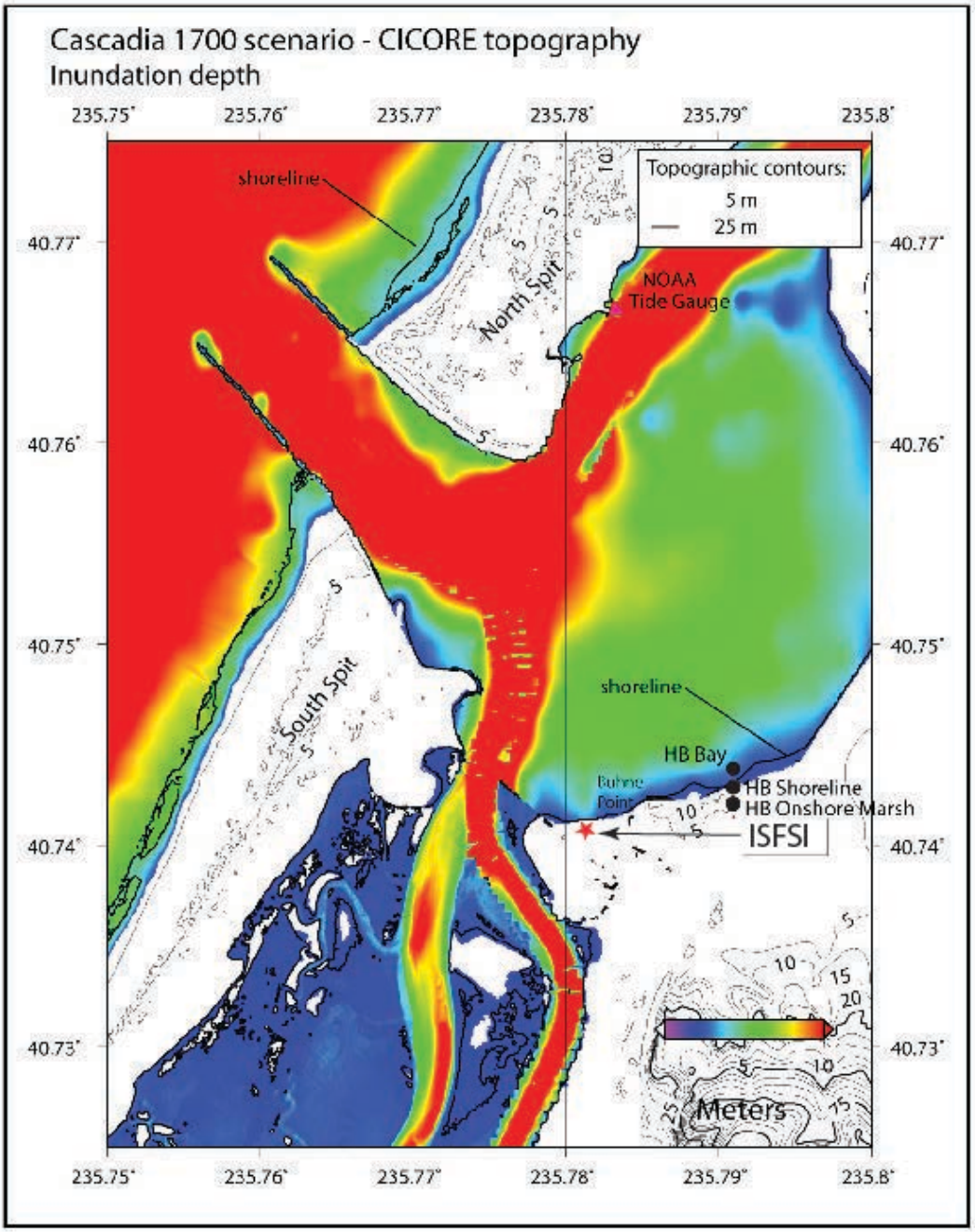

Figure 1-21. Calculated maximum tsunami runup heights from the Cascadia 1700 C.E. scenario at Buhne Hill. The black dots are specific elevations described in the text of the PG&E (2015) report.

1.5.2.2 Cascadia-Little Salmon Fault Scenario

The Cascadia-Little Salmon fault scenario assumes that the CSZ turns onshore at the LSF and that the two faults rupture together with uplift of Buhne Hill as a result of movement on the LSF. The modeled uplift of Buhne Hill is shown on Figure 1-22. Uplift at the site is heavily dependent on the variability of the displacement on the LSF and the larger Cascadia rupture. Based on the

geologic information available, it was estimated at about 1.6 - 1.7 m (+0.5/-1.0 m). The modeled inundation at Buhne Hill is shown on Figure 1--23. Inundation heights above MSL ('ground level') at the HBGS for this scenario are 5 to 7 m (17 to 23 ft.) (Table 1-2).

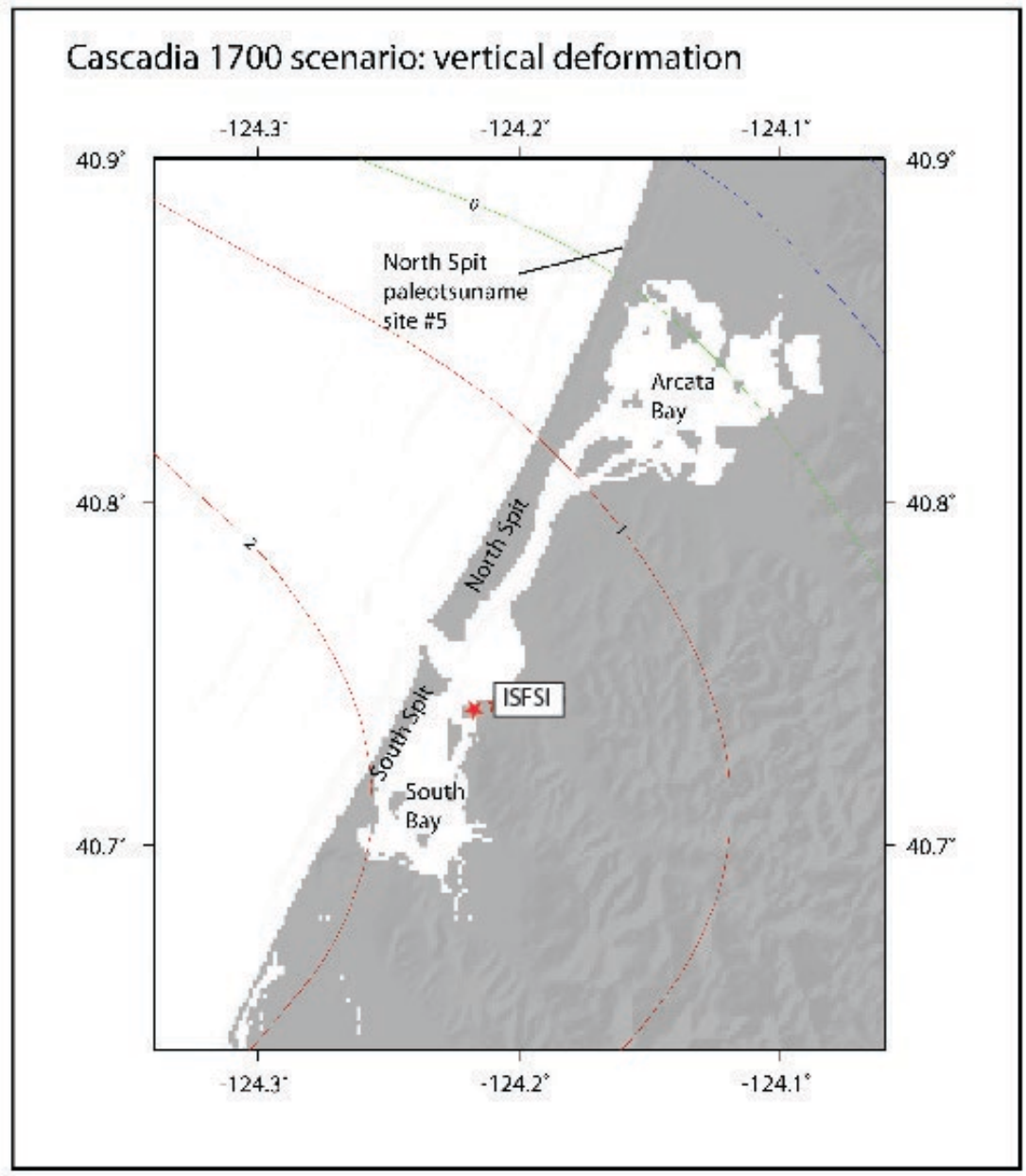

Figure 1-22. Calculated estimated vertical deformation at Humboldt Bay for the Cascadia-Little Salmon scenario. Contours in meters.

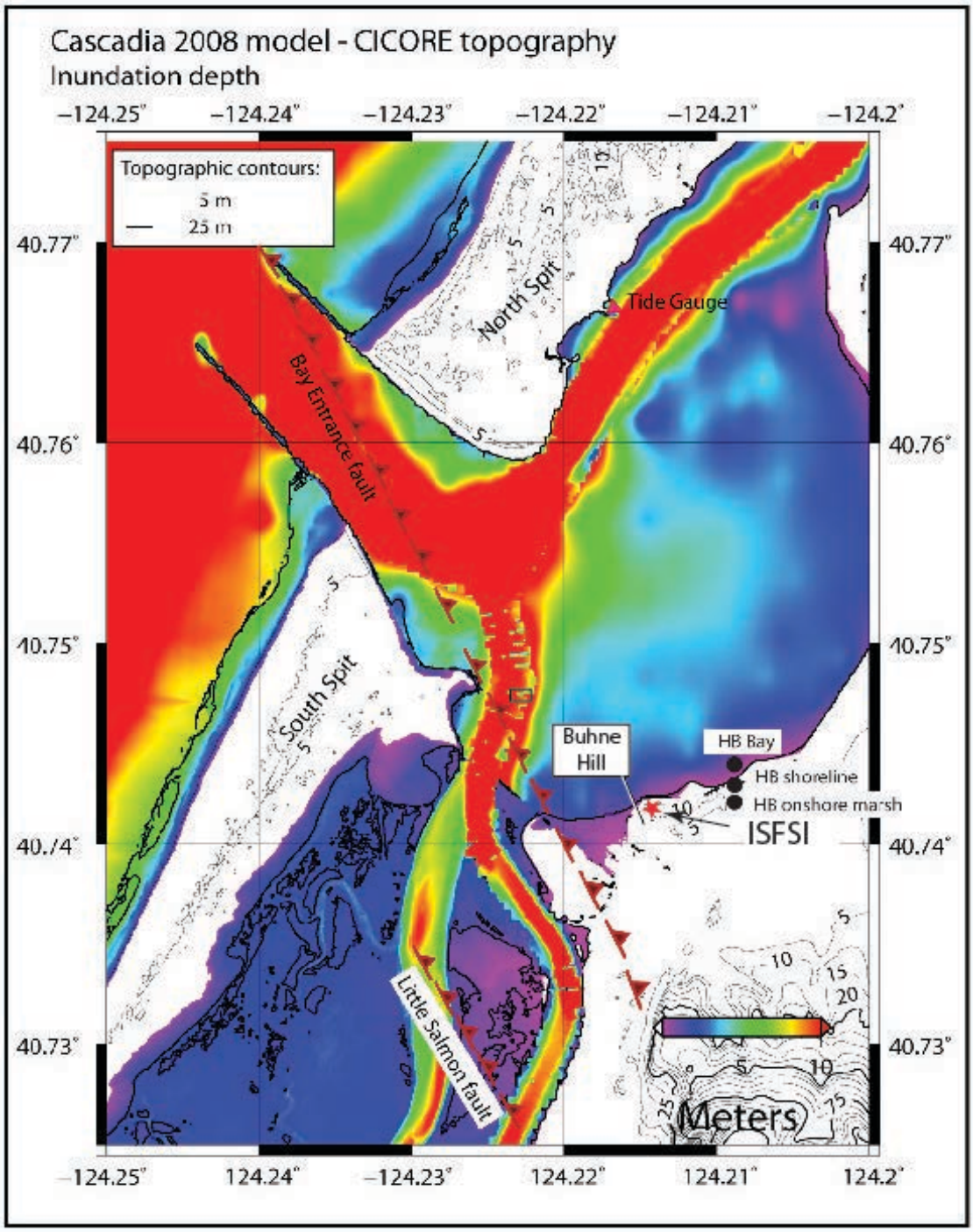

Figure 1-23. Calculated maximum tsunami runup heights for the Cascadia-Little Salmon fault model based on the CICORE DEM.

1.5.2.3 Offshore Landslide Scenarios

Hypothetical offshore landslide tsunami potential from three sites in the Trinidad Canyon and four sites in the Eel River Canyon were assessed (Figure 1-24). The largest runup estimate at the HBGS is 0.2 m (0.6 ft.) (Table 1).

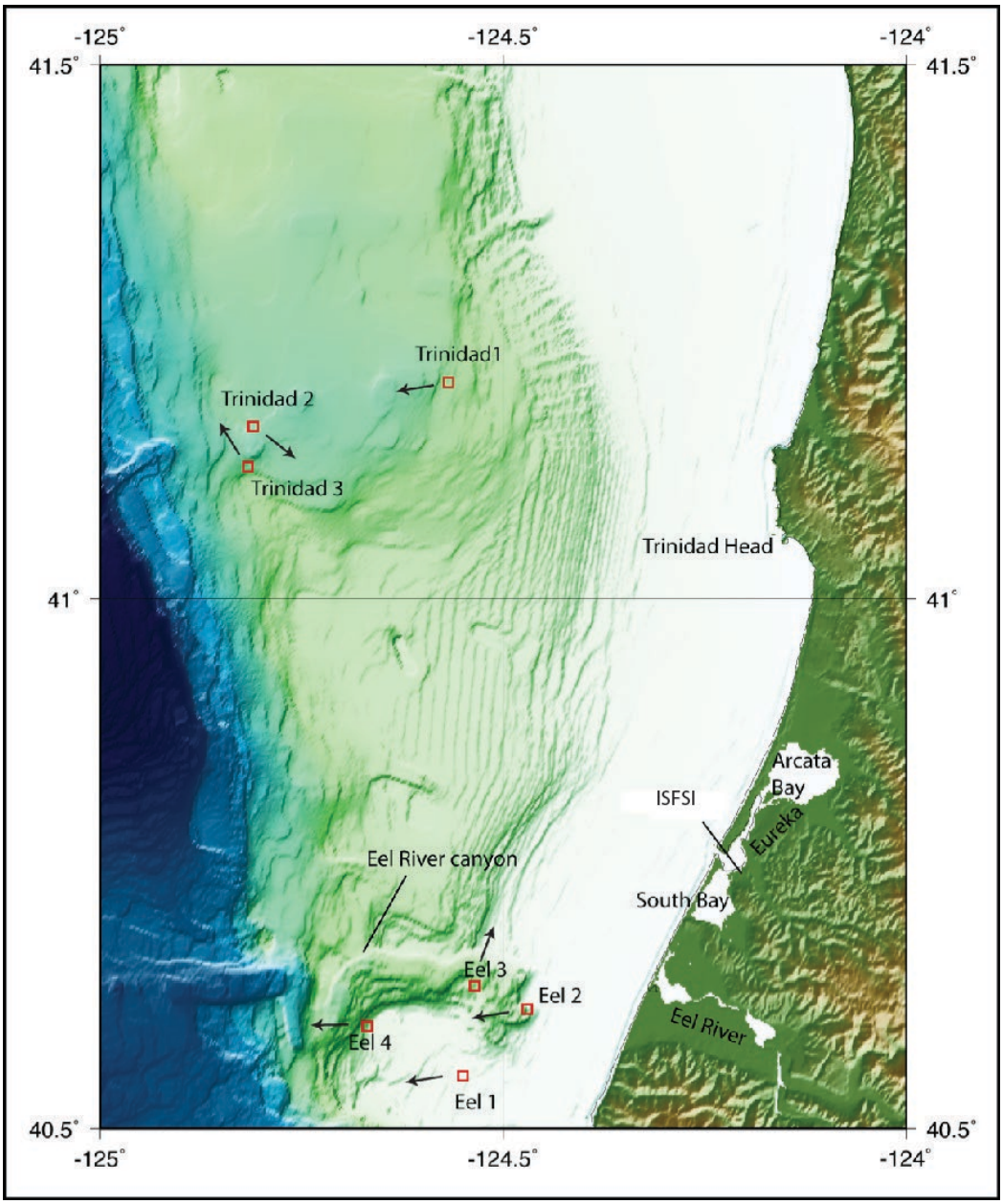

Figure 1-24. Locations of hypothetical submarine landslide simulation source zones in the offshore Trinidad and Eel River canyons. Arrows indicate assumed landslide direction.

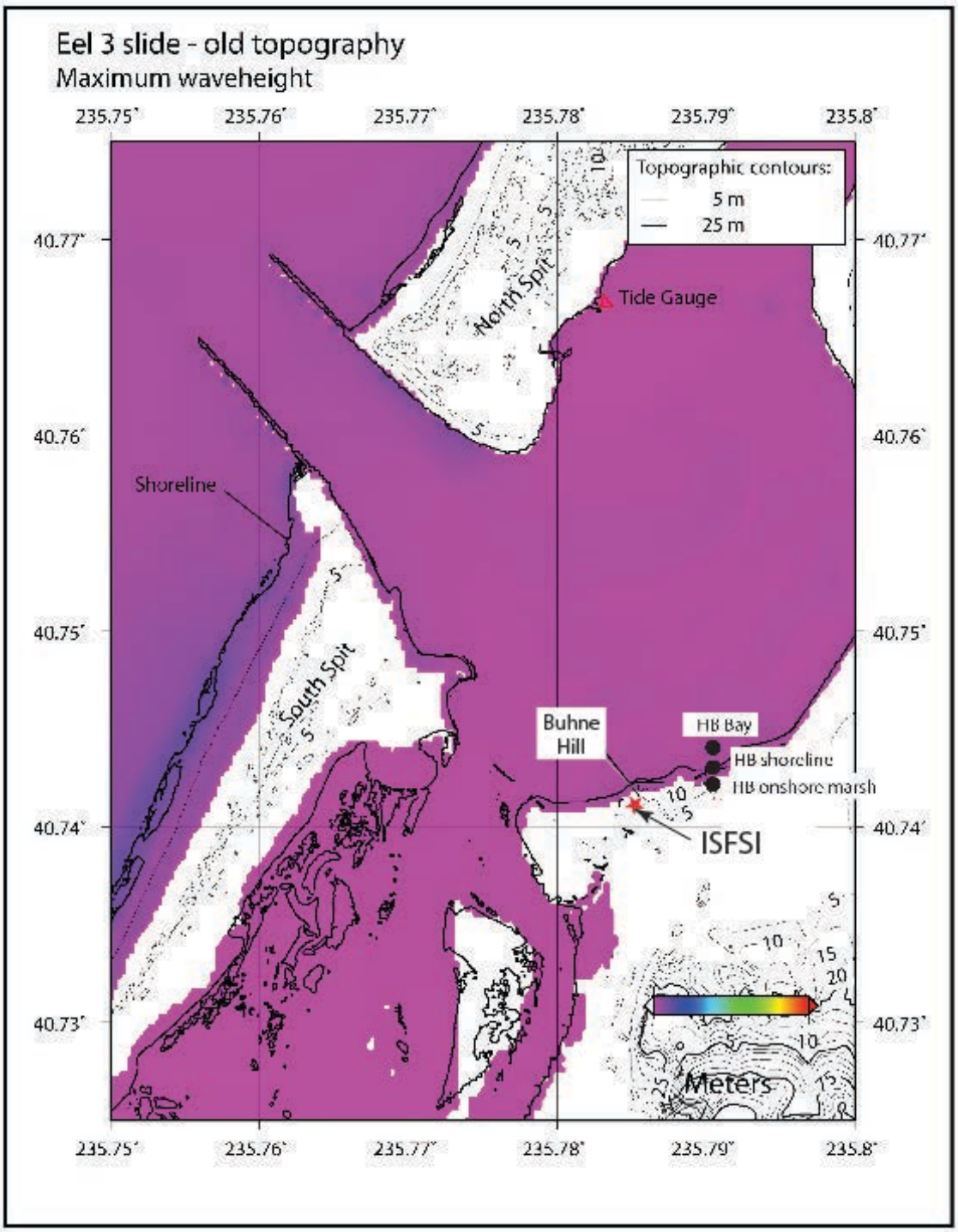

Figure 1-25. Calculated maximum tsunami inundation (colored area) and runup at Buhne Hill from the Eel Canyon landslide 3 scenario (refer to Figure 1-24 for the source location and Table 1-2 for model wave heights).

1.5.2.4 Comparison of the 1700 C.E. Scenario to the Paleotsunami Record

The paleoseismic record described in the ISFSI report (PG&E, 2003) provided further confidence in the modeling results for the 1700 C.E. scenario. Specifically, the model results closely match the paleotsunami record at Redwood Creek (Figure 1-26) and North Spit (Figure 1-27).

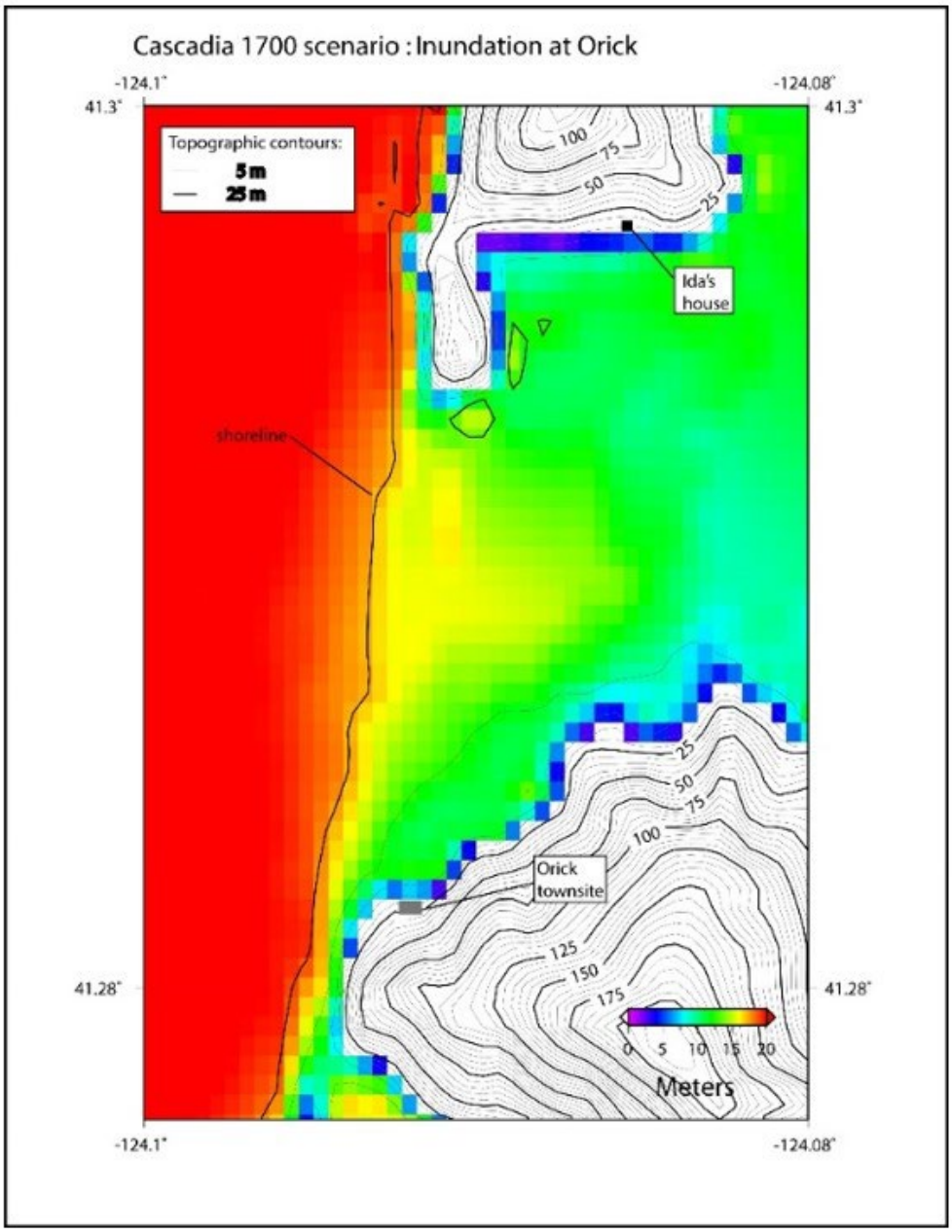

Figure 1-26. Redwood Creek area showing paleotsunami sites at Orick and at Ida's House. The modeled inundation just reaches the two sites, consistent with the oral traditions of the Orick (Yurok) Tribe.

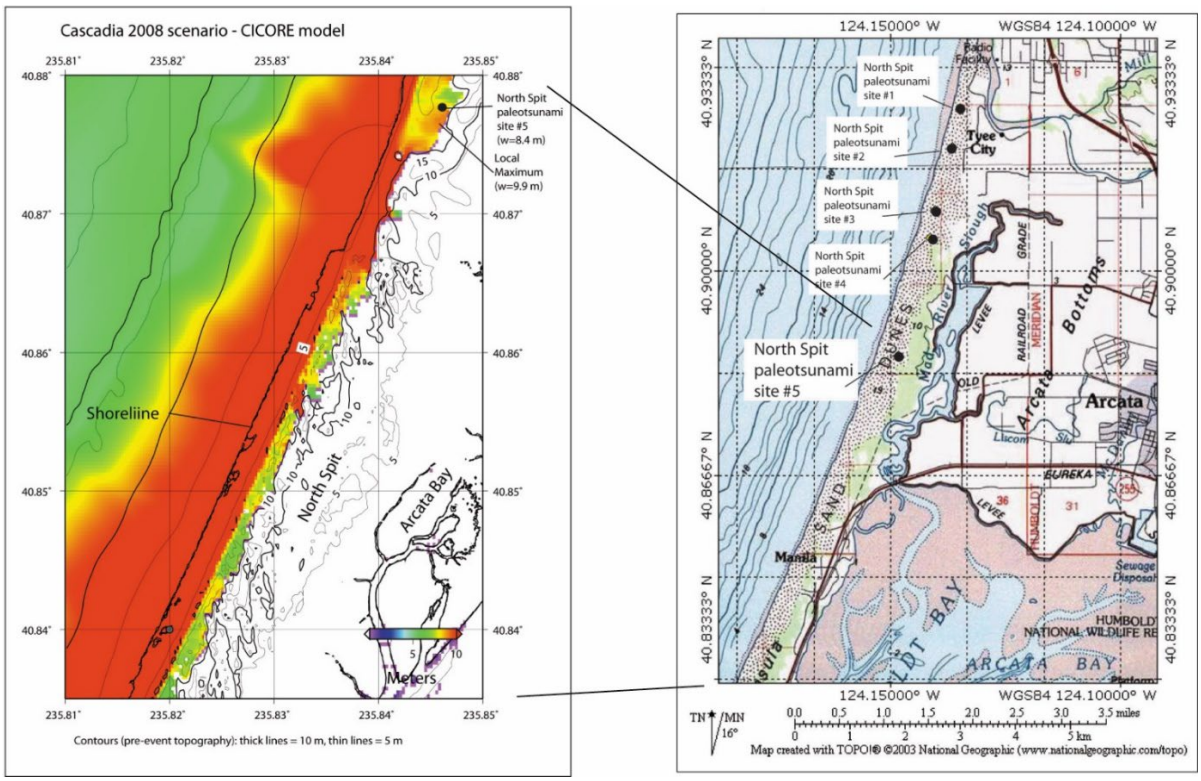

Figure 1-27. Paleotsunami sites on the North Spit and calculated maximum tsunami inundation (colored area) at the North Spit for the Cascadia 1700 C.E. scenario. Gravel lag in the dunes is interpreted to be a paleotsunami deposit (Leroy, 2006). The calculated uplift of the coast at paleotsunami site #5 is about zero after the event.

1.6 2020 Assessment of Projected Shoreline Elevations at Buhne Hill from Sea Level Rise and Tectonic Events to the Year 2120

In 2020, PG&E updated the estimated relative sea-level change at the ISFSI site on Buhne Hill, with the analysis conducted by LCI (2020). The basic tectonic framework that had been developed for the site in previous studies remained, but it was improved using the findings from additional investigations in the Humboldt Bay area (Figure 1-28). The rate of relative sea level rise in Humboldt County was found to be generally higher than the rate previously estimated by PG&E (2005). The new analysis used sea-level rise estimates based on a high greenhouse-gas-emission forecast by the IPCC (2019) that increases the rate of sea level rise due to greater and faster melting of the Greenland and West Antarctic ice sheets compared to earlier estimates by the IPCC (2001).

Recent vertical land-level data for the Humboldt Bay region (Patton et al., 2017) indicate that Humboldt Bay is experiencing interseismic subsidence (Figure 1-29) rather than the interseismic uplift assumed by PG&E (2008). The geodetic data show a modern subsidence rate for Humboldt Bay of approximately 2 mm/yr (0.08 in/yr). Projection of this rate to the year 2120 provides a maximum decrease in elevation of the ISFSI from 13.4 m (44 ft.) to 12.04 ± 0.37 m (39.5 ± 1.2 ft.) in the 100 years between 2020 and 2120 assuming a sea level rise of 1.0 to 1.7 m (3.2 to 5.7 ft.) during the same time period.

If a large earthquake were to occur on the CSZ or LSF, abrupt, coseismic uplift of the ISFSI would counteract the accumulated subsidence and result in an increase in the elevation of Buhne Hill, possibly to an elevation above its current position. However, the interseismic subsidence would require coseismic uplift during earthquakes on the CSZ and/or LSF in order to produce the observed geologic long-term rate of uplift at Buhne Hill and the marine terrace data east of Humboldt Bay (Figure 1-16) (PG&E, 2003, 2005). The forecasted scenarios to the year 2120 are illustrated on Figures 1-30 and 1-31.

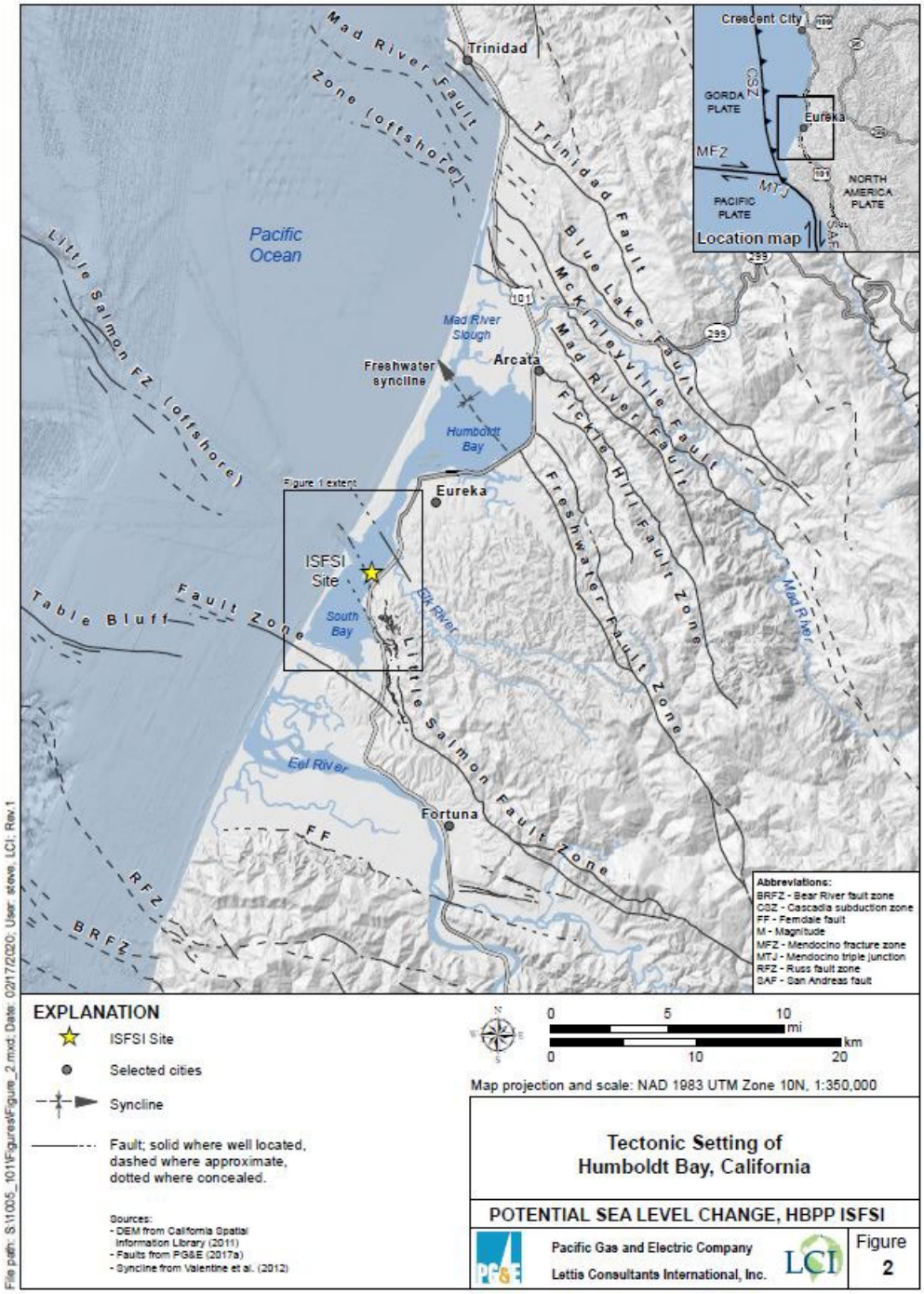

Figure 1-28. Faults in the Humboldt Bay area (from LCI, 2020; their Figure 2)

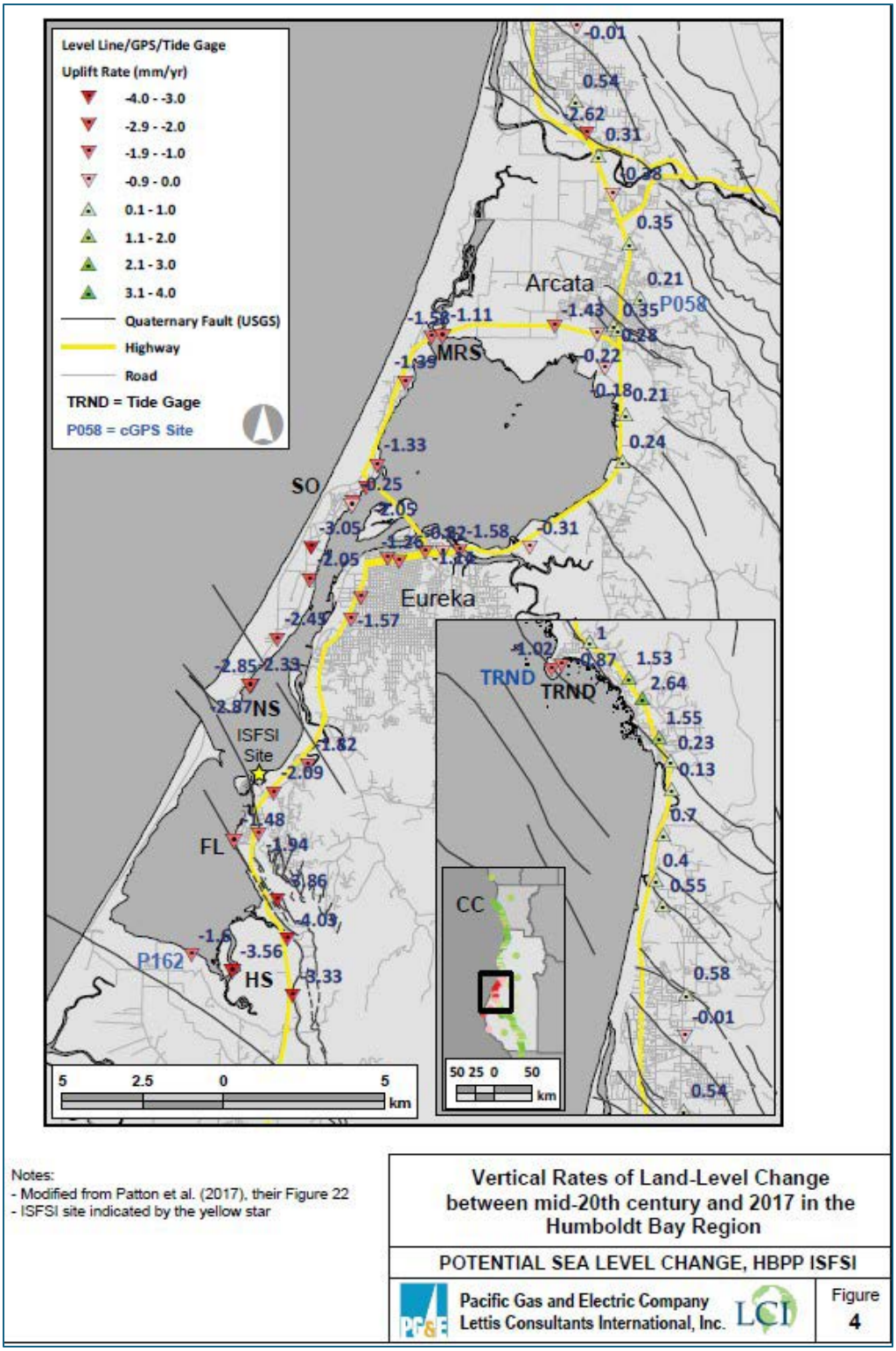

Figure 1-29. Vertical rates of land-level change between ~1950 and 2017 in the Humboldt Bay Region (from LCI, 2020; their Figure 4).

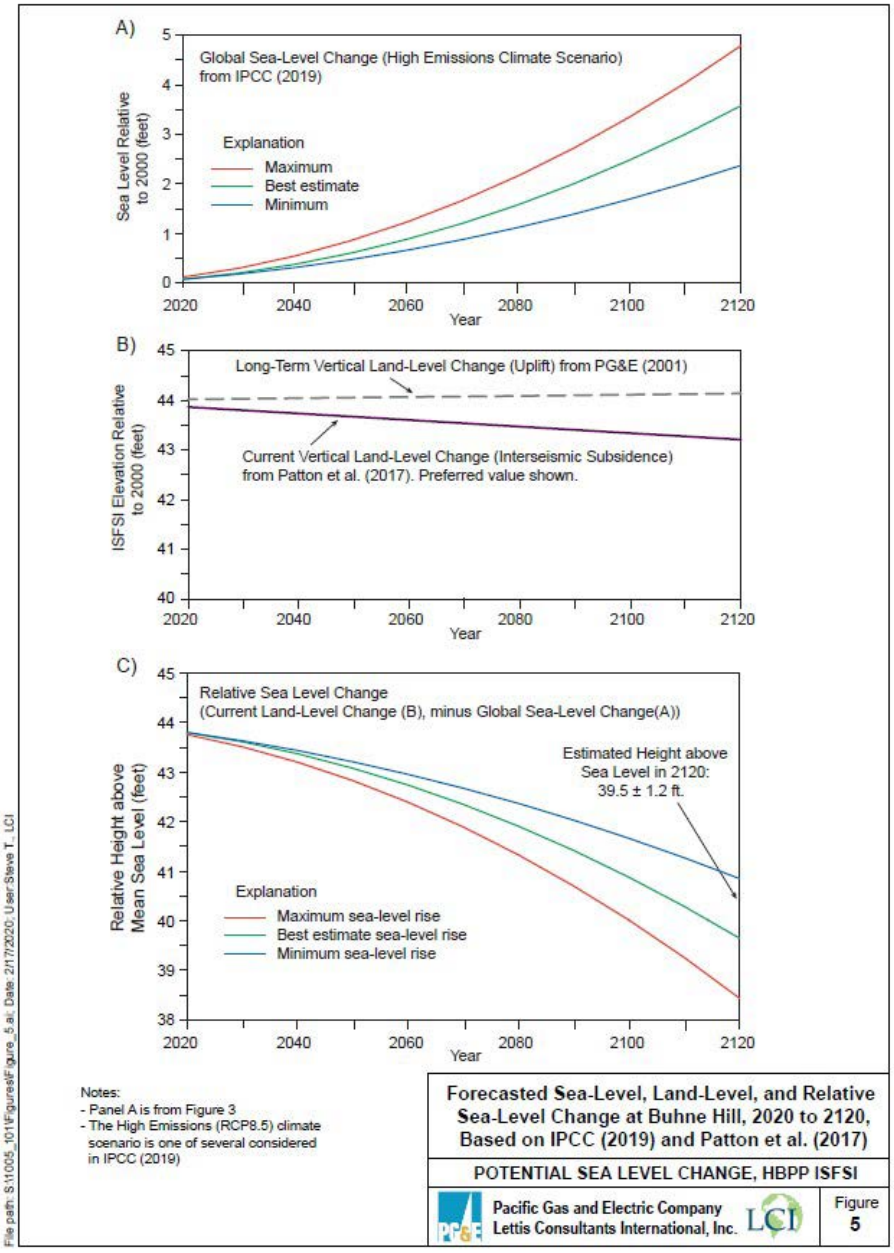

Figure 1-30. Forecast of sea level at Buhne Hill to the year 2120 combining projected sea level rise and subsidence rates in Humboldt Bay (from LCI, 2020; their Figure 5).

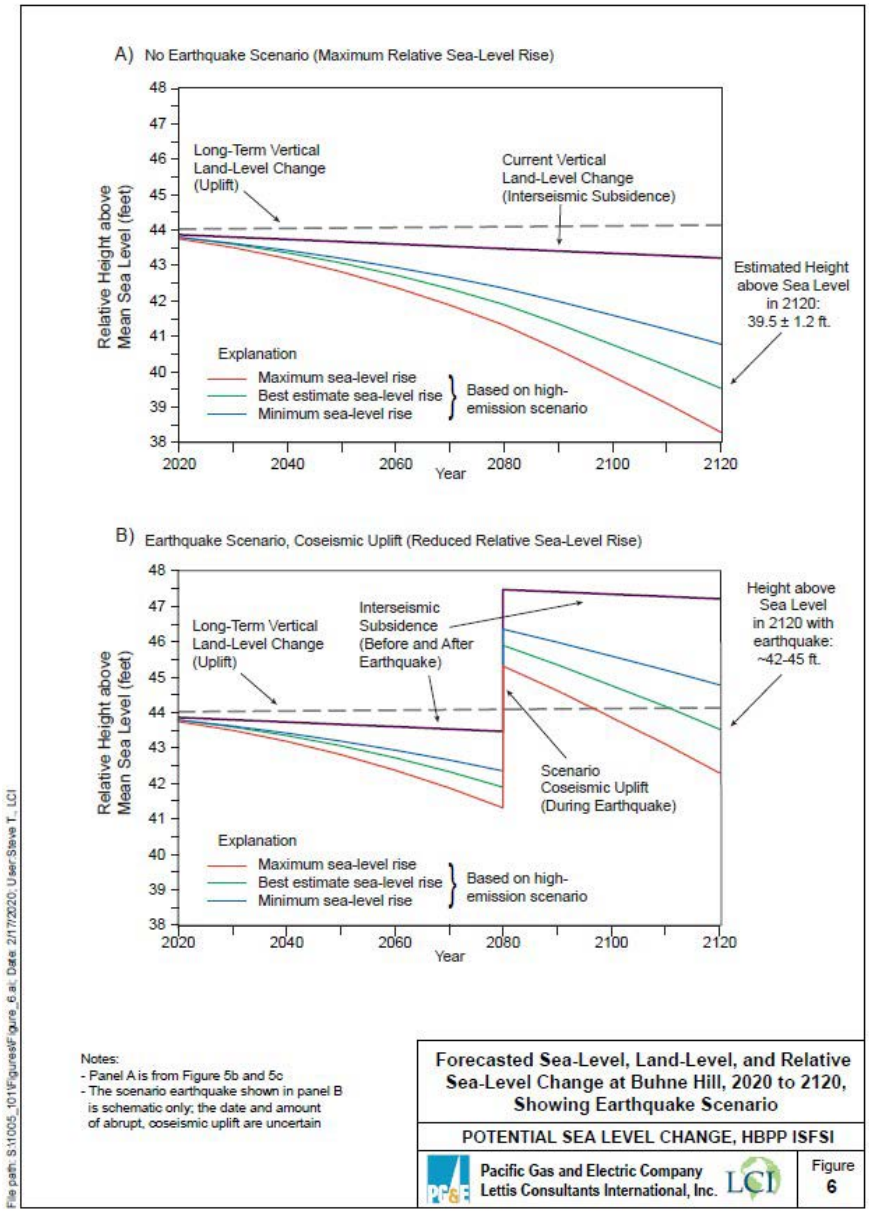

Figure 1-31. Forecast of sea level at Buhne Hill to the year 2120 combining projected sea level rise and tectonic subsidence rates in Humboldt Bay with a Cascadia and /or Little Salmon fault event uplifting Buhne Hill (from LCI, 2020; their Figure 6).

1.7 Summary of Tsunami Runup and Sea Level Rise Estimates Through 2008

Table 1-2 summarizes the various estimates of tsunami runups at the ISFSI at Buhne Hill. The original references are either relative to MLLW or MSL. These have been calculated to NAVD88 and also shown as MHW for easy comparison. The runups are also related to the 44-foot elevation of the ISFSI to show how high the facility is expected to be above each of the estimated runup levels.

Table 1-2. Runup Estimates at Buhne Hill and Distance Below Top of the ISFSI

Source	Runup Estimate at Buhne Hill	Vertical Distance Below ISFSI at 44 ft NAVD88 Elevation to Maximum Runup Level
Wiegel (1965) Calculated 10% in 1,000 yr: + 25.5 ft MLLW. 25.03 ft NAVD88 ; adjusted for MHW 30.75 ft	30.75 MHW	44 -30.75 = **13.25 ft**
PG&E (1985) Calculated using Houston & Garcia (1980) procedure 100 yr <10.6 ft MLLW, 10.13 ft NAVD88; adjusted for MHW 15.85 ft 500 yr <20.7 ft MLLW, 20.23 ft NAVD88; adjusted for MHW 25.95 ft	<15.85 MHW <25.95 ft MHW	44-15.85= 28.15 ft 44-25.95 = **18.05 ft**
PG&E (1985) Calculated using Brandsma et al. (1979) procedure for entrance to HB at 16.1 ft; 15.63 ft NAVD88; adjusted for MHW 21.35 ft	<21.351 ft MLLW	44-<21.35 = **<22.65 ft**
PG&E (2003) Empirical estimate from worldwide data at entrance to Humboldt Bay (Plafker, 2002b): M 8.8 Cascadia event <35 ft MLLW 34.53 ft NAVD88; adjusted for MHW 40.25 ft M 8.5 to 9.2 event <30 to 40 ft MLLW 39.53 NAVD88; adjusted for MHW 45.25	<40.25 ft MHW <45.25 ft MHW	44 MSL-<40.25 =**<3.75 ft** 44-<45.25 = **<-1.25 ft**
Observation at HBPP Intake for 1964 event was 9.6 ft" in note from G. E. Altman, PG&E: Time, 1:30 PM, 28 March 1964 12.85 NAVD88; adjusted for MHW 18.57	18.57 MHW 12.1 MHW	44-9.6 = **34.4 ft** **44 – 12.1 = 31.9**
Whitmore (1993) Modeled Cascadia M8.8 offshore of 8.7 ft MLLW. Onshore with 32% reduction = 5.9 ft. 5.43 NAVD88; adjusted for MHW 11.15	11.15 ft MHW	44-11.15 = **32.85 ft**
Bernard et al. (1994) Model and 30% judgment for input wave amplitude 33ft offshore = 10 ft 9.53 NAVD88; adjusted for MHW15.25	15.25 ft MHW	44-6 = **28.75 ft**
Lamberson et al. (1998) Wave arbitrary amplitude (6 m))19.7ft offshore at 63% onshore = 12.4 ft onshore 11.93 NAVD88; adjusted for MHW 17.65	17.65 MHW	44-17.65 = **26.35 ft**
Myers et al. (1999) Results of finite-element model for tsunami wave propagation with 30 ft offshore 29.53 NAVD88; adjusted for MHW 36.25	36.25 ft MHW	44-<19 = >**8.75 ft**
Carver et al. (1998) in PG&E (2003) Runup at the mouth of Humboldt Bay from paleotsunami from the 1700 Cascadia tsunami: 30 to 40 feet MLLW. Attenuated by 0.7= 21.5 to 27 ft. 21.03 to 26.53 ft NAVD88; adjusted for MHW 26.75 to 32.25 ft. Attenuated by 0.9=28 to 36 ft; 27.53 to 35.53 NAVD88; adjusted for MHW 33.25 to 41.25 ft	@0.7 26.75 MHW 32.25 ft MHW @0.9 33.25 ft MHW 41.25 MHW	44-26.25=**17.25** 44-32.25 = **10.75 ft** 44-36 = **10.75 ft** 44-41.25**=2.75**

Source	Runup Estimate at Buhne Hill	Vertical Distance Below ISFSI at 44 ft NAVD88 Elevation to Maximum Runup Level
1700 CE Cascadia model includes 4.1 meters uplift w/o Little Salmon faulting. Model predicts 5.2 m (14.8 ft) MSL offshore of North Spit and 4.5 m (14.8 ft) MSL onshore at N end of Buhne Hill. NAVD88 18.05 NAVD88; adjusted for MHW 23.77	23.77ft MHW	44-23.7 = **20.23 ft**
Cascadia-Little Salmon fault models Cascadia + Little Salmon model elevation change from sea level rise and tectonics at Buhne Point +1.9 m (6.2 ft.) included in model results. Wave height at north end of Buhne Hill is 7.5 m MSL (24.6 ft). 27.85 NAVD88; adjusted for MHW 33.57	33.57 MHW	44-16 = **10.43 ft**
Hypothetical Alaska M_w 9.1 Wave heights are 2.3 m (7.5 ft) at Buhne Hill MSL 10.75 NAVD88, adjusted for MHW 16.47	16.47 MHW	16.47 ft = **27.53 ft**
Hypothetical offshore landslide in Eel River canyon #3. Wave heights are 0.6 ft MSL 3.85 NAVD88, adjusted for MHW 9.57 ft	9.57 MHW ft	44-9.57 = 34.43 ft

NOTES:
1) See Figure 1- 5 for relative tides and reference datum (NAVD88)
2) The 2008 Model results are based on uplift of Buhne Hill in the Cascadia scenarios to approximate the data at that time.

Figure 1-13 is a simplified cross-section across Humboldt Bay, from the Pacific Ocean to Buhne Hill, that summarizes the various estimates of tsunami runup (and inundation) at Buhne Hill developed since the first tsunami assessment study in 1965. These estimates are based on various analytic models, expert opinions, and from studies of paleotsunami runups on the North Coast. Where appropriate, the results of a given study are presented as a vertical bar that captures the tidal range or the estimated runup values. The upper panel in Figure 1-13 shows the location of the cross-section presented in the lower panel.

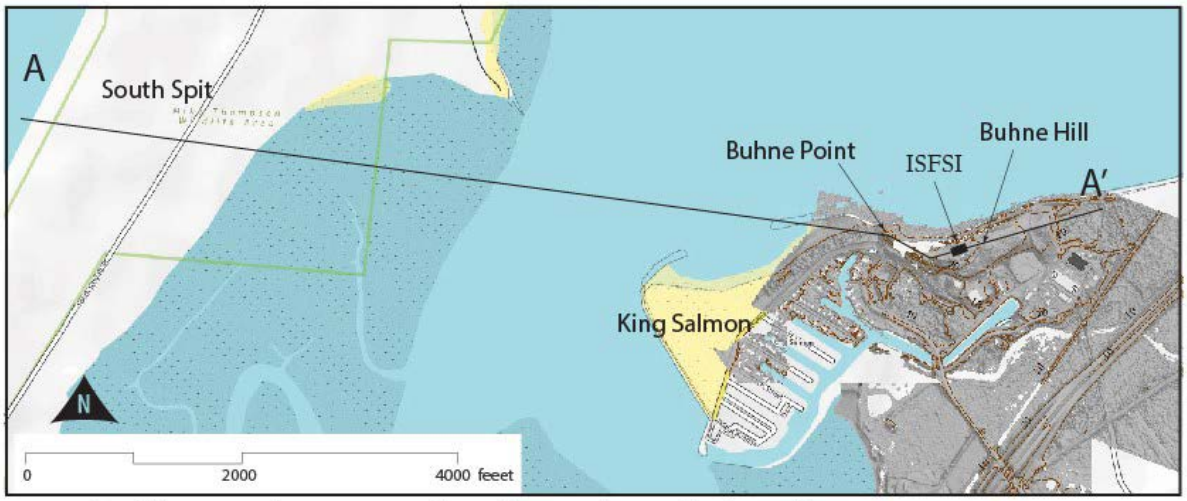

Map of Profile A A' South Spit across Buhne Hill to Marsh East of Buhne Hill

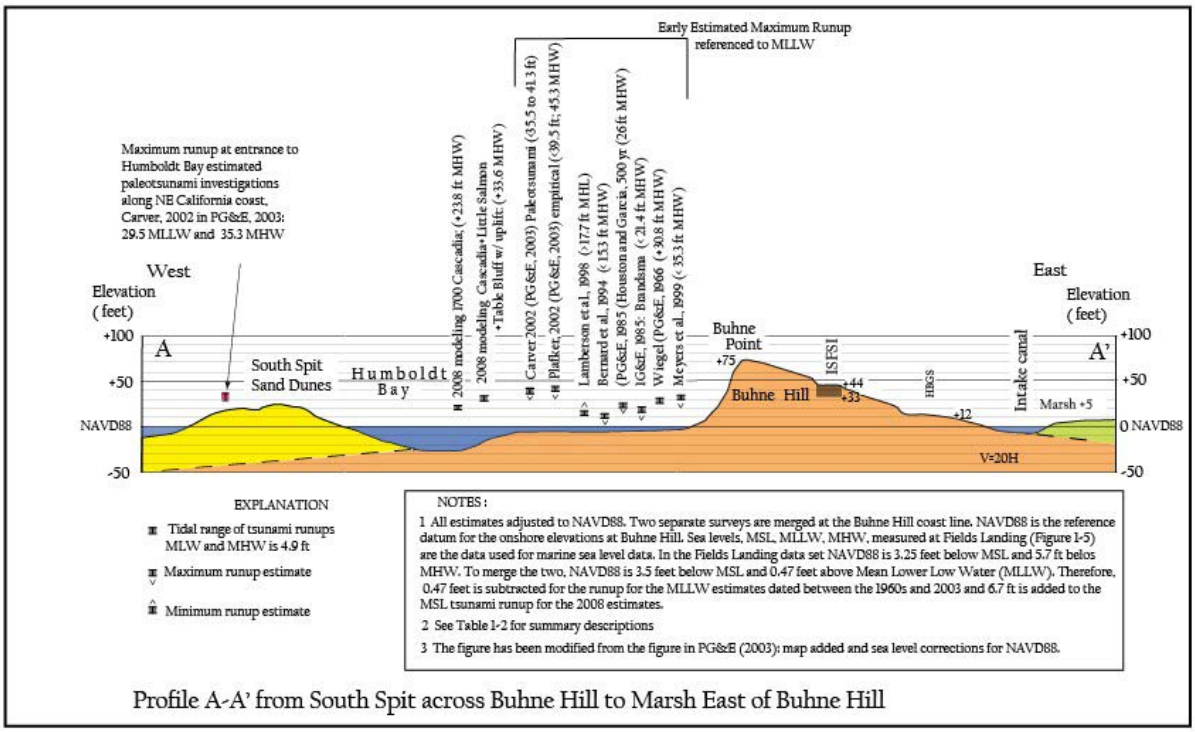

Profile A-A' from South Spit across Buhne Hill to Marsh East of Buhne Hill

Figure 1-13. Schematic cross-section across Humboldt Bay to Buhne Hill showing the previously estimated runups through 2008 at the ISFSI and Buhne Hill

2.0 2024 UPDATE

Out of its entire service territory, the PG&E electric and gas systems located in the greater Humboldt Bay area have the highest tsunami risk. As a result, over the years, PG&E has performed several tsunami studies centered on its facilities located along the east margin of Humboldt Bay, as described in the previous chapter. Given that substantial new information and modeling pertinent to the Cascadia subduction zone (CSZ) and the tsunami hazard in the region have been developed by the seismic community, PG&E conducted this tsunami hazard update for the Humboldt Bay ISFSI. This update includes new information on the following items:

- Bathymetry and geophysical data along offshore southern Cascadia
- Updated characterization of the Cascadia seismic (and tsunami) sources
- Vertical land motion (subsidence and/or uplift)
- Sea-level rise
- Recent local geologic and seismic investigations
- Humboldt Bay tsunami modeling studies

Dr. Mark Hemphill-Haley, retired professor from CalPoly Humboldt, compiled available data on the CSZ and Little Salmon fault for the current update. Dr. Hong Kie Thio, Analyst at AECOM, updated the probabilistic tsunami model they prepared for the State, emphasizing tsunami runups and currents at Buhne Hill and the ISFSI. The information presented in the sections below is summarized from the individual reports prepared by these researchers, which are included herein as appendices. The information is divided into sections in accordance with the order of the individual reports, as follows:

Section 2.1 New Bathymetry and Geophysical Data Along Southern Cascadia
Section 2.2 Segmentation, Recurrence and Wedge Fault Structural Models
Section 2.3 Vertical Land Motions
Section 2.4 Tsunami Hazard Modeling Updates
Section 2.5 Humboldt Bay Tsunami Studies
Section 2.6 Recent Investigations Related to the Geology at Humboldt Hill

2.1 New Bathymetry and Geophysical Data Along Southern Cascadia

The tsunami hazard modeling referenced by Page and Nishenko (2015) in the 2015 update used the most up-to-date bathymetric information available at that time. As stated in the report, Page and Nishenko (2015) combined several data sets to construct the topography and bathymetry of the study area. Significant updates to some data sources are relevant and need to be considered in any updates to the tsunami hazard models for Humboldt Bay and Buhne Hill.

2.1.1 Nearshore And Within Humboldt Bay Bathymetry, Including On-Land Topography

This 2024 update relies on National Oceanic and Atmospheric Administration (NOAA) topobathy (topography and bathymetry) lidar data collected in 2019 that has been processed to generate a 0.3-m (1-ft.) digital elevation model (DEM[1]) with a point density of 35.44 points per

[1] A Digital Elevation Model (DEM) is a representation of the bare ground (bare earth) topographic surface of the Earth excluding trees, buildings, and any other surface objects.

square meter (pts/m2). The lidar data are available at https://portal.opentopography.org/noaa Dataset?noaaID=9026. However, this topobathy lidar does not include deep channels within Humboldt Bay (Figure 2-1).

Prior to the 2019 lidar dataset, the California Coastal Conservancy (jointly with other agencies) provided coverage of nearshore (500 m) topography along with bathymetry out to 4.8 km (3 miles) (Figure 2-2). This product included 2009-2011 data merged with 2013 data. The point density for these data sets is sparser (1.34 pts/m2) than the 2019 lidar data. These older data sets are available at https://portal.opentopography.org/noaaDataset?noaaID=2612.

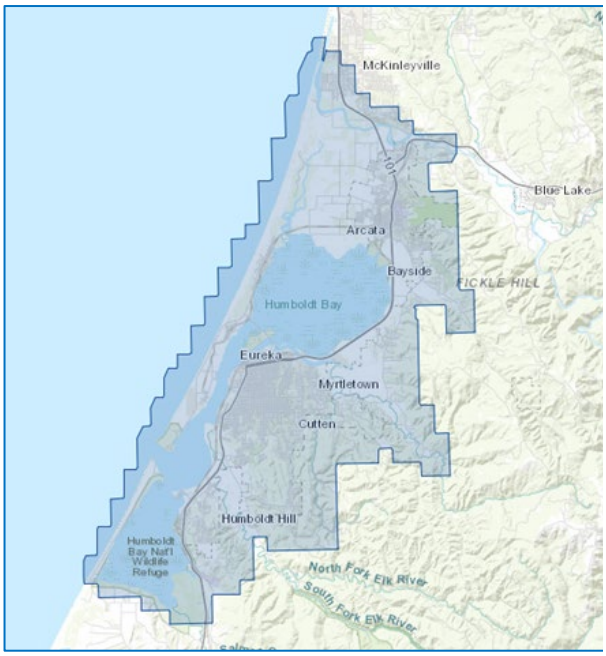

Figure 2-1. Coverage Map for 2019 NOAA Lidar

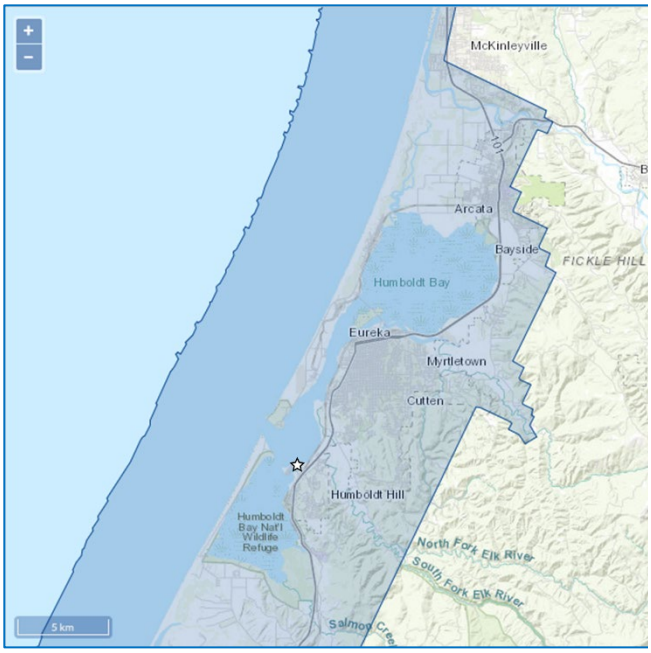

Figure 2-2. Coverage for 2009-2011 Topobathy Lidar from Approximately 10-m Elevation Onland to California 3-Mile State Water Boundary

2.1.2 Offshore Bathymetry

Hill et al. (2020) compiled data from all available sources to evaluate the offshore structure and geomorphology along the Cascadia margin, from Cape Mendocino to the Oregon border (Figure 2-3). The Hill et al. (2020) datasets resulted in nearly complete bathymetric coverage with 10- to 40-m (~33- to 130-ft) resolution and dense crossings of seismic reflection profiles throughout the region. The datasets are available at https://www.ngdc.noaa.gov and https://walrus.wr.usgs.gov/NAMSS/.

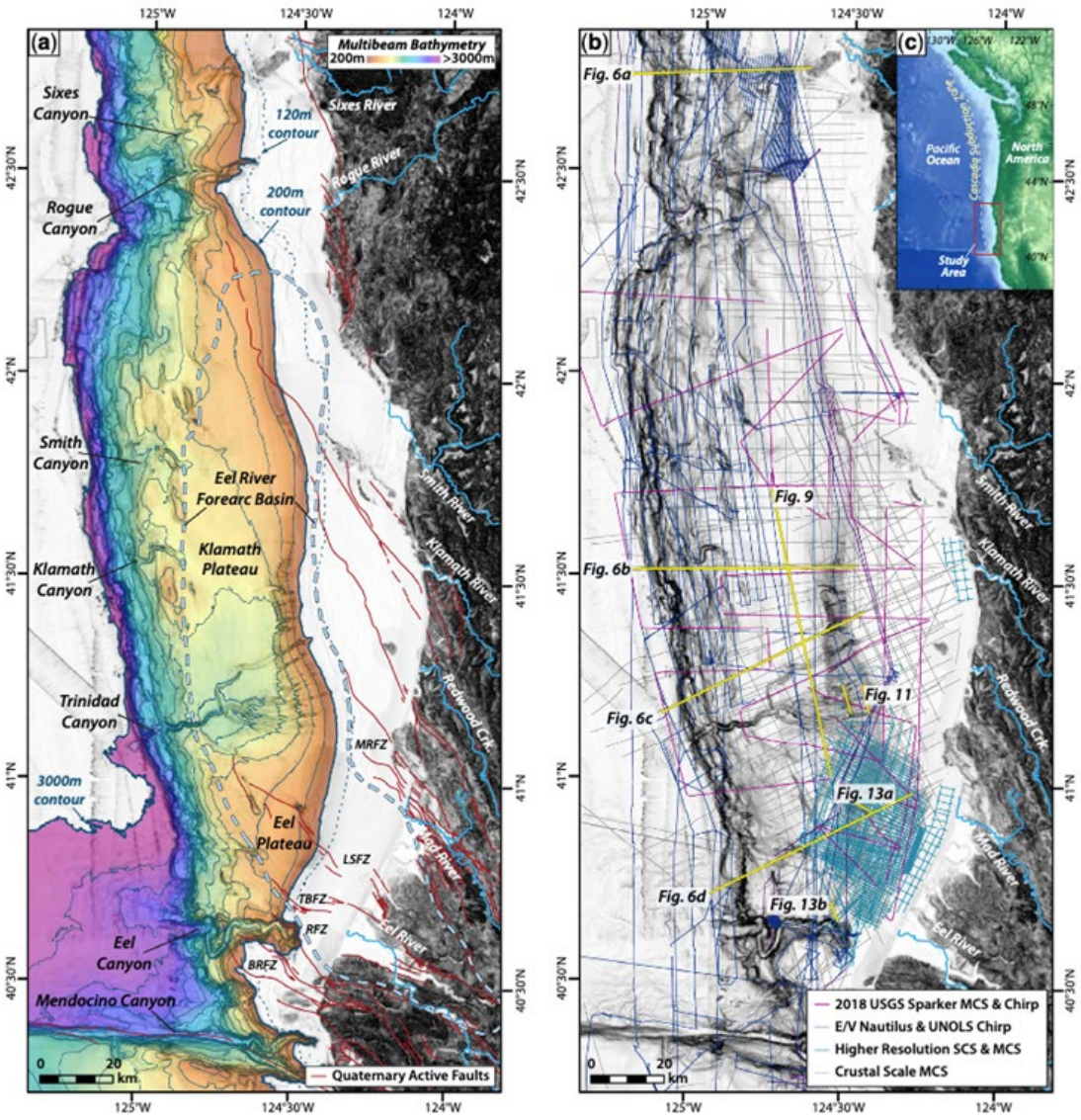

Figure 2-3. (a) Location Map Showing the Bathymetry, Major Rivers and Structural Features of the Southern Cascadia Region. The region is bounded to the north by Rogue and Sixes canyons, and to the south by the Mendocino Triple Junction (MTJ) (from Hill et al., 2020). The Eel River forearc basin (dashed blue outline) lies primarily offshore. Dark red lines are faults from the USGS Quaternary Fault and Fold Database (2020). Bathymetric contour spacing is 200 m; several key isobaths are noted, including the approximate sea-level lowstand shoreline (c. 120 m; dotted blue line), the shelf break at c. 200 m, and the c. 3000-m isobath that marks the base of slope along much of the region.
(b) Trackline Coverage of Seismic Datasets for Southern Cascadia. These include a range of high-resolution Sparker and Air Gun Multichannel Seismic (MCS) and Chirp sub-bottom profiles, as well as legacy and crustal-scale MCS from the 1970s to 1990s.

2.2 Updated Characterization of Cascadia Sources

Since Page and Nishenko (2015), significant new research has been published that better characterizes the CSZ. The following subsections summarize peer-reviewed publications and publicly available reports.

In addition to numerous individual studies, in 2023 the National Science Foundation awarded $15 million dollars to establish the nation's first subduction zone earthquake hazards research center, the Cascadia Region Earthquake Science Center (CRESCENT). CRESCENT has three overarching goals:

1. Develop a better foundational understanding of CSZ earthquakes and their associated hazards and to transfer this knowledge to other subduction zones
2. Promote diversity and train the next generation of geoscientists to address the challenges presented by our dynamic planet
3. Provide a systematic approach to collaboration between researchers in academia and those in agencies that have mandates to produce hazard information that stakeholders, practitioners, and the public at large can trust and use

Consistent with these goals, and No. 3 in particular, PG&E Geosciences staff and consultants have attended collaborative meetings and closely followed up with and contributed to the research originating from this new platform.

2.2.1 Segmentation and Magnitude

Most of the recent studies into segmentation of the CSZ have focused on offshore Oregon and Washington, with lesser attention paid to northern California. Here we summarize two recently proposed segmentation models, and mention the other post-2015 published research papers. Details are provided in Appendix C.

Wang and Tréhu (2016) suggest there are areas of adjacent low- and high-slip along the CSZ that may also coincide with Episodic Tremor and Slip (ETS) segments (Figure 2-4), as first proposed by Brudzinski and Allen (2007).

Watt and Brothers (2020) identify four distinct regions of the CSZ based on outer wedge width and steepness, along with patterns of structural vergence and wedge shape (Figure 2-5). These regions are: 1) Vancouver Island, 2) Washington, 3) north and central Oregon, and 4) southern Oregon and northern California. These authors posit that differences in the outer-wedge morphology are associated with along-strike megathrust segmentation, which are also defined by differences in oceanic asthenospheric velocities, episodic tremor and slip occurrences, plate locking models and seismicity around the boundaries. They also propose that variations in the morphotectonics of the CSZ may be related to differences in wedge strength, megathrust friction (possibly due to roughness of down-going slab), and slip behavior.

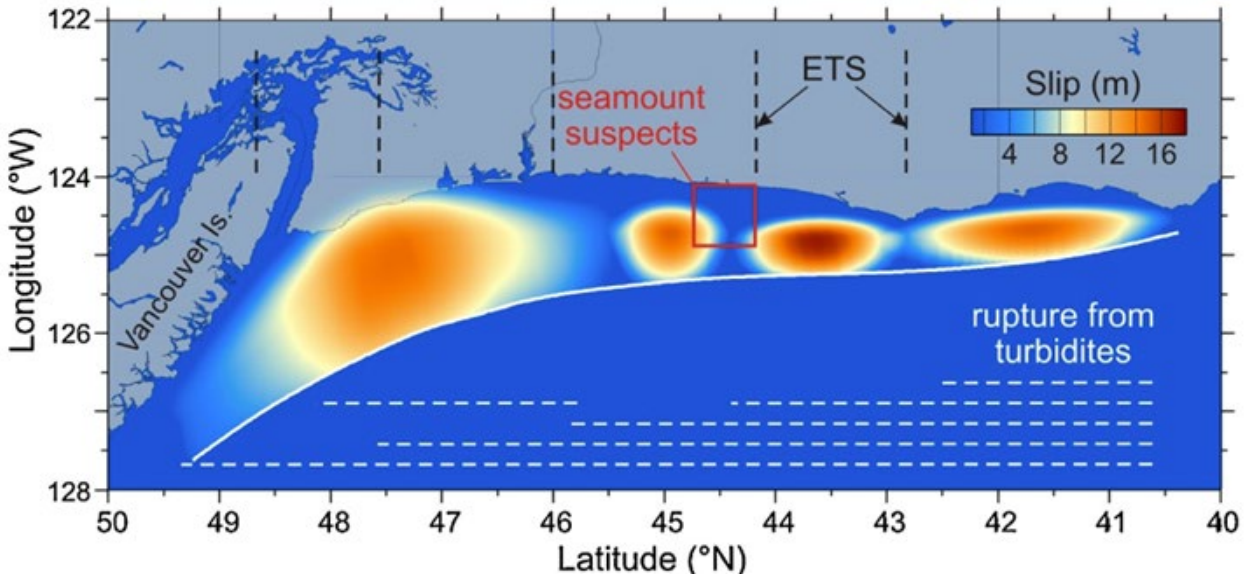

Figure 2-4. Proposed variations in megathrust slip behavior along the Cascadia margin (from Wang and Tréhu, 2016). The oval colors immediately east of the megathrust are proposed slip distributions associated with the 1700 C.E. earthquake. Black dashed lines are ETS boundaries (Brudzinski and Allen, 2007). White dashed lines suggest rupture extents based on turbidite occurrence (Goldfinger et al., 2012). Based on the turbidite evidence, Wang and Tréhu (2016) suggest subduction zone events are more frequent at the CSZ's southern end (southern Oregon and northern California).

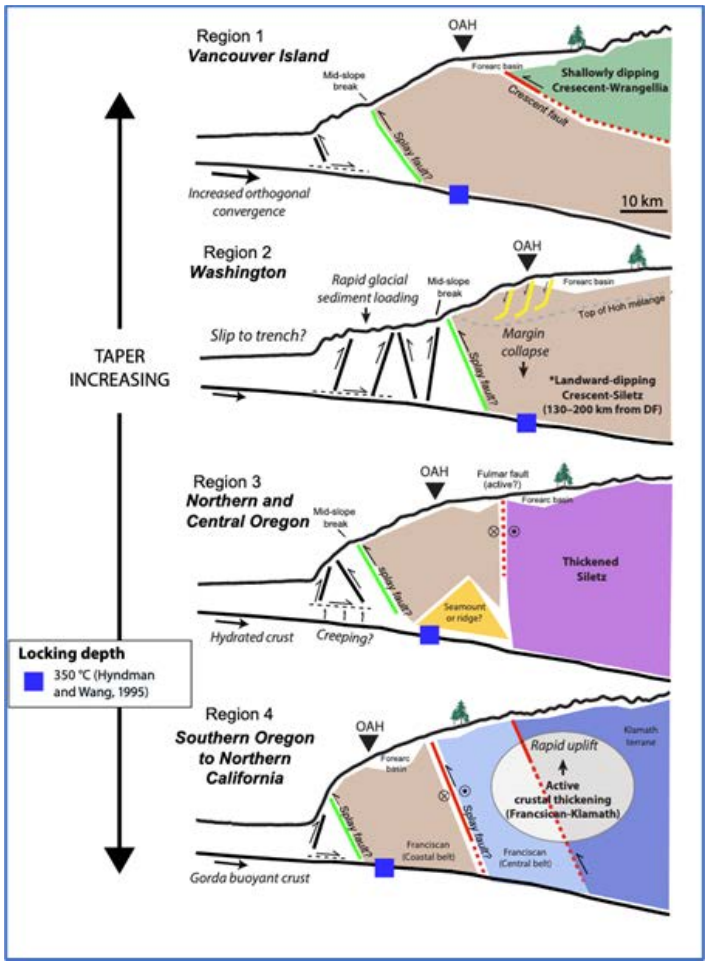

Figure 2-5. **Regional conceptual models illustrating the first-order along-strike variability in morphology and structure along Cascadia's marine forearc in relation to outer wedge taper and strength heterogeneities in the upper plate** (from Watt and Brothers, 2020). It appears that megathrust splay faults are commonly associated with backstop boundaries. Trees depict approximate position of the shoreline within each region. DF—deformation front. Note that outer wedge taper is lowest in region 2 and increases to the north and south. OAH—outer arc high. Note the steep outer wedge in region 4 (Gorda) and landward-vergent thrust near the megathrust tip.

Walton et al. (2021) provide evidence for differences in properties along strike within the subduction margin, both in the upper and lower plates, and prefer a model whereby the rupture during the 1700 C.E. event was not homogeneous but instead consisted of patches of high slip separated by low-slip portions of the megathrust, as proposed by Wang et al. (2013). They also discuss how the heterogenous nature of the subduction zone may influence rupture length and correspondingly, earthquake magnitude. They describe how persistent rupture barriers may be responsible for more frequent, smaller ruptures in southern Cascadia (i.e., **M** <9 earthquakes), south of Cape Blanco. Bilek and Lay (2018) also analyzed the heterogeneity of the subducting plate.

Carbotte et al. (2024) reviewed evidence gathered by offshore high-resolution bathymetry and geophysics along the subduction zone from the California/Oregon border, and found large variability in the oceanic plate that may result in heterogeneity in rupture along the subduction

zone. Bodmer et al. (2018) used teleseismic delay time data to image seismic velocities (tomography) of the entire CSZ. Their imaging shows that the high-velocity, dense subducting slab is underlain by discontinuous warm and buoyant mantle at between 100- and 300-km (62- and 186-mi) depth. Their data suggests that strong plate locking, caused by buoyant mantle, is occurring in northern and southern Cascadia and thus may be responsible for rupture segmentation of the subduction zone. Fan and Zhao (2021) reviewed the slip histories of six **M**~9 subduction zones and, using tomographic imaging, interpret that low-velocity anomalies beneath the subducting slab were locations of mainshock hypocenters. Although the hypocenter of the 1700 C.E. Cascadia earthquake is not known, they identify two large low-velocity zones (one located at southern Cascadia) that they suggest may be candidate locations. Harrichhausen et al. (2024) conducted numerical modeling to evaluate coupling between the subduction zone and crustal faults in northern Cascadia and conclude that at that location, the upper-plate faults are not being driven much by the subducting plate.

McKenzie et al. (2022) used GPS data along the length of Cascadia to better understand the role of upper plate rheology and its connection to locking depth of the subduction zone. They assume that the locked portion of the subduction zone has remained in its current position over the last hundreds to thousands of years, and compare magnitude estimates from their model to paleoseismic estimates. In southern Cascadia, to ~43°N latitude, they posit that a **M** 8.3-8.4 event with a recurrence interval of 300 years is permissible (consistent with paleoseismic estimates of 220 to 400 years) and estimates of **M** 8.2-8.4 events.

Episodic tremor and slip (ETS) and role in segmentation models was first identified and described by Dragert et al. (2001) and by Rogers and Dragert (2003) along the northern Cascadia margin. Others have also investigated the issue and the results to date indicate that the relation between the top of the ETS zone and the base of the seismogenic zone, as well as any causal relation between ETS activity and megathrust events, is poorly understood.

2.2.2 Wedge and Fault Tip Morphology

New tsunami modeling now includes the structure and geometry of the megathrust deformation zone near the trench-ward tip of the accretionary wedge (Figure 2-6). This geometry points out the potential role of steeply dipping coseismic faults with significant displacements in greatly increasing tsunami wave heights. Additionally, it may be that larger vertical displacements near the wedge tip produce similar or larger tsunami amplitudes during smaller (**M** 7-8) events than **M** 8-9 events associated with near-horizontal slip at the base of the wedge.

Ledeczi et al. (2024) conducted high-resolution, near-surface seismic reflection analysis of about 400 km (~250 mi) of Cascadia offshore of Washington and Oregon (Figure 2-7). They found numerous landward- and seaward-vergent faults with scarps and folds displaying tens of meters of relief in late Quaternary sediments and surfaces. Although they did not conduct this analysis at the southern portion of Cascadia, similarities in accretionary wedge morphology imaged near Humboldt Bay (Figure 2-2), including an active oceanward, steep deformation front and presence of scarps in late Quaternary sediments, suggest similar behavior might be expected.

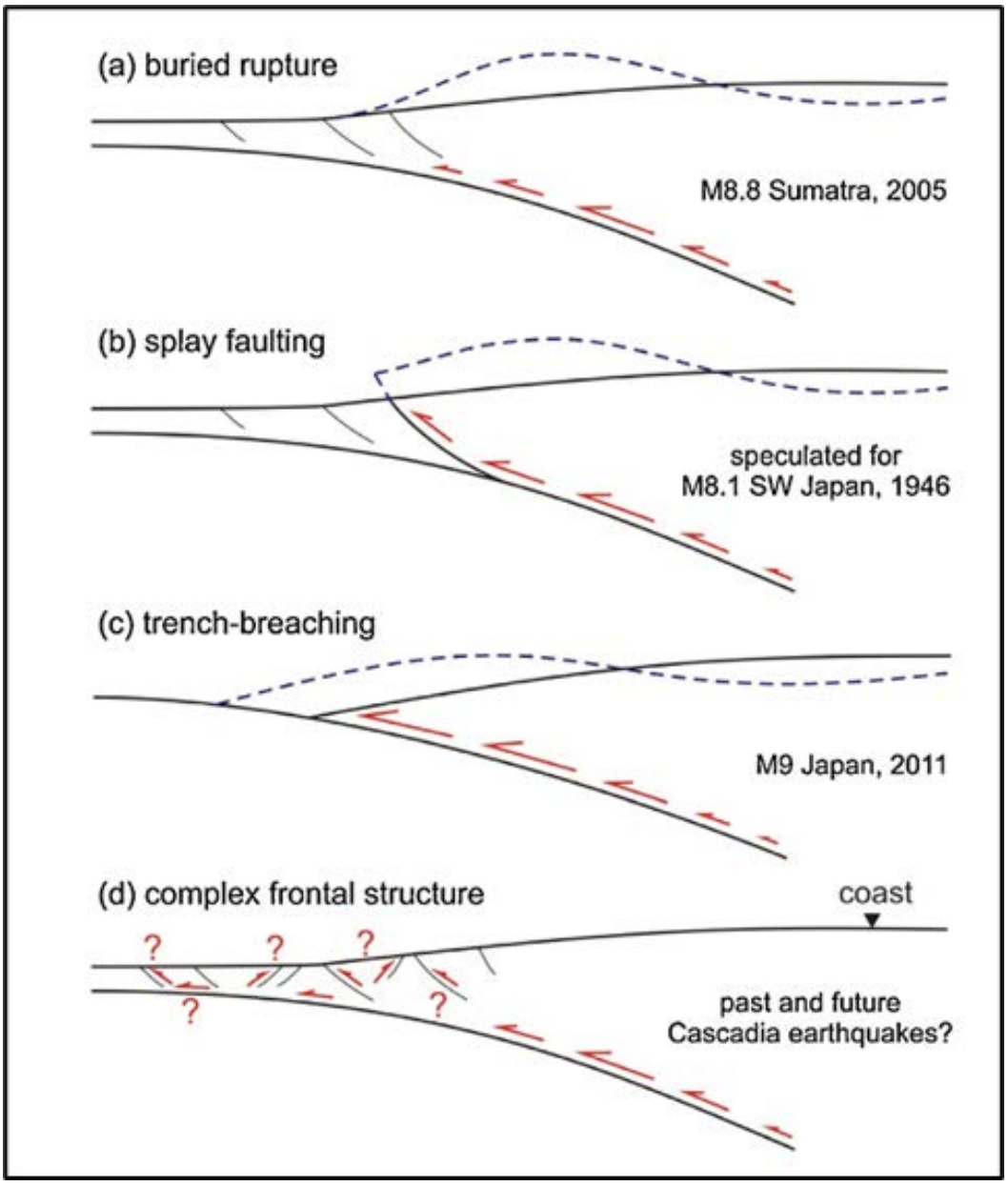

Figure 2-6. Potential accretionary wedge deformation scenarios associated with subduction zone megathrust rupture
(from Wang and Trehu, 2016, their figure 5).

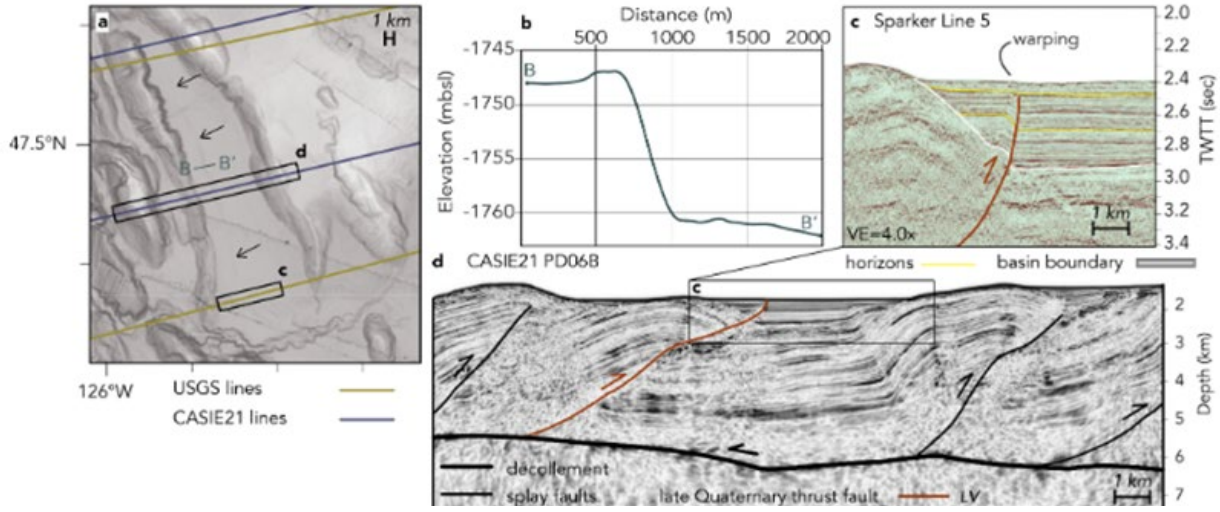

Figure 2-7. Seismic reflection profile of a landward-vergent thrust in offshore northern Washington (from Ledeczi et al. 2024, their Figure 3). (a) map view of fault area with arrows pointing to fault scarp; (b) bathymetric profile of the fault scarp indicating about 13 m (~43 ft.) of relief on the seafloor; (c) sparker profile showing the faulted and folded older sediments and warping of late Quaternary cover sediments; and (d) projection of the fault onto the larger deformation front and connection to the décollement.

2.2.3 Recurrence

Recent proposed segmentation models of Cascadia are based on geophysical and geological along-strike similarities and differences, ETS occurrence, megathrust event recurrence based on ages and distributions of tsunami and turbidite deposits, and on land evidence of subsidence and tsunami inundation (Figure 2-8).

In their summary of knowledge of the Cascadia subduction zone, Walton et al. (2021) state that "*Despite outstanding geologic records of past megathrust events, large uncertainty of the magnitude and frequency of CSZ earthquakes remains.*" Most paleoseismologists agree that the most recent event at Cascadia occurred on 1700 C.E., and that it was a full-margin rupture that created a M 8.7 to 9.2 earthquake (e.g., Atwater et al., 2005; Nelson et al., 2020; Walton et al., 2021).

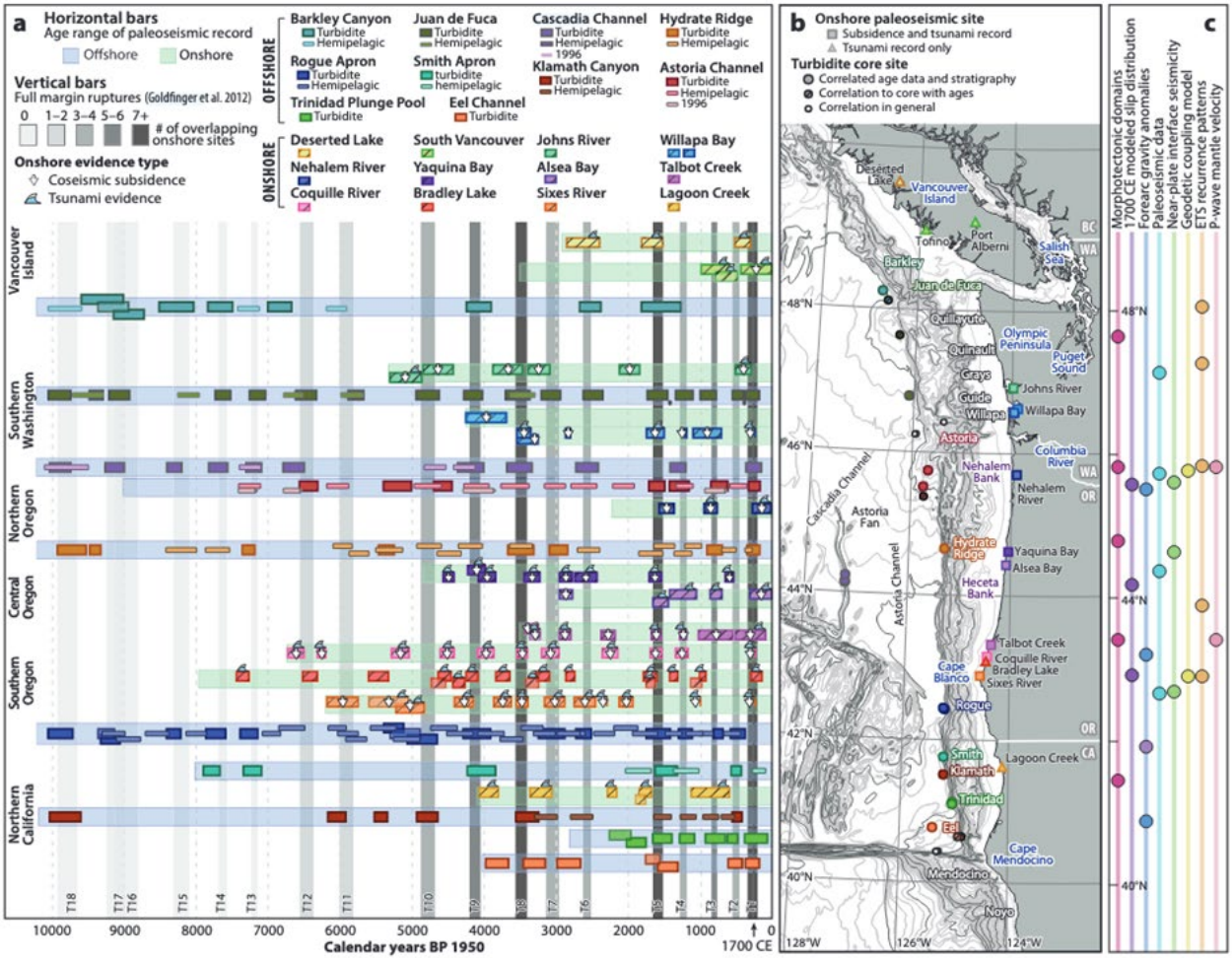

Figure 2-8. Onshore and offshore evidence for earthquakes and tsunamis along Cascadia (from Walton et al., 2021, their figure 4).

However, other researchers have shown that ruptures on individual segments of the CSZ are possible. Melgar (2021) suggests a tsunami of the size recorded in Japan could have been generated by a 400-km (250-mi) long (**M** 8.7) southern Cascadia rupture. He states that this hypothesis is not in conflict with the subsidence and dating information available provided that at least four **M** <8.7 earthquakes occurring years to decades after the 1700 C.E. event satisfy the subsidence story to the north. He also states that these events would likely not produce a tsunami large enough to be part of Japan's written record.

Salaree et al. (2021) conducted an analysis of physics-based **M** 7.5- to 9.2-related deformation of the subduction zone between central Oregon and southern Washington to evaluate the tsunami hazard relative to shoreline characteristics, bathymetry and rupture characteristics. They conclude that the largest and most widespread tsunami amplitudes result from ruptures at or starting near mid-latitude portions of the CSZ and that, based on the choice of slip model, a **M** >8.5 event can produce tsunami amplitudes exceeding 50% of those from a **M** 9.2 rupture. Based on these results, these researchers surmise that **M** 8.5 earthquakes have a higher probability of occurrence (shorter recurrence interval) and hence may pose a more significant hazard than a larger event.

On-land-supported recurrence estimates for CSZ events in Washington and northernmost Oregon are based on ten widely correlated buried soils, often accompanied by overlying tsunami deposits, that yield an average recurrence interval of 500-540 years for the last 5000 years (Atwater and Hemphill-Haley, 1997; Nelson et al., 2006; Walton et al., 2021). In southern Oregon and northern California, a record of 12 potential earthquakes and tsunamis provide an average recurrence interval of ~390 years (Witter et al., 2003; Priest et al., 2014, 2017; Graehl et al., 2015; Milker et al., 2016; Walton et al., 2021; Padgett et al., 2021, 2022). Margin-wide rupture recurrence intervals of 500-530 years are estimated from offshore turbidite records (Goldfinger et al., 2012), however there are concerns about these estimates (see below).

Offshore records of turbidite production proposed by Goldfinger et al. (2012, 2013) provide a much more extensive record of earthquake history than the onshore record. However, questions as to the potential for storm-generated turbidites and overinterpretation of some correlations (Atwater et al., 2014; Goldfinger et al., 2016; Lindh, 2016; Walton et al., 2021) have left some doubt as to the error associated with this proposed longer record offshore.

Padgett (2021, 2022) estimated the ages of coseismic subsidence events in northern Humboldt Bay (Table 2-1). They conclude that the magnitudes of subsidence are different for these events suggesting full- and partial margin ruptures may be recorded in the marsh stratigraphy. Additionally, they correlate these events to others as far north as Talbot Creek in southern Oregon, a distance of about 300 km (186 mi) that is compatible with smaller rupture events (Figure 2-9).

Table 2-1. Coseismic Subsidence Estimates Combined from Three Sites in Northern Humboldt Bay (from Padgett et al., 2021, 2022). The averages and ranges of ages are from Padgett et al. (2022), with the exception of the ca. 1620 cal yr B.P. event, which is from Padgett et al. (2021).

Age of Earthquake (youngest at top)	Estimate of Coseismic Subsidence
250 cal yr B.P. (1700 C.E.)	**Average**: 0.6 ± 0.1 m (2 ± 0.3 ft.) **Range**: 0.2 ± 0.3 to 1.0 ± 0.4 m (0.7 ± 1 to 3 ± 1.3 ft.)
ca. 875 cal yr B.P.	**Average**: 0.4 ± 0.2 m (1.3 ± 0.7 ft.) **Range**: 0.4 ± 0.4 to 0.5 ± 0.4 m (1.3 ± 1.3 to 1.6 ± 1.3 ft.)
ca. 1120 cal yr B.P.	**Average**: 0.7 ± 0.2 m (2.6 ± 0.7 ft.) **Range**: 0.5 ± 0.4 to 0.8 ± 0.5 m (1.6 ± 1.3 to 2.6 ± 1.6 ft.)
ca. 1620 cal yr B.P.	> 0.9m (> 3 ft.)

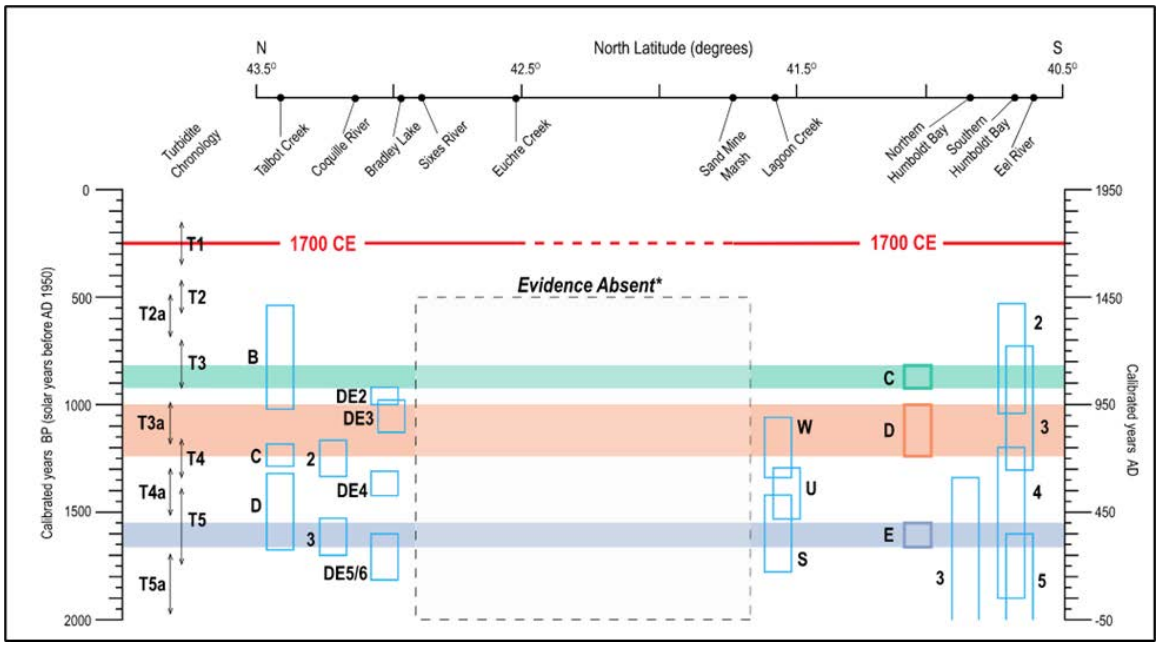

Figure 2-9. Comparison of interpreted coseismic subsidence events from Humboldt County North to Southern Oregon (from Padgett et al., 2021). The 1700 C.E. event, and events C, D and E at northern Humboldt Bay appear to correlate with events at other locations, strongly suggesting at least 300 km (186 mi) of contemporaneous rupture.

2.2.4 Offshore Landslides

Hill et al. (2020) conducted a bathymetric and seismic reflection analysis of the CSZ margin from Oregon to Cape Mendocino primarily to evaluate offshore landsliding (Figures 2-10, 2-11 and 2-12). They provide high resolution images of the accretionary wedge in the vicinity of the subducting Gorda plate and in the vicinity of Humboldt Bay. Landslides can produce tsunamis and have been used as indicators of strong shaking during large earthquakes (e.g., Goldfinger et al., 2012, 2013). The California section of the CSZ appears to have fewer slope failure features relative to areas to the north, however. Their interpretation of this part of the offshore margin is shown on Figures 2-10, 2-11 and 2-12.

Existing submarine landslides off the coast of Humboldt Bay are concentrated in steep walls of offshore river canyons (e.g., Eel River) and at the edge of the coastal platform (Figure 2-11). These failures include turbidite flows (evacuated scars and sediment accumulations) and cohesive slumps/slides. Turbidite flows do not appear to represent significant tsunami sources; instead, larger cohesive slumps/slides appear to be the primary tsunamigenic sources. The shelf edge occurs about 20 to 40 km (12.4 to 24.8 mi) offshore Humboldt Bay, and this distance is a reasonable approximation of the distance for modeled tsunami submarine landslide sources.

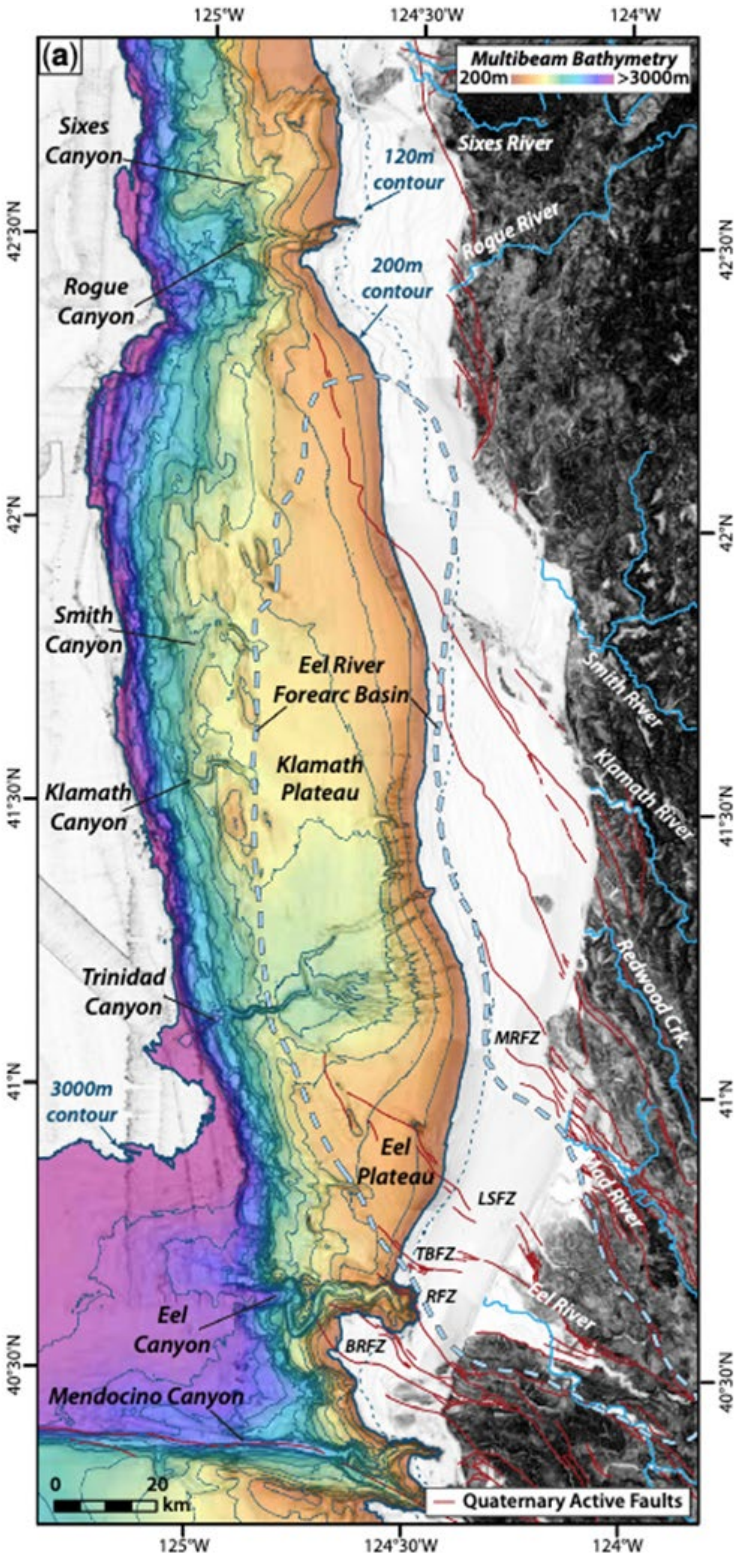

Figure 2-10. Bathymetry, major rivers and structural features of the southern Cascadia margin (from Hill et al. 2020). The steepest part of the accretionary prism is located near the base of the slope. Note the Eel and Trinidad canyons in the vicinity of Humboldt Bay. Also note the steep oceanward tip of the wedge.

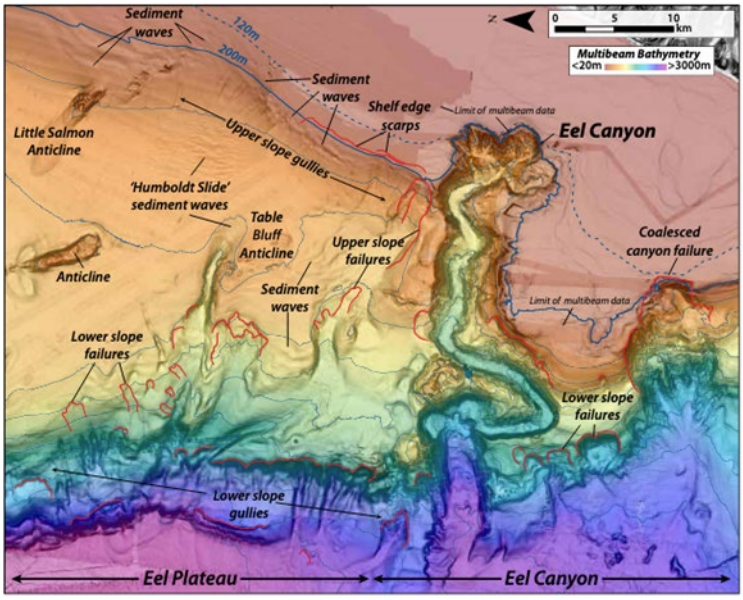

Figure 2-11. Bathymetry of the southernmost subduction margin at Eel Canyon. Noticeable are the presence of folds associated with the Little Salmon and Table Bluff faults. Also notable are significant submarine landslide features including sediment waves, coalesced canyon headwall failures and smaller individual failures, mainly located in the steeper outer part of the wedge (from Hill et al., 2020).

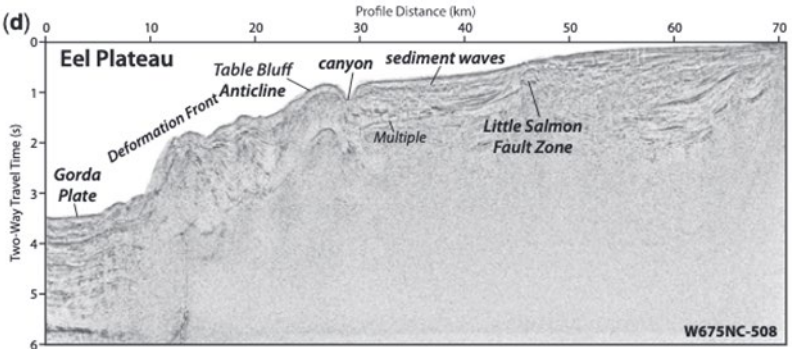

Figure 2-12. Sparker profile crossing the Little Salmon and Table Bluff faults. Profile also shows the steep deformation front characteristic of this portion of the subduction margin and the absence of a well-defined trench (from Hill et al., 2020).

2.3 Vertical Land Motion

Vertical land motion (VLM) encompasses both uplift (positive) and subsidence (negative) of a datum on land. Relative sea level (RSL) change is relative change between absolute changes in sea level and VLM. Changes in RSL can be quantified by accounting for VLM and absolute sea level changes at a site. Along an active tectonic margin, VLM can be influenced by both coseismic and interseismic land-level changes, with these occurring at different temporal and physical scales. In the vicinity of Humboldt Bay, coseismic land-level changes may accompany large-magnitude earthquakes, including those possible from rupture of the CSZ megathrust and/or other large local thrust or reverse faults within the accretionary prism. In subduction zone earthquakes, whether the vertical land movement is up, down, or neutral depends on the location

of the site relative to a flexure point in the overriding plate above the megathrust. In the most recent full-margin rupture of the CSZ, in 1700 C.E., all coastal sites evaluated between Northern California and Vancouver Island experienced coseismic subsidence; to date no evidence of coseismic uplift as a result of this event has been found.

Unlike the temporary inundation from climatic events such as coastal storms or floods, coseismically subsided areas abruptly drop from elevations unaffected by sea level to areas permanently inundated by tides. Strong evidence for past instances of abrupt coseismic subsidence at coastal sites is the stratigraphic juxtaposition of two dissimilar kinds of sedimentary deposits in sharp contact with one another: an organic-rich soil (peat) indicating a former marsh, meadow, or coastal woodland—a type of environment which would be infrequently or possibly never submerged by tides—abruptly overlain by thick deposits of mud indicative of a lower intertidal setting such as a tidal flat (as depicted on Figure 2-13). Examples of these mud-over-soil stratigraphic sequences have been documented along the full length of the CSZ, including in Humboldt Bay and the Eel River estuary.

Padgett et al. (2019, 2021, 2022) (Figures 2-14 and 2-15) describe sites in North Bay (Arcata Bay) that record four earthquake-driven subsidence events from CSZ earthquakes. The age of the four events with the estimated amounts of coseismic subsidence per event are summarized in Table 2-1. The combined results of the various paleoseismic studies for North Bay suggest that coseismic subsidence on the order of 0.5 to 1 m (1.6 to 3.3 ft.), or more, is possible in future CSZ earthquakes.

Witter et al. (2001, p. 44) compiled evidence for coseismic subsidence accompanying rupture of the Little Salmon fault (LSF) in South Bay and reported that the "*data suggest that submergence in the footwall of the Little Salmon fault occurs during upper-plate earthquakes*." Significantly, based on the results at their study sites near College of the Redwoods and Hookton Slough, these authors concluded that although subsidence accompanied rupture on the LSF, the LSF ruptures were in turn triggered by and coincident with ruptures in the CSZ megathrust. "*Evidence for subsidence of the [LSF] western fault scarp along with stratigraphic records of abrupt soil submergence suggests that coseismic subsidence of the Humboldt Bay region also accompanied upper-plate seismicity. We conclude that where evidence for slip on the Little Salmon fault and regional coseismic subsidence coincide, the evidence supports an interpretation of upper-plate faulting triggered by rupture on the southern Cascadia plate-interface*" (Witter et al., 2001, p. 41). Therefore, it is possible for Humboldt Bay coseismic subsidence to occasionally be associated with rupture on faults in the accretionary prism in addition to the deformation associated with rupture of the southern CSZ megathrust. The onshore faults in the upper plate of the CSZ are unique to the North Coast where the accretionary wedge of the subduction zone trends onshore.

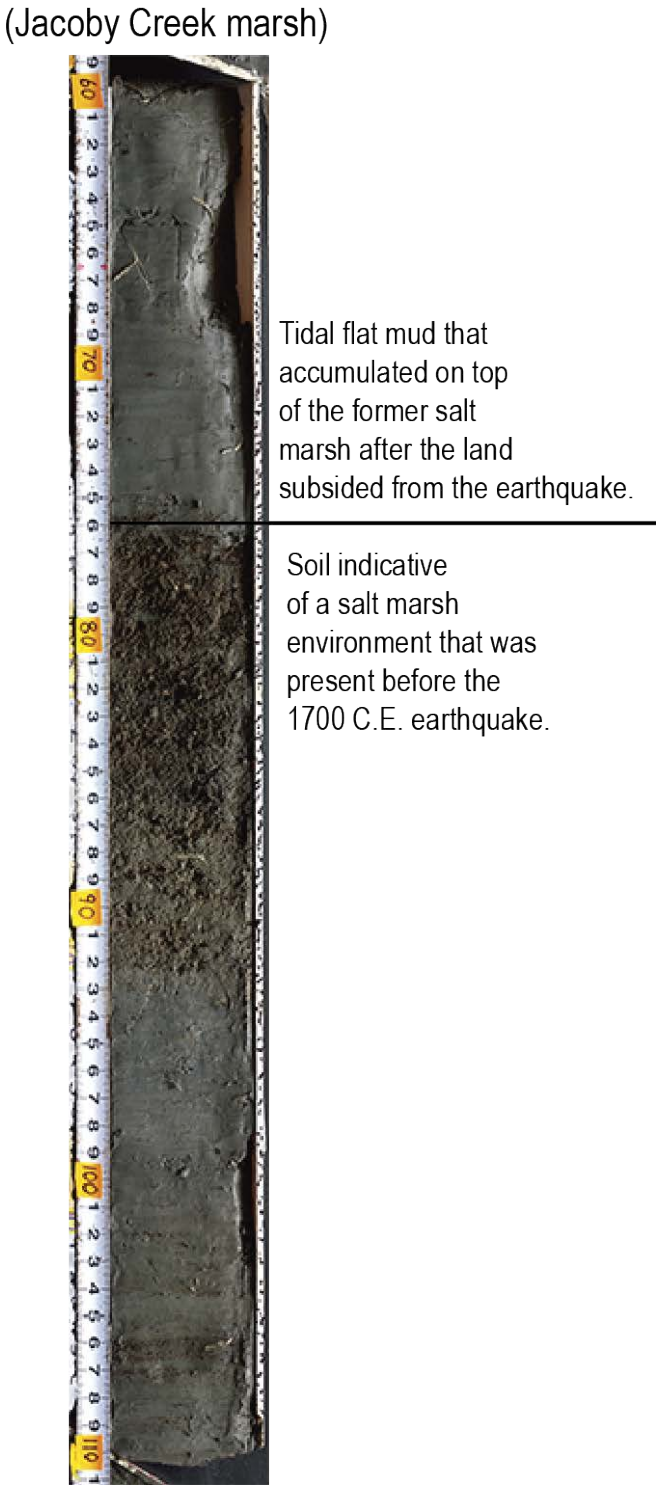

Figure 2-13. Photo of a core collected from Jacoby Creek Marsh at the edge of North Bay (Arcata Bay).
The stratigraphy shows the remains of a marsh soil that was buried by tidal flat mud through coseismic subsidence following the CSZ earthquake in 1700 C.E.
(Photo and interpretation by Eileen Hemphill-Haley).

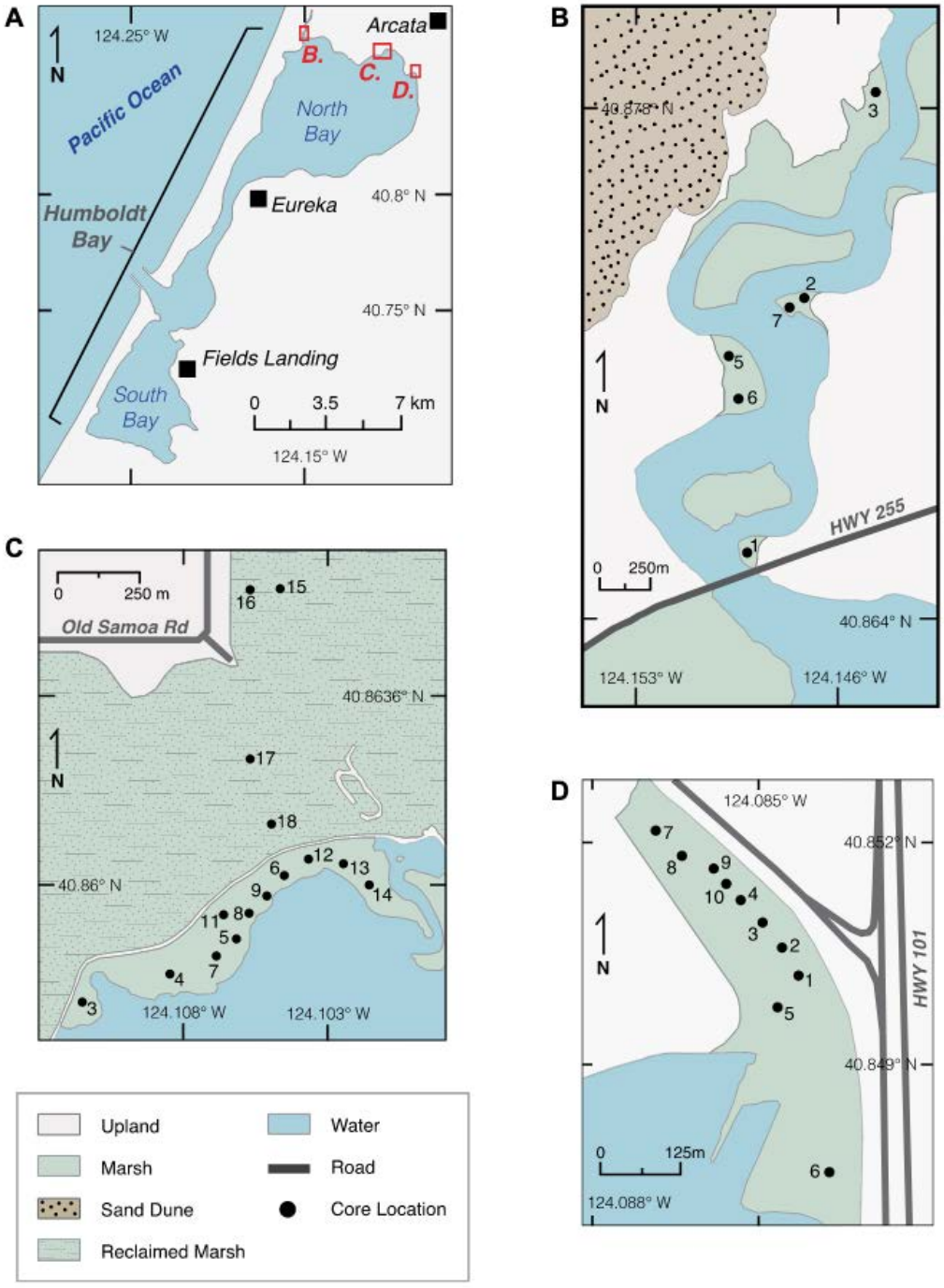

Figure 2-14. Locations of marsh borings on the margin of North Bay
(from Padgett et al., 2021, their Figure 2).

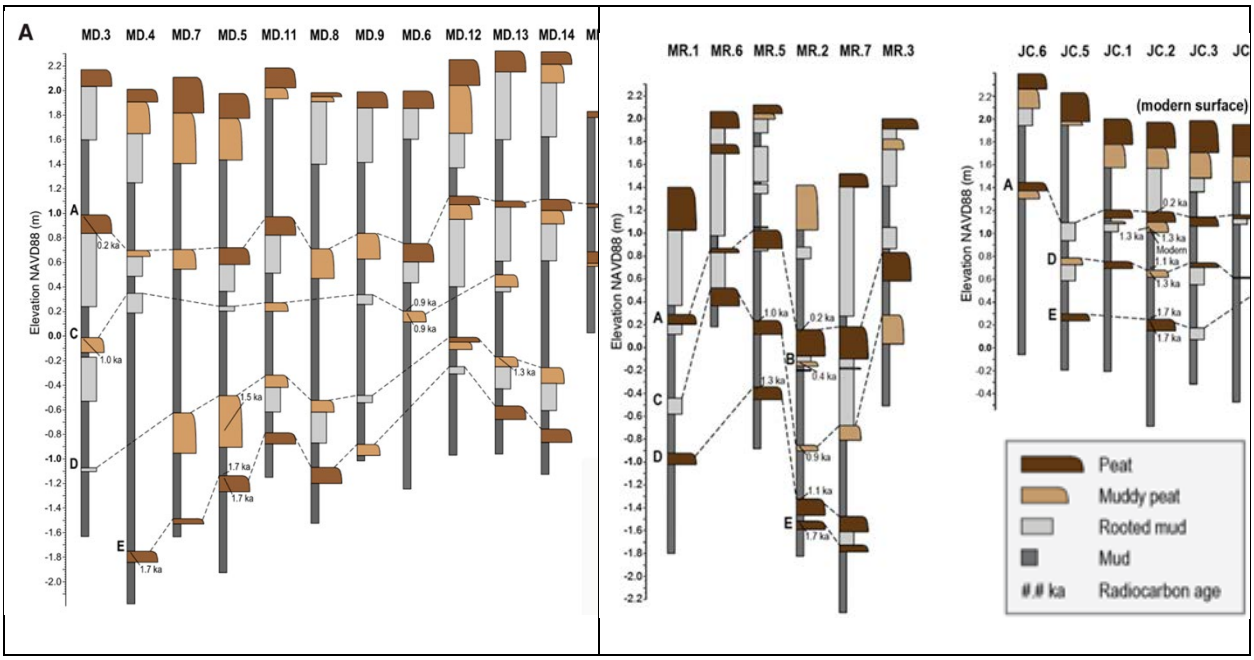

Figure 2-15. Core diagrams (from Padgett et al., 2021, 2022) showing multiple times in the past that areas of northern Humboldt Bay coseismically subsided and former marshes (indicated by the dark reddish brown to brown "peat" intervals) were buried by thick accumulations of intertidal mud (indicated by gray intervals). Following subsidence, the land builds back up over time to an elevation high enough to support marsh growth again, until the next great earthquake and subsequent burial.
MD = McDaniel Creek; MR = Mad River Slough; JC = Jacoby Creek.

2.3.1 Coseismic and Interseismic Uplift

As mentioned in Section 2.3 above, there is no direct evidence for coseismic uplift along the CSZ related to megathrust earthquakes, as all studied sites show evidence of coseismic subsidence (e.g., Nelson et al., 2006; Hutchinson and Clague, 2017). However, an uplift signal has been documented along the north coast of Humboldt County (Woodward-Clyde Consultants, 1980; Burke and Carver, 1992; Swan et al., 2002; McCrory, 2000), and uplift is also indicated from Humboldt Bay to northern Washington by a series of marine terraces at least 200,000 years old in the coastal hills above the coast. This permanent, long-term strain signal is interpreted as evidence that megathrust earthquakes do not completely release all interseismic elastic strain stored along the subduction zone (Stanton et al., 2024). At Humboldt Bay, these terraces are thought to record the progressive regional uplift of the accretionary sediments above the megathrust, while adjacent synclines (i.e., Arcata Bay – Freshwater Syncline and South Bay – South Bay Syncline) are absent of terraces, indicating that these low-lying areas do not record the regional uplift signal seen elsewhere in Humboldt Bay (Figure 2-16). An older record of uplift is noted in the separation of the base of Neogene sediments forming the cores of the folds where it is estimated that more than 3,400 m (~11,150 ft.) of separation exists across the Little Salmon and Table Bluff faults (Ogle, 1953; Kelsey and Carver, 1988; Swan et al., 2002; Vadurro, 2006). These terraces record a longer-term trend of tectonic uplift that has accumulated over many episodes of megathrust activity and not the interspersed, episodic coseismic events.

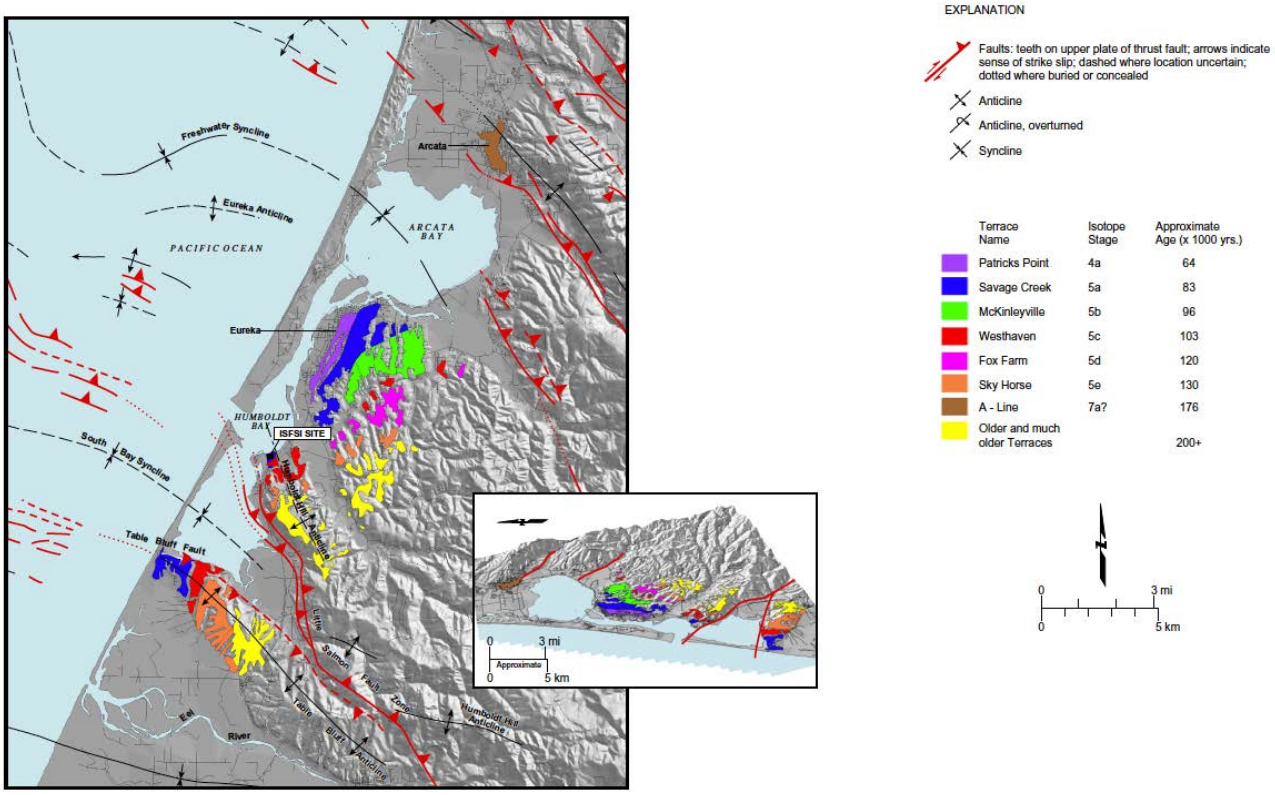

Figure 2-16. Marine terrace sequence within Humboldt Bay, California (from Swan et al., 2002, their Figure 3-6). Note that the terraces record progressive uplift of anticlinal folds as they grow, presumably coseismically, above thrust faults, including the Table Bluff fault, Little Salmon fault, and an unnamed structure beneath Eureka.
Marine terrace geomorphology is absent from intervening synclines.

North of Humboldt Bay, near Trinidad, California, Padgett et al. (2019) describe upper plate deformation associated with the Trinidad fault and anticline (Figures 2-17 and 2-18). They identified five uplifted and deformed marine terraces ranging in age from 80ka to <500 ka that yield an average maximum uplift rate of ~1mm/yr (~3.3ft./ky). This uplift rate estimate is approximately three times that described near Buhne Point by Lettis and Thompson (2020), who calculated a long-term regional uplift of 0.36 mm/yr (1.2 ft./ky), while Page and Nishenko (2015) report that the National Research Council (2012) estimated the area north of Cape Mendocino is rising interseismically at a rate of between 1.5 mm/yr (4.92 ft./ky) and 3.0 mm/yr (9.8 ft./ky). Patton et al. (2023) report an interseismic uplift signal near Trinidad of approximately 2.66 mm/yr (8.7 ft./ky).

2.3.2 Interseismic Subsidence at Humboldt Bay

In addition to episodic coseismic subsidence at Humboldt Bay from great earthquakes, Patton et al. (2017, 2023) have shown that Humboldt Bay is interseismically subsiding at a rate estimated at millimeters per year (Figures 2-19 and 2-20). Specifically, these authors report the following rates of land subsidence:

- South Humboldt Bay/Hookton Slough (3.56 mm/yr)

- Fields Landing (2.66 mm/yr)
- North Spit (3.21 mm/yr)
- Samoa (3.05 mm/yr)
- Arcata Bay/Mad River Slough (1.58 mm/yr)

Patton et al. (2023) used data from tide gages, benchmark releveling and Global Navigational Satellite System (GNSS) to reevaluate VLM rates in the Humboldt Bay area. One plausible interpretation of the data is that the relatively high rates of interseismic subsidence are recording the effects of a locked megathrust boundary, with the overriding North America plate being pulled downward as subduction of the Gorda plate continues beneath it (Savage et al., 1991; Hyndman and Wang, 1995; Wang et al., 2003; Wang and Tréhu, 2016). Another explanation for the relatively high rate of subsidence in Humboldt Bay is that the sites are underlain by soft sediments (Patton et al., 2017, 2023), and compaction of these soft sediments contribute to the relative high subsidence rate measured there. This is suggested by Blackwell et al. (2020), who analyzed large datasets of multitemporal interferometric synthetic aperture radar (InSAR).

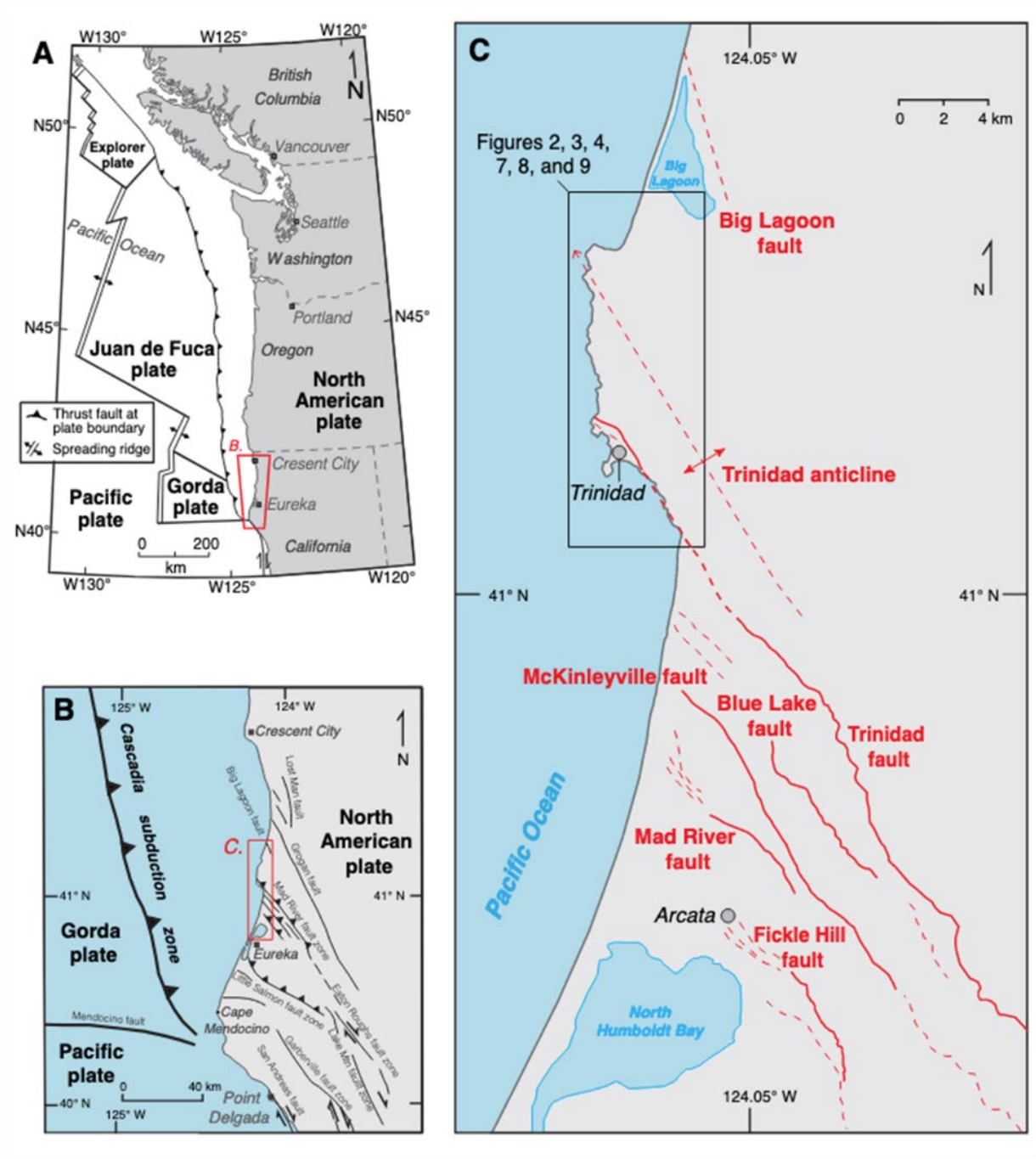

Figure 2-17. Configuration of (A) fold and thrust belt faults at the southernmost end of the Cascadia subduction zone (from Padgett et al., 2019). **(B) Location of the Mad River fault zone, within the fold and thrust belt, consisting of five strands; the Trinidad fault is the northernmost. (C) Enlarged section of the Mad River fault zone.** All bold lines represent southeast-vergent thrust faults dipping to the northeast. Also, notable is the Trinidad anticline formed in the hanging wall of the thrust fault.

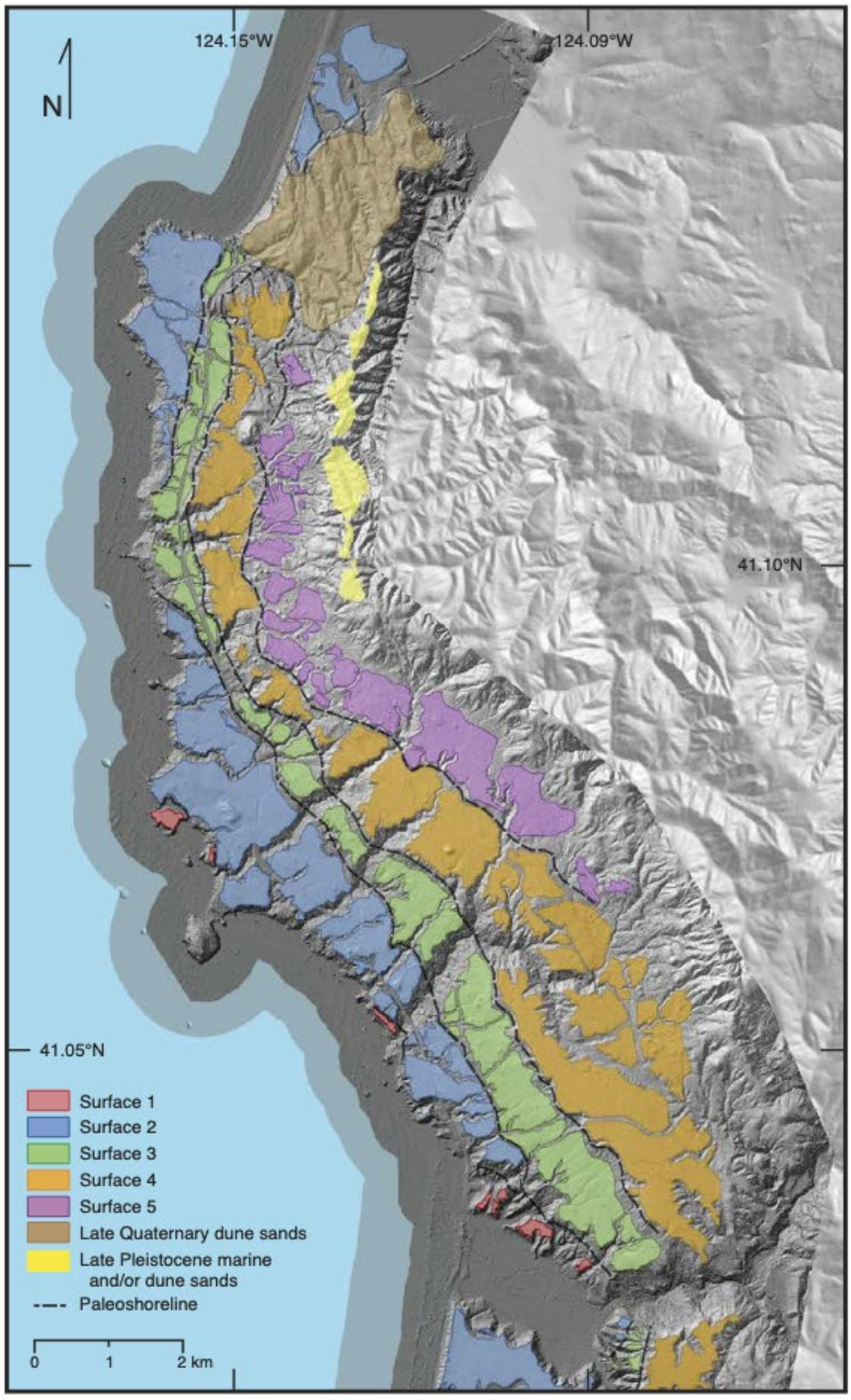

Figure 2-18. Mapped marine terrace surfaces (denoted 1, 2, 3, 4 and 5) near Trinidad, California (from Padgett et al., 2019, their Figure 7). Paleoshorelines (terrace back edges) are delineated as black dashed lines.

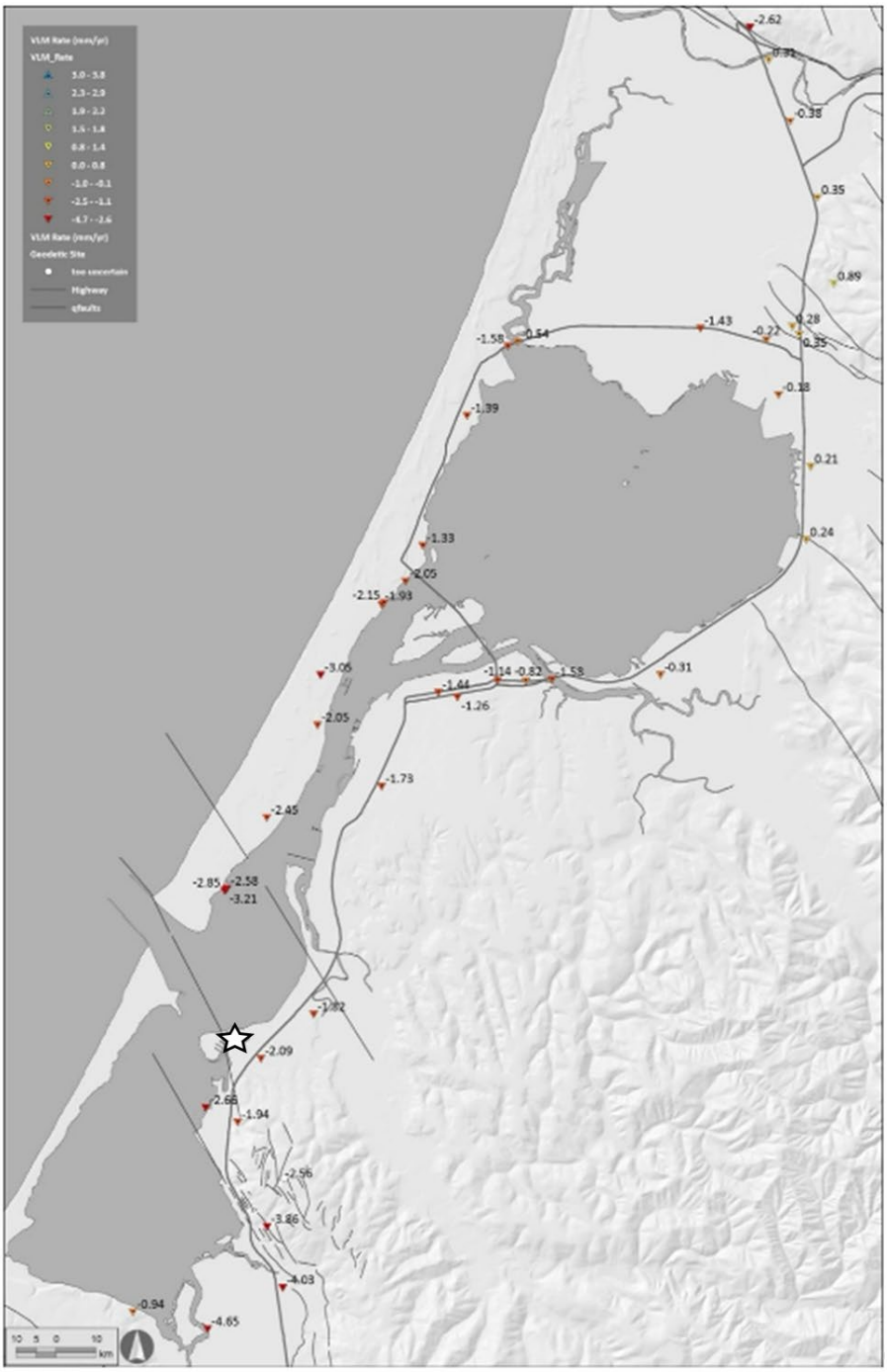

Figure 2-19: Vertical land motion (VLM) for the Humboldt Bay area (modified from Patton et al., 2023). Interseismic VLM estimates are based on GNSS Geodetic data and first-order level-line surveys and tide-gauge data. Downward pointing triangles denote subsiding areas while upward-pointing triangles indicate uplift. Triangles are color-coded to indicate ranges of rates. Highest rates of subsidence occur along the margin of Humboldt Bay (red to orange colors). They are largely bound on the north by the Mad River fault zone (top of figure) and by the Little Salmon fault zone to the south (at Buhne Hill – white star). Figure 2-20 provides a profile of interseismic VLM along the same area as this figure.

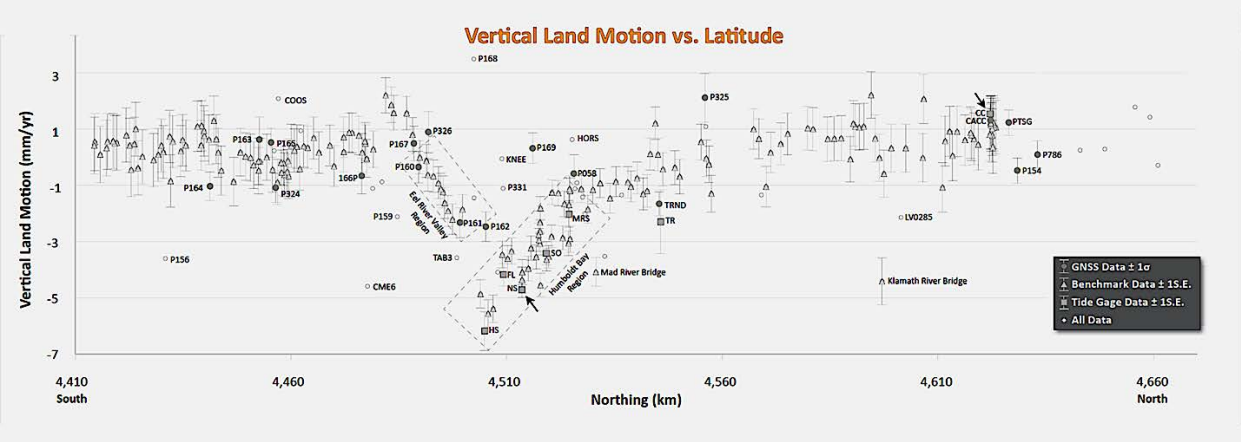

Figure 2-20. Plot of vertical land motion (VLM) versus latitude inland of the Cascadia subduction zone (from Patton et al., 2023). Black arrows point to the locations of North Spit (NS) and Crescent City (CC). North Spit is closer to the megathrust and also within the zone of crustal faults such as the Little Salmon and Mad River fault zones. Note the significant negative vertical motion within Humboldt Bay relative to CC.

Patton et al. (2017, 2023) interpret the data as showing that Humboldt Bay is interseismically subsiding along Highway 101 at a rate ranging from 1.82 mm/yr (0.07 in/yr) immediately north of Buhne Point to 2.66 mm/yr (0.1 in/yr) south of Buhne Point (Figure 2-19). These values differ slightly from those used by Lettis and Thompson (2020), who used a subsidence value of 2mm/yr (0.08 in/yr), likely reflecting an averaging of these estimates.

The accepted interseismic and coseismic models for subduction zones were first proposed by Plafker (1972) following the 1960 **M** 9.5 Chile and 1964 **M** 9.2 Alaska earthquakes, and by Atwater (1987) following investigations of coastal Cascadia that suggest that portions of the coast that are interseismically subsiding will subsequently coseismically uplift. However, the current interseismic subsidence signal for all parts of Humboldt Bay (Patton et al., 2017, 2023) is increased by the evidence for substantial coseismic subsidence for at least the last four CSZ earthquakes in both South and North Bay (Witter et al., 2001; Patton, 2004; Padgett et al., 2021, 2022). The data from Humboldt Bay is consistent with pre-seismic subsidence documented in the Upper Cook Inlet region of Alaska prior to the 1964 earthquake and earlier earthquakes (Zong et al., 2003; Shennan and Hamilton, 2006). Specifically, that area had slowly been subsiding prior to the 1964 **M** 9.2 earthquake, and then dropped >2 m (>6.6 ft.) within minutes as a result of the mainshock event.

It is possible that interseismic and coseismic strains on the adjacent crustal faults in Humboldt Bay (including the Table Bluff, Little Salmon and Fickle Hill faults) are also being manifested in the permanent strain record. If so, it is not certain whether the coseismic change in land level as a result of a megathrust rupture will be up or down (uplift or subsidence).

2.3.3 Vertical Land Motion Uncertainty Complications at Humboldt Bay

Patton et al. (2023) suggest that complications in resolving VLM around Humboldt Bay are not only due to the interseismic loading along the Cascadia subduction megathrust but also due to the local crustal faults. A large part of the uncertainty is the presence of the fold and thrust belt structures located within the accretionary prism that transect the onland and near offshore parts

of the coast at Humboldt Bay. As described earlier, the paleoseismic evidence for coseismic events on the Little Salmon fault is accompanied by upper plate folding that may include uplift directly above the fault and subsidence on either side (Witter et al., 2001). This deformation is smaller in scale than that expected along the Cascadia megathrust, but over time, it can result in a significant geomorphic feature (i.e., Arcata Bay is largely a syncline formed within the lower plate footwall of the Fickle Hill fault with the hanging wall represented by uplifted terraces at Arcata).

The preponderance of studies on regional subsidence address tectonically driven subsidence. However, subsidence can alternatively also be driven by long-term soft-sediment compaction. Subsidence magnitudes and rates similar to those inferred to be from tectonic causes in the Humboldt region have been measured and attributed instead to sediment compaction in coastal areas such as San Francisco Bay and San Diego Bay (e.g., Blackwell et al., 2020). Thus, it bears repeating that some of the interseismic subsidence signal may be due to soft sediment compaction (e.g., Blackwell et al., 2020), especially along the shores of Humboldt Bay.

Even though the cause of, and future potential for, coseismic ground level changes and regional subsidence are not well understood, it is prudent to consider potential implications of coseismic land level changes in tsunami inundation models.

2.4 Sea Level Rise

Future sea level rise (SLR) and the rates of sea level change are important aspects of VLM and potential tsunami inundation. The estimates of SLR are also reevaluated periodically by various researchers and agencies, and hence, are also revisited for this update. Page and Nishenko (2015) and LCI (2020) addressed future sea level at the Humboldt ISFSI site using global and regional estimates of sea level rise. Page and Nishenko (2015) used the guidance from the National Research Council (2012) to estimate the 100-year minimum and maximum SLR projections for the year 2115 of 0.1 m (0.3 ft.) and 1.4 m (4.7 ft.), respectively (Table 2-2). LCI (2020) used sea-level rise rates provided by the IPCC (2019) to estimate a 100-year minimum and maximum SLR at the ISFSI for the year 2120 of 0.3 (1 ft.) and 1.5 m (5 ft.), respectively (Table 2-2).

Since the LCI (2020) assessment, several newer SLR estimates projected to the year 2100 have been released, including those by Horton et al. (2020), Sweet et al. (2022), IPCC (2022), and Ocean Protection Council (OPC, 2024). These SLR projections range from low values of 0.2 to 0.4 m (0.7 to 1.4 ft.) to high values of 0.9 to 2.0 m (2.8 to 6.6 ft.). Projections as far as 2150 (Sea-level Rise Leadership Team and Ocean Protection Council [SLRT&OPC], 2022; Sweet et al., 2022) provide minimum SLR estimates of 0.3 to 0.4 m (1 to 1.3 ft.) and maximum SLR estimates of 3.3 to 3.6 m (10.8 to 11.9 ft.). For the purposes of this update, however, the aim is to calculate the estimated rise in sea level at the ISFSI to the year 2045, when the license for the facility expires. Using the various SLR rates provided in the literature, we estimate minimum and (conservatively) maximum SLRs of 0.1 and 0.4 m (0.4 and 1.4 ft), respectively. The conservatively high SLR estimate of 1.9 ft. is used in this update to add to the calculated tsunami runup estimate to evaluate the tsunami hazard at the ISFSI.

Table 2-2. SLR Rate Comparisons with Oldest at Top
Baseline information from Page and Nishenko (2015) and Lettis and Thompson (2020) are highlighted in gray.

SLR Rates	Minimum		Intermediate		Maximum	
	(in/yr)	(mm/yr)	(in/yr)	(mm/yr)	(in/yr)	(mm/yr)
Burgette (2009)	0.08	2.0			0.1	2.54
Page and Nishenko (2015)					0.16	4.06
LCI (2020) using IPCC (2019)	0.3	8			0.6	15
He et al. (2022) GLOBAL	0.06	1.5			0.07	1.78
Patton et al. (2023) using Montillet (2018)	0.07	1.8			0.08	2.03
OPC (2024) 2025 2100	 0.1 0.1	 2.5 2.5	 0.3 0.8	 7.6 20.3	 0.7 1.3	 17.78 33.02

*Note: Only references providing rates were included in the comparison table.

2.4.2 Impact of Sea Level Rise Estimates on Tsunami Runup Estimates

Recent Probabilistic Tsunami Hazard Assessments (PTHAs) typically do not include SLR in their models (González et al., 2009; Selva et al., 2016; De Risi and Goda, 2016; Park et al., 2017; Davies et al., 2018; Small and Melgar, 2021; Goda, 2023) and only recently has it become a consideration (Li et al., 2018; Nagai et al., 2020; Sepúlveda et al., 2021; Alhamdi et al., 2022). However, future PTHAs may have to consider SLR. Lettis and Thompson (2020) described this possibility when they projected a 100-year SLR change in elevation for Buhne Hill that includes sea level rise combined with interseismic and coseismic vertical land motion. Thus, a Buhne Hill tsunami runup analysis may involve projection of SLR to the year 2100 or greater, and consideration of the recurrence and lapsed time (since 1700 C.E.) of **M** >8.0 earthquakes along the CSZ.

2.5 Recent Investigations that Relate to Understanding the Geology at Buhne Hill

2.5.1 Crustal Faults Associated with the Little Salmon Fault Zone

Recent investigations into components of the southern CSZ and the Little Salmon fault (LSF) provide insights into the interaction between the Mendocino triple junction (MTJ) and the southern edge of the subduction zone. Several of these investigations were reported in the 2022 Pacific Cell Friends of the Pleistocene (FOP) guidebook for a field trip to the southern Cascadia and Cape Mendocino areas (Patton et al., 2022a). These are non-peer reviewed articles that present original geologic research ranging from graduate thesis projects to U.S. Geological Survey (USGS) investigations. For example, Patton et al. (2022b) mapped a previously unknown fault within southern Humboldt that may be an eastern extent of the Russ fault, a major crustal fault immediately north of Cape Mendocino. Investigations at Cape Mendocino addressed coastal deformation rates and fluvial geomorphology related to MTJ migration (Crawford et al., 2022; Hartshorn et al., 2022; Robinson et al., 2022; Vermeer and Hemphill-Haley, 2022). McPherson et al. (2022) considered the seismological implications of more than 40 years of **M** >5 earthquakes in the MTJ region. Other reports compiled and reviewed include seismological investigations conducted following the 20 Dec 2021 and 20 Dec 2022 **M** >6 earthquakes near Petrolia and Ferndale (Yeck et al., 2023; Yoon and Shelly, 2024; Shelly et al., 2024; Smith et al., 2024).

The crustal faults of the accretionary prism in southern Cascadia have received new attention in the past few years. Trenching and geomorphic investigations of the LSF, and associated Goose Lake and Van Duzen faults have been conducted by Bold and Michalak (2022), Nicovich et al. (2024), and Ladinsky et al. (2022a, 2022b) (Figure 2-21). In addition, a USGS investigation considered the interseismic loading strain budget of the Little Salmon and Mad River fault zones and compared it to regional strain (Materna et al., 2022).

2.5.2 Cape Mendocino

Near Cape Mendocino, multiple investigations have evaluated the marine terraces to estimate the vertical land deformation where coseismic uplift occurred during the 1992 **M** 6.6 and **M** 7 earthquakes (Crawford et al., 2022; Hartshorn et al., 2022; Vermeer and Hemphill-Haley, 2022). Additionally, Robinson et al. (2022) conducted a geomorphic analysis of the response of the nearby Mattole River and its response to uplift associated with migration of the MTJ.

2.5.3 Seismology

Seismological investigations were conducted following the 20 Dec 2021 and 20 Dec 2022 **M** >6 earthquakes near Petrolia and Ferndale, California, respectively (Yeck et al., 2023; Yoon and Shelly, 2024; Shelly et al., 2024; Smith et al., 2024)

2.5.4 Recent Findings on Historical Records

2.5.4.1 The 1964 Tsunami in Humboldt Bay

Thirty-three far-field tsunamis have been recorded on the North Coast since the installation of the first tide gauge at Crescent City in 1933 (Admire et al., 2011, 2014). The NOAA National

Centers for Environmental Information Natural Hazards Viewer provides some information about the effects of the 1964 **M** 9.2 Prince William Sound, Alaska tsunami at Fields Landing and King Salmon, noting that water heights of 1 to 2 m (3 to 7 ft) were observed in that region (Figure 2-22). The associated website https://www.ngdc.noaa.gov/hazel/view/hazards/tsunami/runup-more-info/4349 provides further information about the tsunami in Humboldt Bay.

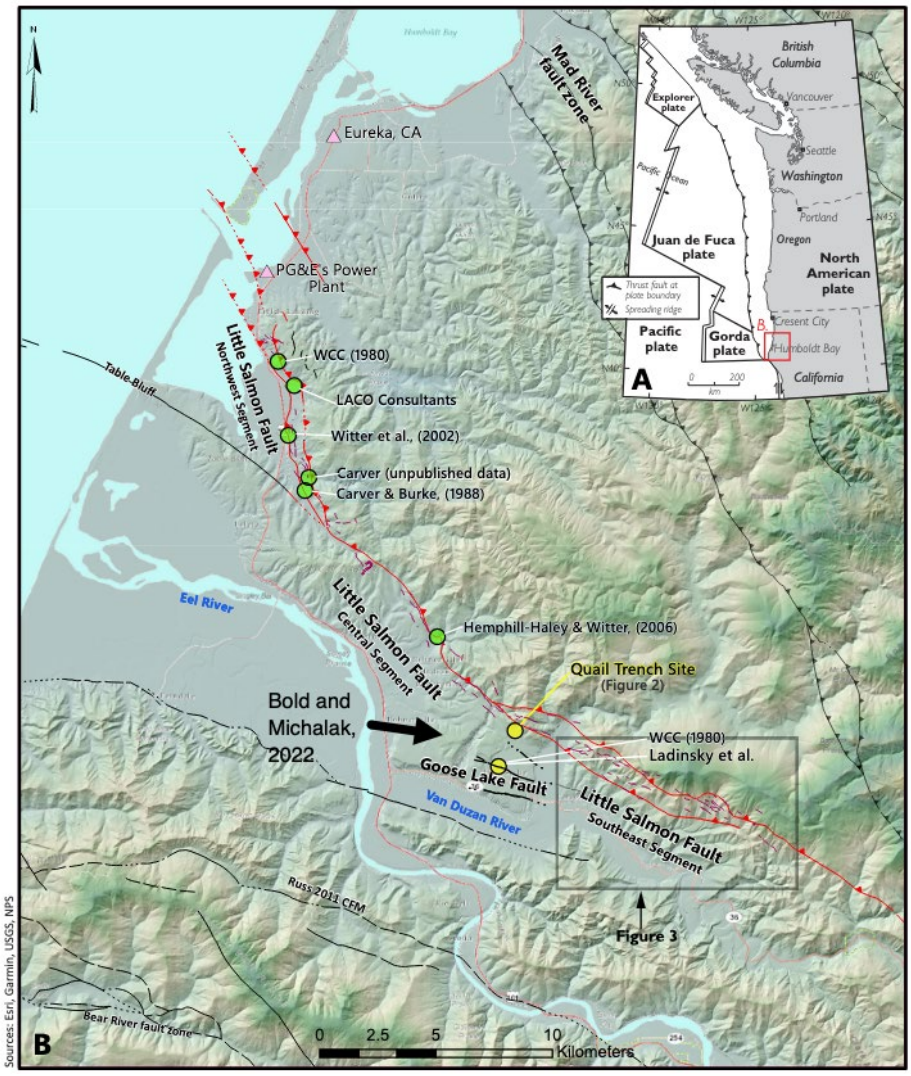

Figure 2-21. Location of paleoseismic investigations along the Little Salmon fault including Bold and Michalak (2022) and Ladinsky et al. (2022b) (from Ladinsky et al., 2022b, their Figure 1).

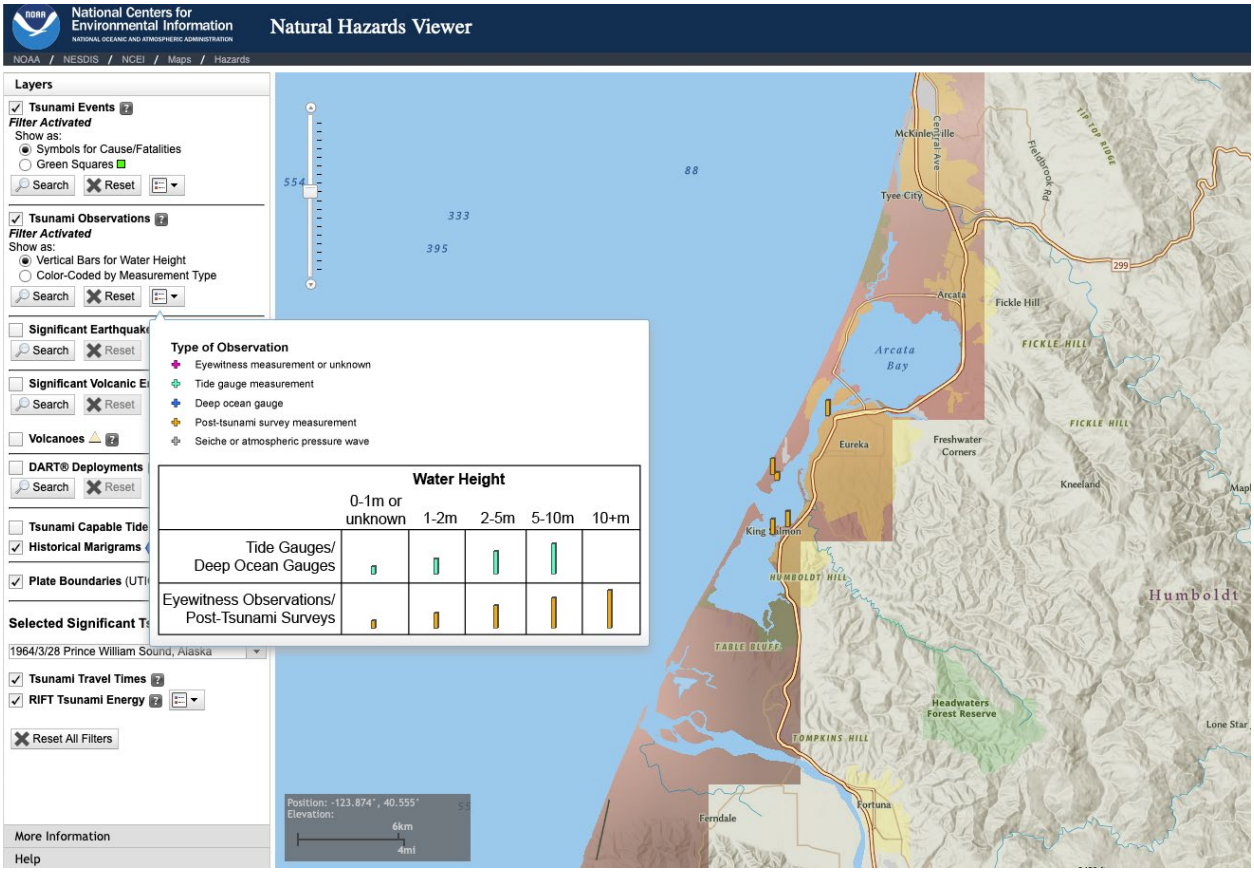

Figure 2-22. Screenshot of NOAA Natural Hazards Viewer webpage showing reported wave heights at King Salmon as a result of the 1964 M 9.2 Prince William Sound, Alaska earthquake (https://www.ncei.noaa.gov/maps/hazards/?tsEvent=1954).

Lander et al. (1993) reported that: *"The Eureka Boat Basin suffered little damage but the water rose over the ten-foot seawall and eight feet into the street at the height of the rise. The tide was six feet. The bay was filled with logs and debris. Half of the sea and channel markers were moved off their stations by the surge. Nine changes in the tide were reported between midnight and 4:30 A.M. with an eight to nine feet tide at the channel entrance. It was like someone pulled the cork out of the bay. The velocity was tremendous. It came back in just as fast and kept repeating."*

Robert Wiegel (1965) reported: *"…maximum run-up elevations above the tide stages as probably 3.1 feet at the Coast Guard Station on North Spit, about 4.7 to 5.1 feet at the Municipal Marina, Eureka about 4.5 feet at the entrance to King Salmon Slough, and 3.8 feet at the Pacific Gas and Electric Power Plant intake (0.6 miles upstream on the King Salmon Slough)."*

The NEIC site also documents that Magoon (1965) stated that there were: "*…14 knot currents in the channel opposite the Coast Guard Station. Professor Gast, Humboldt State College, estimated the maximum height as 14 feet (7 foot amplitude) based on water lines on docks and structures."*

2.5.4.2 1964 Tsunami Currents in Humboldt Bay

Destructive tsunamis forces include not only the landward force and flooding of the incoming waves, but also the erosion and deposition by backwash as debris-filled water rushes back to the ocean, typically at high flow velocities in several pulses. The combined landward flow and subsequent backwash can result in areas of coastal erosion and deposition in the nearshore as well as sediment scour in ports and harbors. These morphodynamic effects of tsunami inundation could erode Buhne Hill on the bluff side. The top of the bluff is set 21 m (70 ft) away from the ISFSI providing protective buffer from potential erosion.

Acoustic Doppler Current Profilers (ADCP) have been installed in Humboldt Bay (Figure 2-23) to measure tsunami and other currents (Admire et al., 2014). The ADCPs were operational during the 2010 **M** 8.8 Chile and 2011 **M** 9.0 Tohoku-Oki, Japan earthquakes, and were able to calculate peak tsunami wave amplitude and peak current speeds for both events. Admire et al. (2014) report that tsunami currents within Humboldt Bay from the 2010 Chile earthquake lasted for approximately 30 hours with peak velocities of about 0.35 m/s (1.15 ft/s) and peak water amplitudes of about 0.23 m (0.75 ft). The 2011 Japan earthquake resulted in a tsunami signal in the bay that lasted more than 40 hours, with water velocities of between 0.6 and 0.84 m/s (2.0 and 2.8 ft/s) measured during the first 2 hours with a peak amplitude of 0.81 m (2.6 ft). Some of the ADCP locations reported by Admire et al. (2014) are part of the Physical Oceanographic Real-time System (PORTS) project, a collaborative effort at Humboldt Bay between NOAA and Cal Poly Humboldt (https://tidesandcurrents.noaa.gov/ports/index.html?port=hb). PORTS currently maintains a continuous monitoring system in Humboldt Bay in the event of tsunami activity to acquire *"Better estimates of the currents generated by tsunamis [which] can be used to improve numerical modeling and to provide better understanding of the hazards in ports and harbors caused by currents"* (Admire et al., 2014, p. 3402).

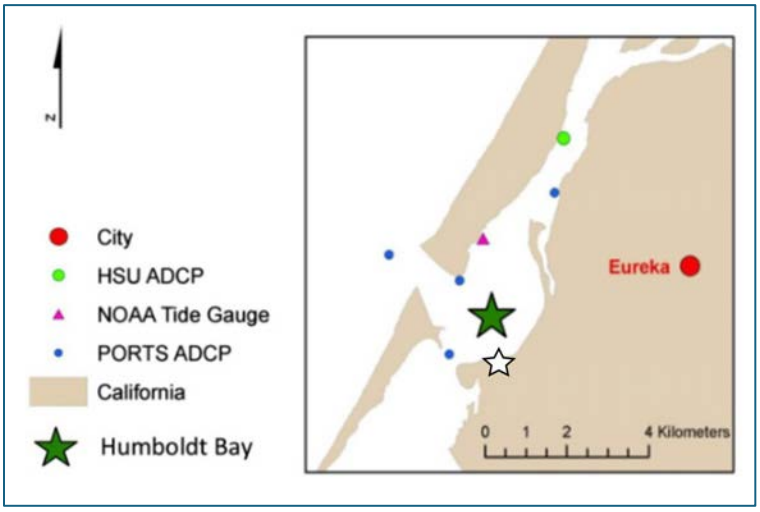

Figure 2-23. Humboldt Bay with NOAA tide gauge site (pink triangle), Acoustic Doppler Current Profiler (ADCP) (green dot), and ADCP sites deployed as part of ongoing NOAA PORTS project (blue dots). White star indicates approximate location of ISFSI.
(Modified from Admire et al., 2014).

2.5.5 Updates on Paleotsunami Record for the North Coast at Humboldt Bay

To date, no definitive tsunami deposits have been identified at study locations along North Bay (Arcata Bay). This may be because the bay is relatively sheltered from the Pacific Ocean by intervening high sand dunes between the mouth of Humboldt Bay and the Mad River (Engelhart et al., 2016; Hemphill-Haley, 2017; Padgett et al., 2021, 2022; Pritchard, 2004).

Similarly, Patton (2004) found no evidence at Hookton Slough for a tsunami deposit associated with the ~ **M** 9.0 CSZ earthquake in 1700 C.E. The interpretation that a deposit at the South Humboldt Bay sites studied by Carver et al. (1998) represents the 1700 C.E. event is possible but equivocal, given the proximity of the study sites to the ocean and the overlap between the radiocarbon-derived age of the deposit and the ages of known destructive coastal storms in the late 19th century (e.g., Hemphill-Haley et al., 2019). Other older tsunami events are recorded at South Humboldt Bay. Although the stratigraphic record is not definitive, it is likely that the coast at Humboldt Bay was impacted by the CSZ tsunami in 1700 C.E. as there is abundant evidence for this event at coastal sites to the north, including at Crescent City and elsewhere in coastal Del Norte County (Abramson, 1998; Carver et al., 1998; Garrison-Laney, 1998; Hemphill-Haley et al., 2019; Peterson et al., 2011).

2.6 Probabilistic Tsunami Hazard Analysis (PTHA)

2.6.1 2007 Humboldt Bay Study

In 2007, URS (now AECOM) carried out a deterministic tsunami inundation study for the ISFSI site that was included in the Page and Nishenko (2015) assessment report. The main results were based on a 1700-C.E.-type **M** 9 earthquake on the main subduction zone interface with additional movement on the crustal faults in the area, such as the Little Salmon and the Mad River faults. While the scenarios yielded significant inundation in the Humboldt Bay area, locally elevated areas like Buhne Hill remained dry, partly due to the hill's elevation above mean high sea level (MHW). Modeled runup elevations calculated as part of the 2007 study at Buhne Hill ranged between 7.3 to 10.3 m (24 to 34 ft) (MHW).

2.6.2 Tsunami Hazard Modeling Updates

The tsunami hazard due to earthquakes on the Cascadia subduction zone has been the subject of a number of studies since completion of the 2007 URS study. Priest et al. (2013) developed hazard maps for the Oregon coast using a range of scenarios for a Cascadia earthquake with different size events referenced as "T-shirt sizes, S, M, L, XL, XXL." While the models extend along the entire CSZ, the inundation maps were only developed for Oregon, and therefore do not include Humboldt Bay. Likewise, a probabilistic tsunami hazard study by Park et al. (2017) was performed for a small area in Oregon, as are several site-specific models for Seaside, Oregon (González et al., 2009).

New tsunami hazard modeling since Page and Nishenko (2015) and SAFFR (2013) (Figure 2-24) are part of a California-wide tsunami Probabilistic Tsunami Hazard Assessment (PTHA) effort by Thio (2019) that included Humboldt Bay (Figure 2-25). Maps including Humboldt Bay that rely on Thio's (2019) models (Figures 2-26 and 2-27) were produced by the California Geological Survey (CGS, 2021) and the Redwood Coast Tsunami Work Group (RCTWG, https://rctwg.humboldt.edu). No other PTHA analyses have been performed for Humboldt Bay,

but tsunami hazard evaluations conducted along other portions of the CSZ are relevant to the bay and the ISFSI site. For example, Goda (2023a) conducted a PTHA for Vancouver Island, Canada that considers full rupture of the CSZ. Goda concluded that coastal exposure to the subduction zone source and local bathymetry will be major contributors to the variability of tsunami inundation along Vancouver Island. Davies et al. (2018) conducted a global PTHA that included a site near Seaside, Oregon using CSZ as an earthquake and tsunami source. They concluded that a 1/100 exceedance tsunami would have peak wave heights of 5.0 m (16 ft) (MSL) and a 1/500 exceedance event would have peak wave heights of 13.2 m (43.3 ft).

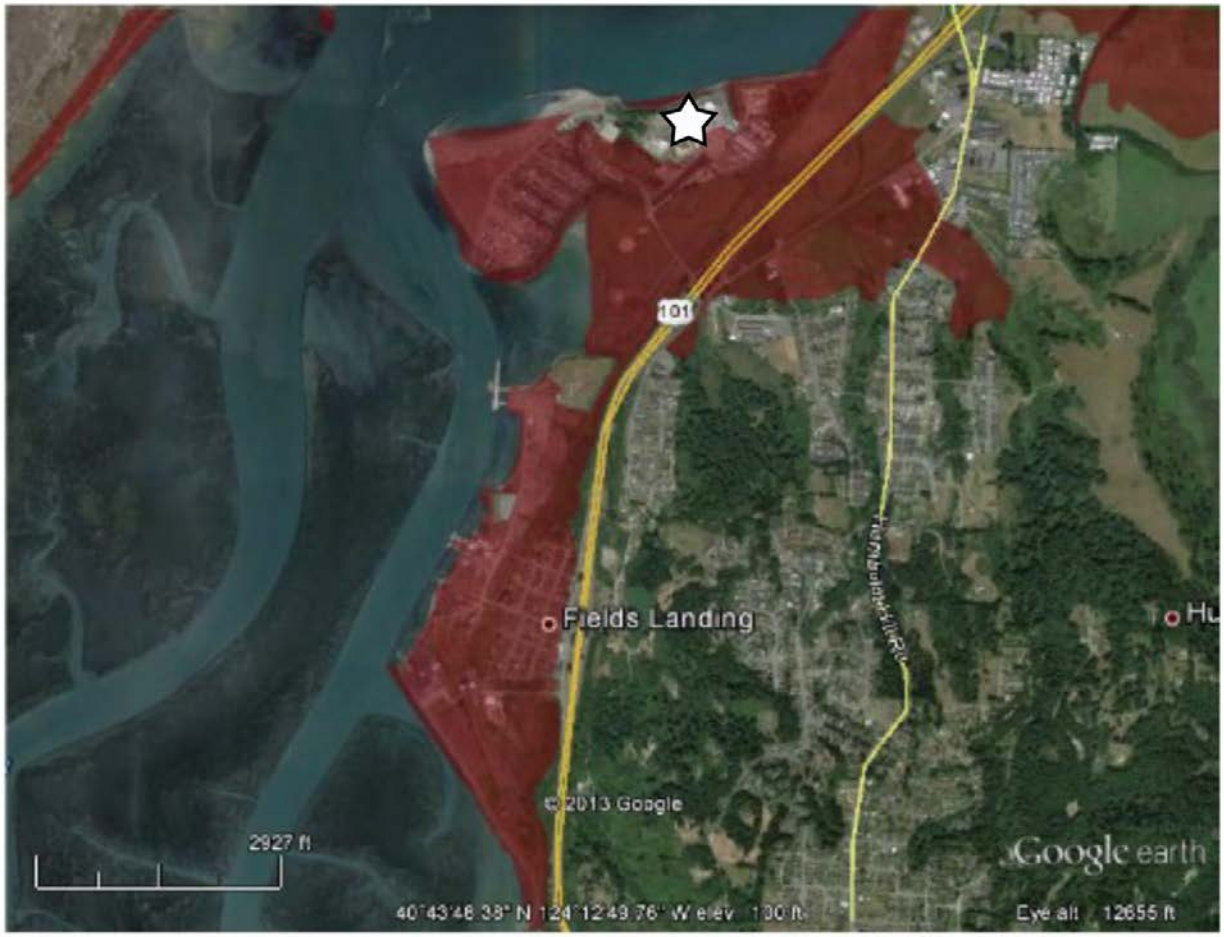

Figure 2-24. Tsunami inundation map of the Fields Landing area including Buhne Point and the ISFSI site (SAFFR Tsunami Modeling Working Group, 2013). Note that most of Buhne Hill and the ISFSI site (white star) are not within the inundation area (red shading).

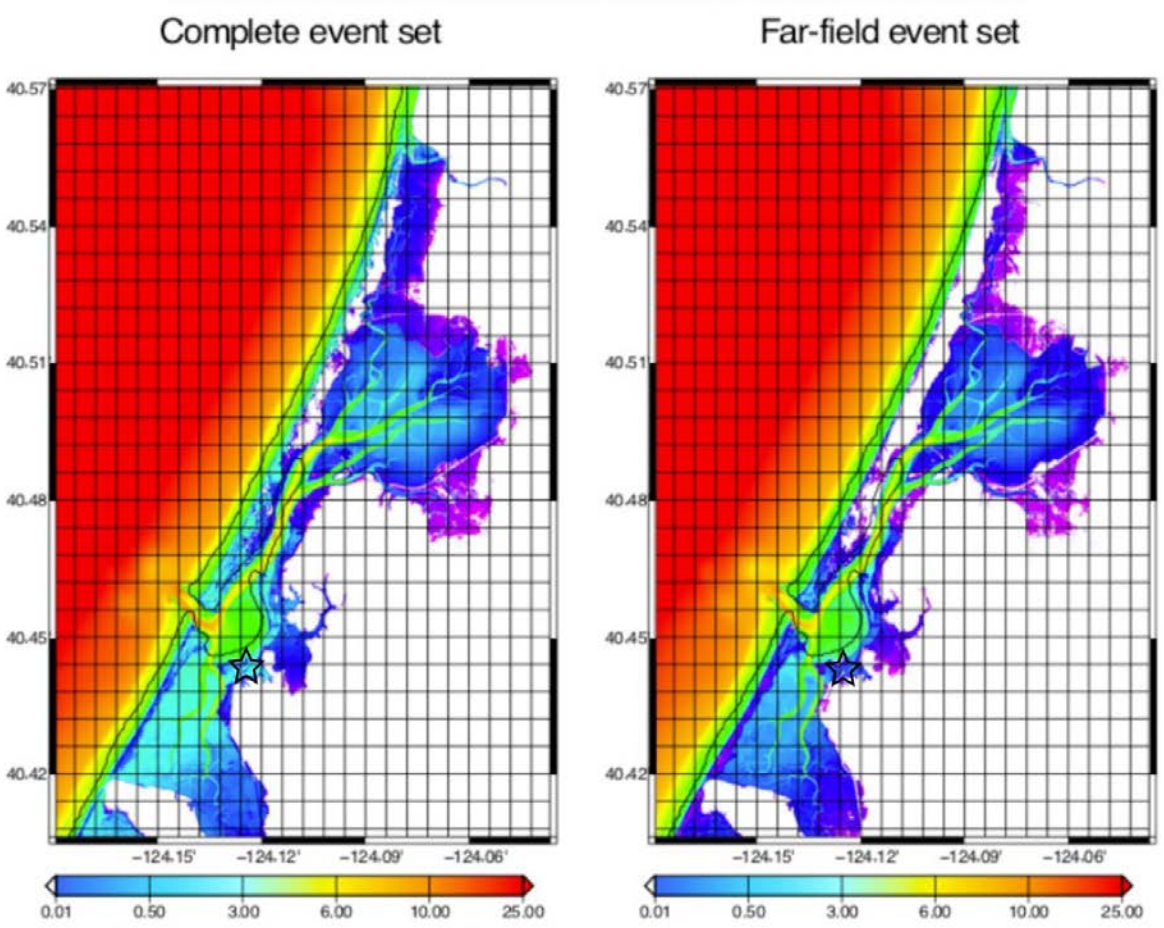

Figure 2-25. Probabilistic tsunami flow depths for Humboldt Bay considering a 2,475-year model (from Thio, 2019). Map on the left includes local and far-field sources, whereas the map on the right considers only far-field sources. Approximate location of ISFSI depicted by open star. As noted in the report, there is no substantial difference in the inundation pattern between the two source models. Elevation units are in meters.

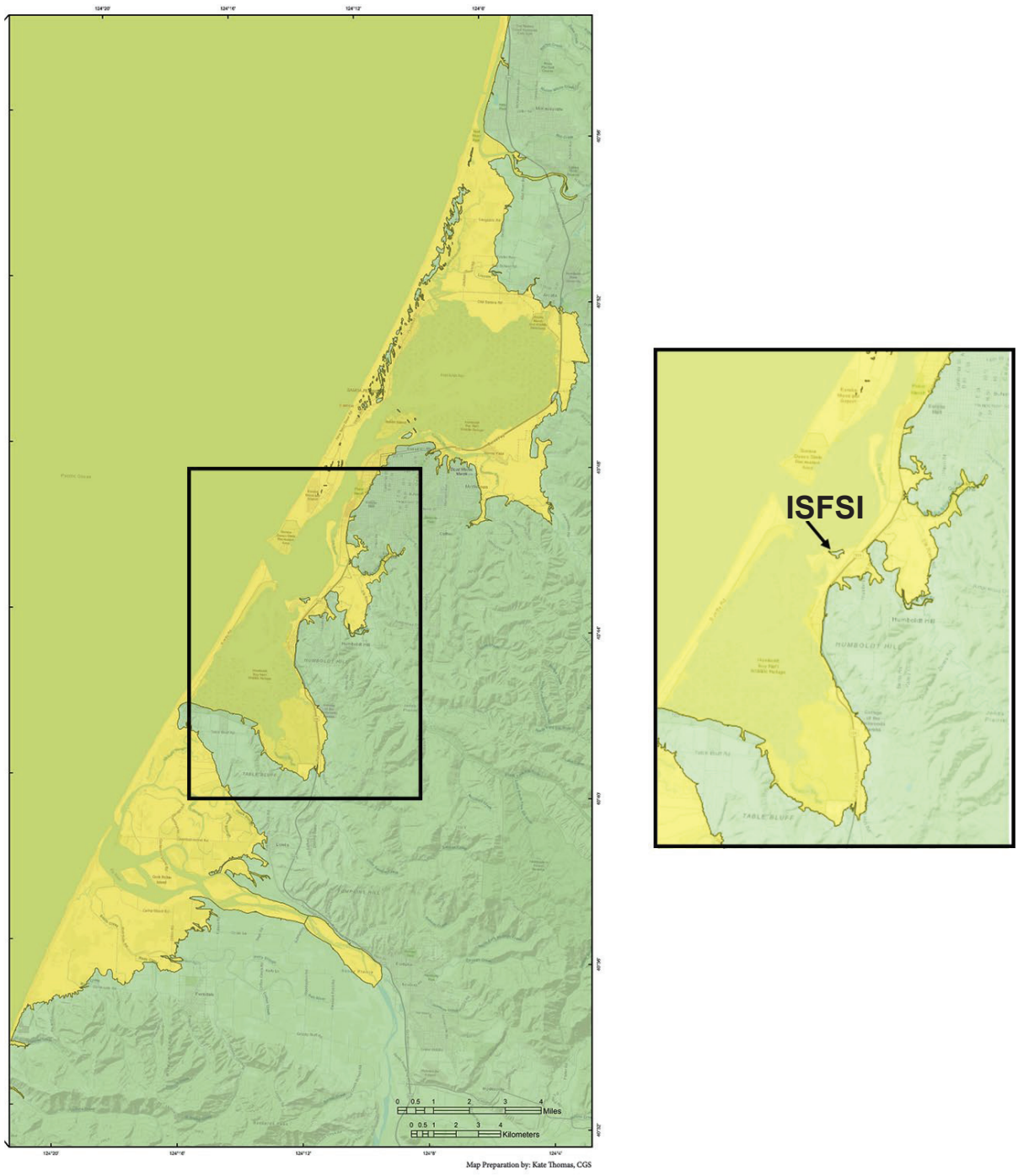

Figure 2-26. Humboldt Bay tsunami inundation map (CGS, 2021).
Areas highlighted in yellow are considered likely to be inundated by a 975-year-average-return-period tsunami event, corresponding to an event with a 5% probability of exceedance in 50 years. At this resolution it is apparent that most of Buhne Hill is not inundated during this scenario.
This map is based on modeling by Thio (2019).

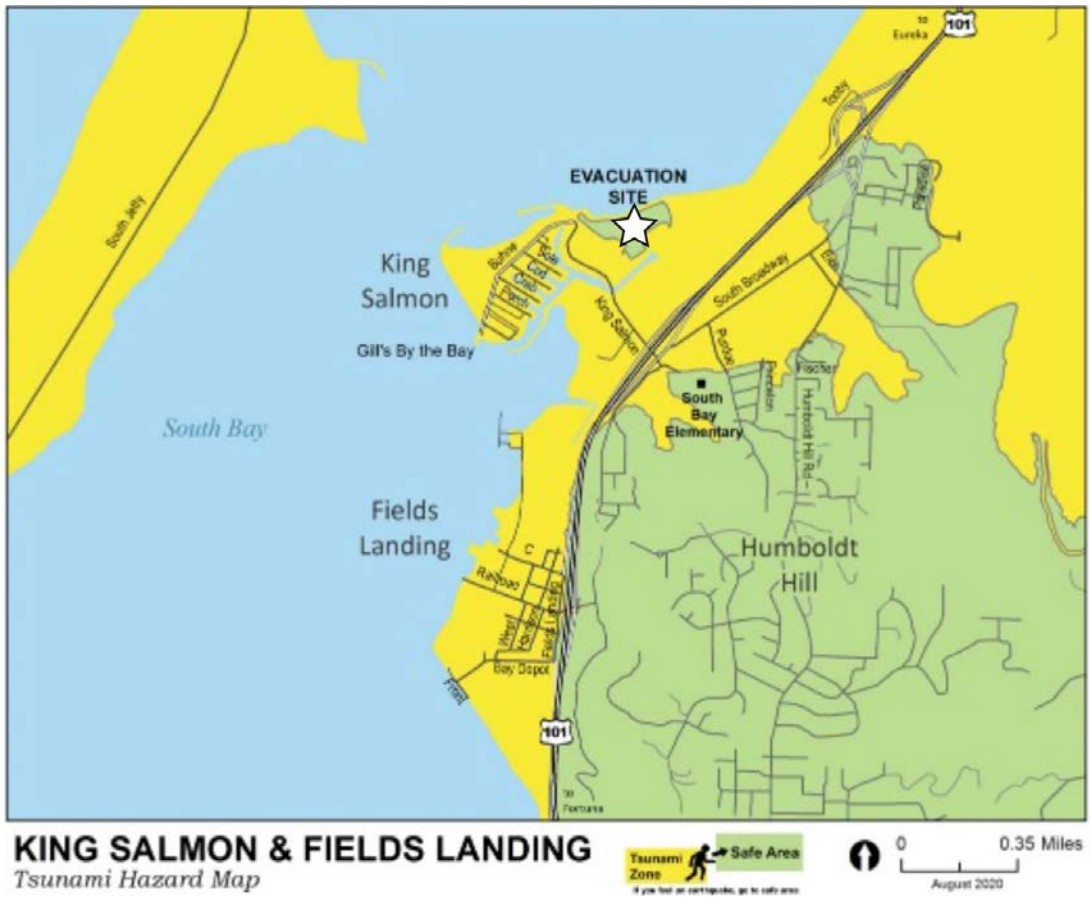

Figure 2-27. Tsunami inundation map for King Salmon and Fields Landing (CGS, 2021). This map was produced in association with the Redwood Coast Tsunami Working Group (RCTWG, https://rctwg.humboldt.edu). Yellow shading indicates areas of inundation. Most of Buhne Hill and the ISFSI site (star) are not inundated in this model, and are instead identified as a local evacuation site. Modeling is based on Thio (2019).

2.6.2.1 Tsunami Maps for ASCE 7 and Similar Developments

2.6.2.1.1 ASCE 7-16/22 Offshore and Inundation Maps

The offshore hazard maps for ASCE 7-16 (ASCE, 2017), the first edition of the building standard to contain a chapter on tsunami impact and design issues, were developed by Thio et al. (2017) and covered the entire US west coast and Hawaii. While the original standard contained tsunami design zones mapped at 60-m (~197-ft) horizontal resolution, California developed its own inundation maps at a resolution of 10 m (~33 ft) for the next update. On the left side of Figure 2-26 we present an example of the CGS (2021) map for Humboldt Bay, with a more detailed map around the ISFSI on the right.

These maps are based on subduction zone sources around the Pacific Basin, which are capable of producing the largest earthquakes in the world. These sources are generally based on the Slab2.0 model (Hayes et al., 2018), which consists of irregularly shaped subduction zone interfaces. Complications like splay faulting and other local tsunami sources, such as crustal faults, were not included in this first version of tsunami hazard models. Similarly, landslide sources were also not

included, as these, with the exception of Alaska, are generally considered to have recurrence intervals well above the 2,475-year return period used in ASCE 7-16/22.

In Humboldt Bay, the tsunami hazard stems primarily from two sources depending on return period, as follows: 1) Alaska sources for short return periods of less than 800 years, and 2) the CSZ for longer return periods. The ASCE 7-16/22 tsunami design zone maps reflect the extent of the 2,475-year-return period tsunami hazard. Dynamic parameters such as velocity and momentum flux prescribed in the standard are computed through an energy-gradeline method available separately from the CGS.

Also included in the design standard are maps showing the probabilistic subsidence estimates for a region, such as those on Figure 2-28. Due to the geometry of the CSZ, which curves landward at its southern terminus, the Humboldt Bay area is situated on the seaward side of the hinge line that separates uplift from subsidence during megathrust earthquakes. As a result, the probability of subsidence at the ISFSI is considered very small compared to that farther north along Oregon and Washington. Additionally, as previously described, the ISFSI is sited on Buhne Hill, a local, fault-bounded topographic high capped by an ~80-ka marine terrace that has been correlated with flights of marine terraces to the east and northeast, on Humboldt Hill and in Eureka. This suggests that either 1) intraseismic regional subsidence in the Humboldt Bay area does not apply to Buhne Hill, and/or 2) the net tectonic motion over several intraseismic and coseismic events is that of uplift. This is an ongoing subject of research.

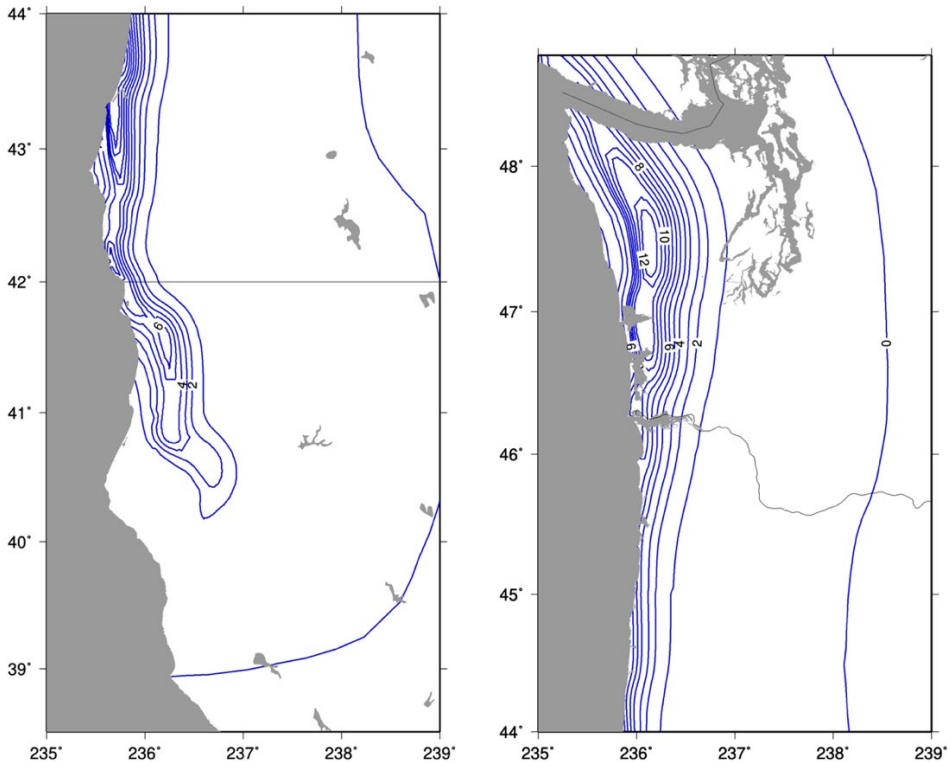

Figure 2-28. Probabilistic subsidence maps from ASCE 7-22.
Note that the probabilistic subsidence in the Humboldt Bay area is less than a meter.

2.6.2.1.2. CGS and DOT Tsunami Hazard Maps

The California Geological Survey (CGS, 2021) developed an extensive set of probabilistic tsunami hazard maps for most of the California coast based on a high-resolution (10-m [~33-ft.]) control grid; the 2021 maps replace the initial ASCE 7-16 inundation maps for the California coastline. The CGS tsunami hazard maps were prepared considering several return periods ranging between 72- and 3,000-year Annual Return Probabilities (ARPs).

Starting in 2016, the Oregon Department of Transportation (DOT), with additional funding from the California, Washington, Alaska and Hawaii Departments of Transportation, supported work to develop a tsunami design document for bridges. The project was completed in 2021 (Lynett et al., 2021). The scope of this project included determining an appropriate hazard level for design, creating a set of tsunami inundation maps at a determined hazard level, and developing a procedure to calculate the loads on bridge components due to tsunami. Figure 2-29 compares the inundation models for Humboldt Bay from the URS (2007) study and the 2,475-yr and 975-yr ARPs developed using the ASCE 7-22 standard.

The DOT project used the 975-year ARP hazard level. This is consistent with the level of other hazards considered for bridge design. Inundation maps were created following the procedure developed and used by the ASCE-7 standard. The 975-yr inundation map for Humboldt Bay is shown on the right panels in Figures 2-29 and 2-30. The runup elevation at Buhne Hill estimated by these three models ranges between 1.5 and 6.4 m (5 and 21 ft) relative to Mean High Water (MHW). The data used for these maps is available by request from the CGS. Note that the ASCE 7-22, DOT, and CGS maps for Humboldt Bay were all derived from the same set of models, with the only difference being that the CGS maps include minor adjustments to the inundation zones to correct for obvious mapping errors.

2.6.2.1.3 ASCE 7-28 Development

Updated tsunami hazard maps are being prepared as part of the ASCE 7-28 development. Update of these maps is primarily focused on a revision to the original source characterizations, and relies on a more community-based development of the rupture models used for the source logic trees (see Figure 2-31).

A major improvement in the ASCE 7-28 model is the more detailed geometry of the subduction zone interface and the modeling of splay faulting and various slip distribution models. Other changes include an improved bathymetry, and widening of the original offshore point locations from the 100-m (330-ft) contour to depths between 100 and 500 m (330 and 1,640 ft). The offshore portion of this effort is scheduled for completion in 2024, whereas the tsunami design zone maps for Oregon and Washington will be finalized by the end of 2025. Analyses for the California coastline adjacent to the CSZ are expected to follow, but there are no planned updates of the tsunami design zones yet.

As with the CGS tsunami hazard maps described above, the ASCE maps are also derived relative to current MHW, a typical datum for flooding studies. Sea-level rise extrapolations are not included in these maps, but the standard provides some guidance on how to account for them.

2.6.2.1.4 Cascadia Logic Tree

The updated Cascadia source model characterization being developed for ASCE 7-28 is significantly more complex and inclusive than that in the original URS (2007) model, which was

based on a narrow interpretation of the USGS source model with simplistic extensions related to slip distributions on the Cascadia fault. The logic tree for the recent ASCE 7-28 model is shown on Figure 2-31. It is based on the upcoming USGS National Seismic Hazard Model (NSHM), the Oregon Department of Geology and Mineral Resources (DOGAMI) model, and a workshop by the USGS Powell Center on tsunami sources (Ross et al., 2021) where the initial logic tree was developed. Follow-up work by Sypus et al. (2024) extended this model by adding numerous details such as an updated interface geometry based on recently acquired offshore surveys (CASIE) and input by specialists on Cascadia tectonics. The logic tree includes several branches on slip distributions (buried, surface-breaking), splay-faulting geometry and more.

While this model is very detailed and well-documented along the Oregon and Washington sections of the CSZ, less attention was paid to the California section. Specifically, the southern end is currently represented by a very simple interface geometry similar to that in the ASCE 7-16 model, without consideration for any crustal and/or splay faults like the LSF. Submarine landslides are not included in these maps for the same reasons as in ASCE 7-16/22. However, the contribution of coseismic submarine landslides to the tsunami hazard is to some extent included in the sigma term of the aleatory variability. Independent crustal faults are not included in these analyses either.

2.6.2.1.5 Offshore Tsunami Hazard

The updated offshore tsunami hazard model for ASCE 7-28 is currently under development for the Oregon and Washington coast and will be extended to the Humboldt Bay area in the near future.

2.6.3 Bathymetry

For the original URS (2007) tsunami study, an improved dataset for several areas around Humboldt Bay had been made available by the Center for Integrative Coastal Observation, Research and Education (CICORE), which is a consortium of several California State Universities. This dataset spans the North Bay (including North Spit), South Bay (including South Spit) and the main shipping channels (Figure 2-32, left panel). The data were obtained through high-resolution surveys using Portable Hyperspectral Imager for Low Light Spectroscopy (PHILLS), LiDAR, and Multibeam Sonar (Sound Navigation and Ranging). The data were resampled with a resolution of approximately 6 m (~19.7 ft) for the detailed inundation modelling.

In 2009, shortly after the URS (2007) report was completed, NOAA updated their model for Humboldt Bay which was subsequently used for the development of the tsunami inundation maps by CGS and ASCE 7-22. The most recent data available for the area is the 2019 lidar survey from NOAA. On Figures 2-32 and 2-33 we present comparisons between the URS (2007) model, the ASCE 7-22 model and the new lidar data. The largest differences appear to be in the North Bay area, but some of these variations may be because the vertical datum used for the lidar data may not the same as for the other two surface models. Around the ISFSI (Figure 2-33), there are also some large differences between the models, especially around the King Salmon, where the lidar model is superior to the others. It appears that the 2007 model overestimates the topography around Buhne Hill, whereas the ASCE model underestimates the topography.

Offshore, the model used for ASCE 7-22 shows significant more detail of the channels compared to the 2007 model, which is much smoother.

The following conclusions can be drawn by comparing these maps:

- The ASCE 7-22 bathymetry shows greater detail than the 2007 model, especially offshore, in the channels and farther out.
- While the 2019 lidar data includes some submarine datapoints, the resolution decreases quickly below a few meters, and apart from some nearshore areas and the wetlands to the north, the bathymetric part of this model is not useful.
- Alternatively, the 2019 lidar onshore topography shows more detail than the ASCE 7-22 and the 2007 models, and at first glance appears to be the more detailed model. In many cases, small topographical features that could significantly influence the tsunami inundation appear to be much better defined in the 2019 lidar model than in the previous two models.
- Further analysis using ground-truthing reference points would provide valuable confirmation, but at first glance a combination of offshore ASCE 7-22 bathymetry and onshore 2019 lidar topography appears to provide the most accurate DEM for the area.

2.6.4 2024 Update

The 2024 update used the CGS (2021) model by selecting two points, one on the seaward side and one on the leeward side of Buhne Hill making the profile X-X’ that crossed the ISFSI (Figure 2-30). The 2,475-year probabilistic scenario was selected as appropriate for the 20 year license extension for the ISFSI with the Humboldt Bay inundation extent shown in Figure (Figure 2-30). The points are 5.2 and 6 m (16.92 ft and 19.62 ft NAVD88) respectively, for the analysis showing the Buhne Hill staying above tsunami runup.

-

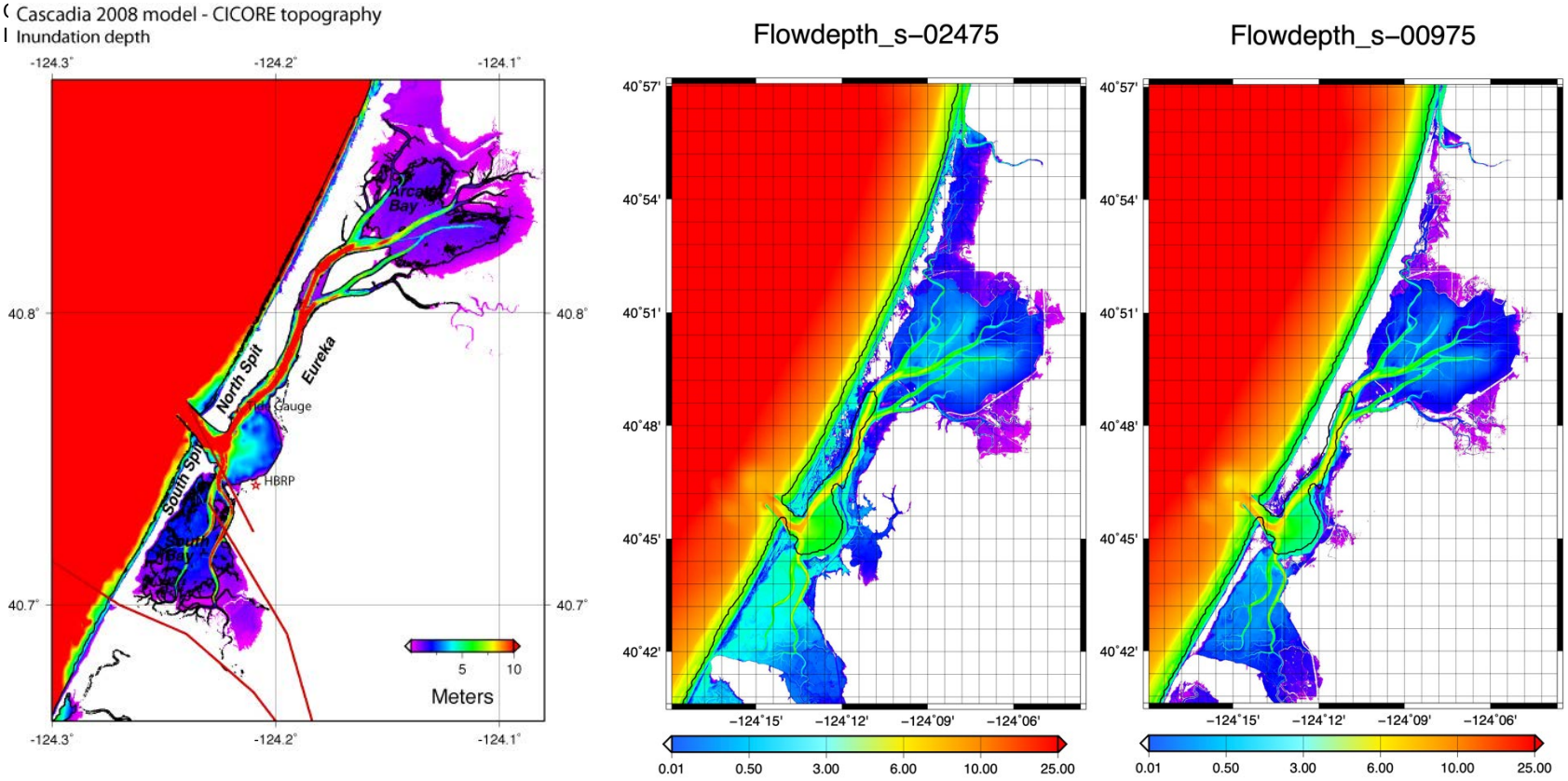

Figure 2-29. Comparison between the URS 2007 inundation model (left), ASCE 7-22 2,475-yr ARP model (middle) and the DOT 975-yr ARP model (right). Note the more extensive inundation throughout the area estimated by the 2,475-yr ARP model, with flooding over the North and South spits. The scale and areal coverage of the 2007 map on the left is different than for the maps in the middle and right.

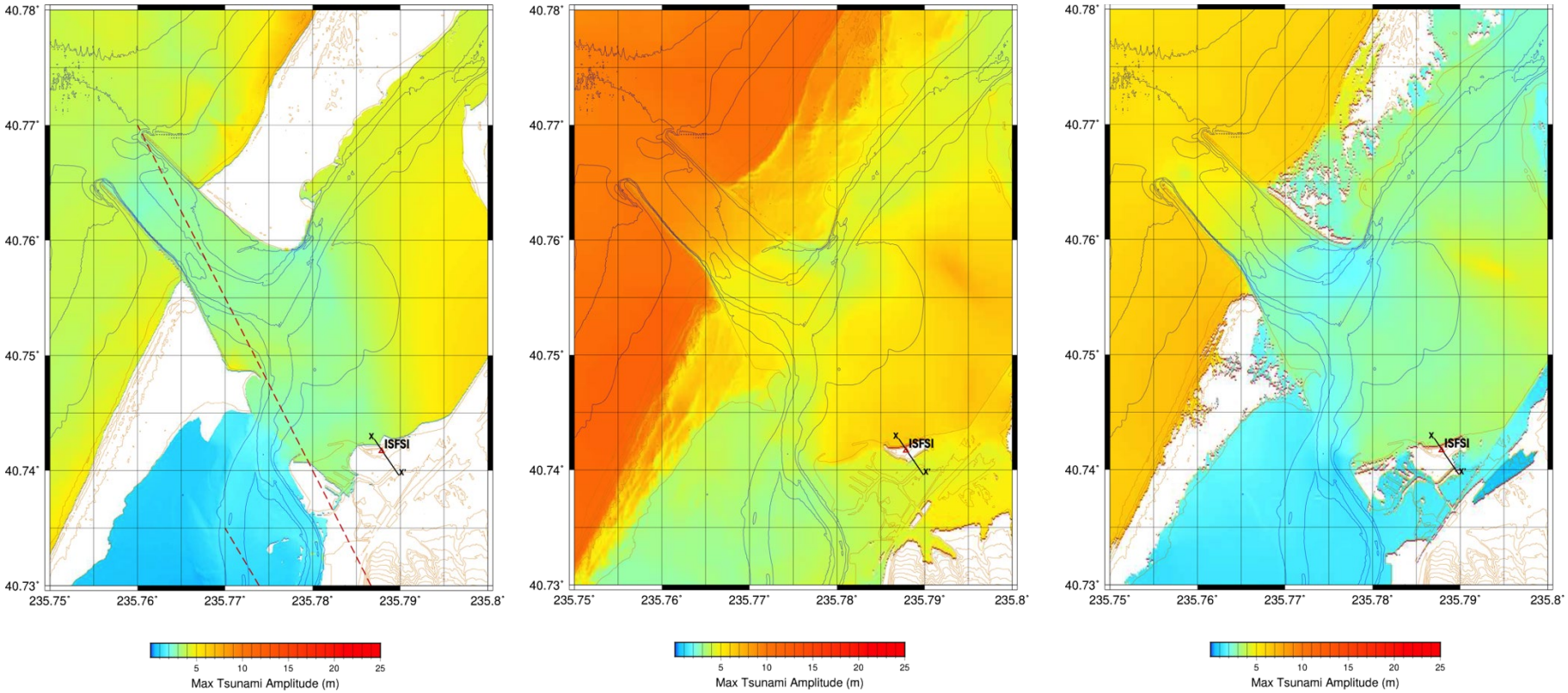

Figure 2-30. Close-up comparison of the inundation maps around PG&E's ISFSI with the URS 2007 model (left), ASCE 7-22 2,475-yr ARP model (middle), and ASCE 7-22 975-yr ARP model (right). In the 2007 model the local crustal faults are shown as dashed lines. The X-X' line is the location of the profile across Buhne Hill in Figure 3-1

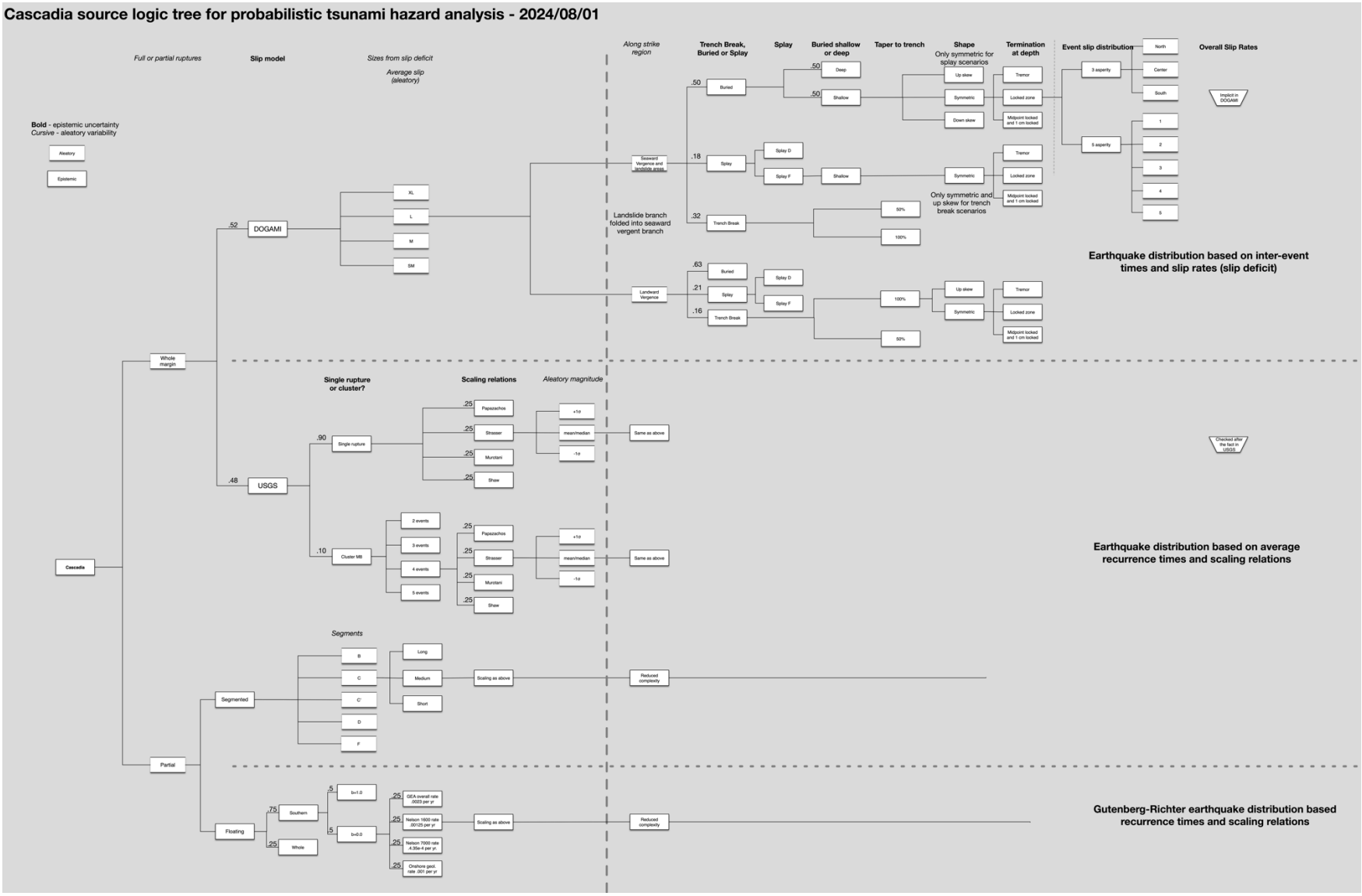

Figure 2-31. New logic tree for the probabilistic source characterization for ASCE 7-28.

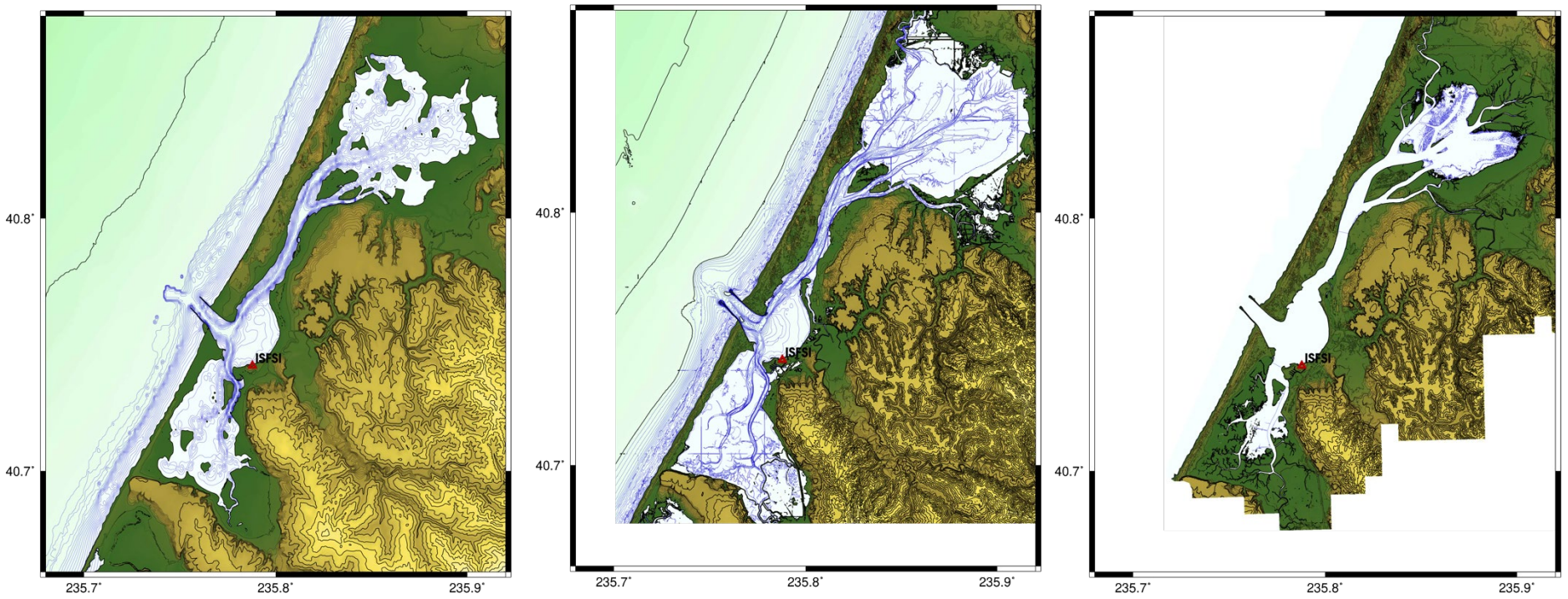

Figure 2-32. Comparison of the LiDAR elevation models for Humboldt Bay between the original URS (2007) study (left), ASCE 7-22 (middle) and 2019 data used for this tsunami assessment update (right). Note that while the first two datasets are referenced to MHW, the 2019 lidar data may have not been equalized to the same vertical datum, which may lead to differences of up to 2 m (~6.5 ft).

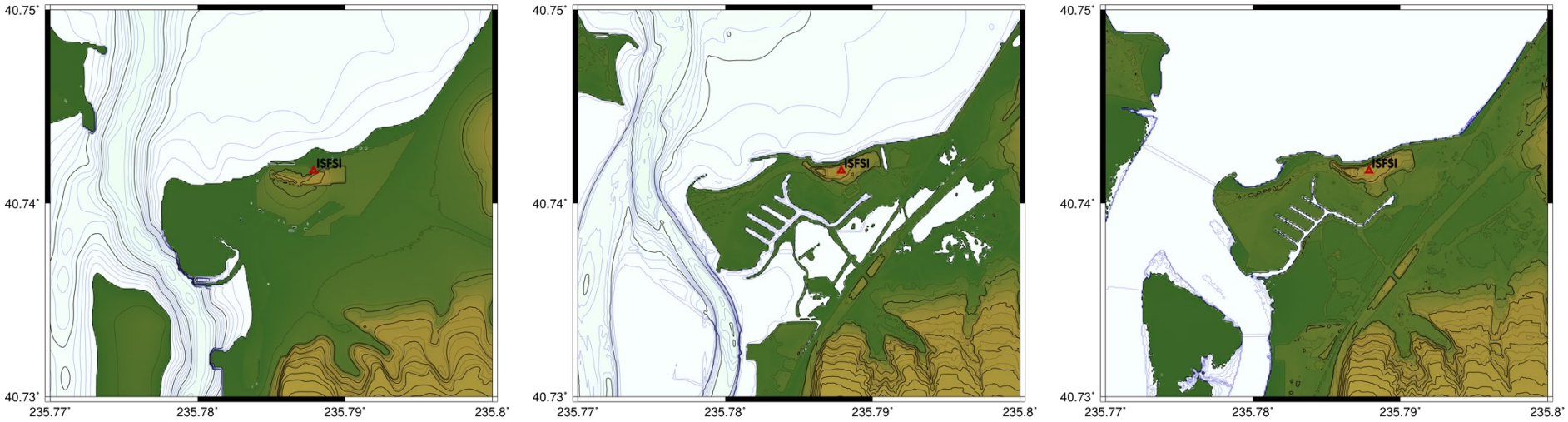

Figure 2-33. Close up of the previous maps around the PG&E facilities. URS (2007) model (left), ASCE 7-22 (middle), and 2019 lidar (right). Left two figures are relative to MHW. The vertical datum of the lidar model is to be determined.

3.0 CONCLUSIONS

This 2024 tsunami assessment update shows that the Humboldt Bay ISFSI is safe from potential tsunami inundation as informed by recent research findings and the review of updated tsunami modeling that has been conducted by others for the Humboldt Bay region. The safety margin (freeboard elevation above the estimated tsunami runup levels) is large enough to capture the margins of error in the runup estimates resulting from current uncertainties in the tsunami sources and in the assumptions and parameters used as inputs in the tsunami models.

This tsunami update for the Humboldt Bay ISFSI is based on new information and probabilistic modeling for estimated runups at Buhne Hill as shown on Figure 3-1. When compared to the earlier runup estimates shown on Figure 1-13 from Section 1, the updated probabilistic inundation level for a 2475-year event, which is a reasonable return period to consider for the 20-year license extension for the facility, are lower. Using the 2475-year return inundation levels, the ISFSI pad is 5.2 m (17 ft) above the projected runup height at the bluff, providing a safety margin (freeboard) from tsunami inundation. The previous 2015 estimates represent a deterministic scenario that was used for the ISFSI design.

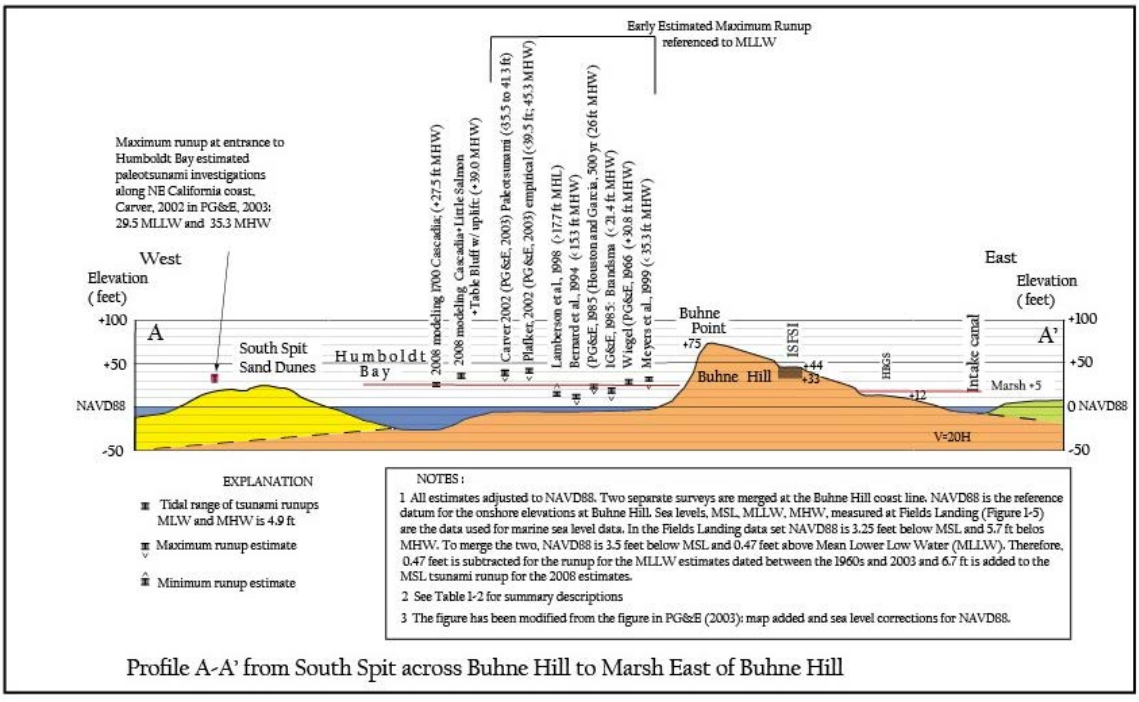

Figure 3-1. Schematic diagram showing previously estimated runup at the Humboldt Bay ISFSI and the 2024 update based on CGS (2021) 2,475-year scenario (modified from PG&E, 2003, Figure 9-20)

The 2024 probabilistic estimates, which incorporate the current research and understanding of tsunami sources and modeling approaches, fall within the 2015 deterministic estimates and within the range of earlier estimates. The estimates from paleotsunami and worldwide data are considered lower than estimated by the authors, so are very conservative estimates. Additionally, the ISFSI was designed as a below ground vault to provide safe containment of the spent fuel

casks even in the event that tsunami inundation would rise to the grade level of the facility, providing conservative defense-in-depth protection.

This chapter summarizes the key new information that was considered as part of the tsunami update for the Humboldt Bay ISFSI. The review consisted of peer-revied scientific publications and publicly available technical reports since the last major update in 2015 (Page and Nishenko, 2015). A summary of the historical background information compiled for the ISFSI through the year 2015 is presented in Chapter 1 and is not repeated here.

This update consisted of the compilation and analysis of the following data:

- Geologic information, including tectonic source model inputs for regional CSZ segmentation and local crustal fault characterization
- Hydrologic information, including new higher-resolution bathymetric data, sea level change projections, and reference datums
- Vertical land movement information using geodetic data to measure interseismic land uplift or subsidence
- Tsunami modeling performed since 2015
- Erosion potential around Buhne Hill as a result of strong tsunami currents

3.1 Geologic Source Information

High-resolution offshore imagery of the accretionary prism (Watt and Brothers, 2020; Hill et al., 2020; Carbotte et al., 2024) provides new information about offshore splay faults in Washington and Oregon (Wang and Tréhu, 2016; Aslam et al., 2021; Ledeczi et al., 2024). Modeling of these faults suggests they could be a high-angle source of large vertical displacements that in turn could produce significantly higher tsunamis than previously modeled for low-angle basal thrust faults as was observed in the 2011 Tohoku-Oki Japan earthquake. This should be taken in consideration for the Buhne Hill site for three reasons, especially if the LSF and the Mad River fault (MRF) are analogs to these kinds of faults:

- An offshore, high-angle LSF and/or MRF rupture could result in larger-than-previously modeled tsunami wave amplitudes
- These faults, being in the accretionary prism, are located closer to the coast than the basal thrust, thus decreasing tsunami arrival times
- If the LSF and/or MRF behave as splay faults and rupture coseismically with the CSZ, they could result in significant coseismic displacements onshore, either subsidence or uplift. Although sparse onshore evidence suggests these faults are low-angle reverse structures, they may be responsible for sufficient vertical displacement over the long-term, resulting in uplift of Buhne Hill

New paleoseismic and interseismic strain modeling of the LSF and associated crustal faults demonstrates the LSF is part of a complex and broad zone of active faults (including the Goose Lake and recently named Van Duzen faults). Materna et al. (2022) and McKenzie and Furlong (2021) modeled interseismic strain and concluded that about 20% of the convergence rate of the CSZ, amounting to about 8 mm/yr (0.31 in/yr), is shared between the LSF and MRF. However, it is not clear how that strain is distributed. Also, dextral shear bleeding north from the San Andreas fault is apparent in geodetic velocity models but not clearly observed in the geologic evidence.

Recurrence estimates for the southern CSZ have not changed significantly, although new segmentation models based on Episodic Tremor and Slip (ETS) events suggest that there may be fundamental segmentation, at least at the base of the seismogenic zone of the CSZ. This is based on observed spatial (structural) and temporal (deformation rates) differences. The southernmost reach of the CSZ appears to be confined to the southern limit of Siletzia (southern Oregon) and extends to the MTJ. Faults in the upper plate (Wells et al., 2017) may serve as fluid depressurization conduits, thus causing heterogeneity in the megathrust normal stress. Also, there is conjecture that the base of the seismogenic zone may coincide with the upper extent of the ETS zone (30 to 50 km [18.6 to 31 mi). This could help in modeling earthquake rupture depth and magnitude.

These new observations and data support recent arguments (see below) against the full-rupture model of Goldfinger et al. (2012) and the accuracy of the repeatability of **M** 9 earthquakes on the CSZ. For example, and counter to the full rupture model, Melgar (2021) modeled potential CSZ tsunamis and finds it is permissible that the 1700 C.E. event could have been just a southern CSZ event, and that the large tsunami detected in Japan was enhanced by near-vertical splay fault rupture in the offshore wedge (as discussed above). He recognizes that his proposed event would need to be followed closely in time by smaller (**M** ~8+) earthquakes to the north that would create the well-documented onshore subsidence signature, but would not create a tsunami large enough to be detected in Japan. One concern regarding this hypothesis is that the available dendrochronology data clearly identifies the time of death of trees along the length of CSZ to have occurred in the same year and possibly even in the same season, requiring a complete rupture involving several large earthquakes within the span of a year (or season).

3.2 Hydrologic Information

Sea level rise (SLR) estimates at Buhne Hill are not considerably different from those presented in previous assessments (Page and Nishenko, 2015; LCI, 2020), with the exception of the Ocean Protection Council (2024) rates that yield a maximum SLR estimate that is significantly higher than any of the earlier models proposed for the region (e.g., Montillet et al., 2018; He et al., 2022). The effect of SLR on tsunami runup estimations only becomes significant in projections 100 years or more in the future.

3.3 Vertical Land Movement

Crawford et al. (2022) suggest that the 1992 earthquake and uplift of the coast at Cape Mendocino was not related to the CSZ megathrust, but the distribution of marine terraces and lack of post-seismic strain recovery enforces the notion that the MTJ is a complicated area.

Paleoseismic evidence for the last four coastal marsh burial events in northern Humboldt Bay are thought to be associated with CSZ megathrust events (Padgett et al., 2021, 2022) and record subsidence of approximately 1 m (3.3 ft) each. This, combined with >2 mm/yr (>0.08 in/yr) of interseismic subsidence of the marsh deposits near Buhne Hill (Patton et al., 2017, 2023) suggest that a future CSZ event could result in coseismic subsidence and not uplift, as has been previously thought. However, the long-term preservation of the elevated Buhne Hill surface is counter to this short-term observation within the surrounding soft sediments. This should be explored for future hazard assessments of Buhne Hill, and this discrepancy should be either resolved, or an alternative mechanism (e.g., structural control for the coseismic uplift of Buhne

Hill as opposed to interseismic and/or coseismic subsidence for the Bay in general) should be considered.

3.4 Tsunami Modeling

Published and in-progress PTHA studies that became available since 2015 were reviewed as part of this update. The California Geological Survey (CGS, 2021) developed an extensive set of probabilistic tsunami hazard maps for most of the California coast, which includes a high-resolution (10-m [~33-ft.]) control grid that replaces the initial ASCE 7-16 inundation maps for California sites with the newer ASCE 7-22 maps. The CGS (2021) 2475-yr model for Humboldt Bay, which is based on ASCE 7-22, was used for a detailed runup at Buhne Hill and verifies that the ISFSI is 5.2 m (17 ft) above the projected runup height at the bluff and ~7.5 m (24 ft) on the leeward side of Buhne Hill.

3.5 Erosion Potential

Historical imagery attests to the erodibility of Buhne Hill bluff, especially since the construction of the Humboldt Bay jetties in the 19th century (Figure 1-4). Currently, the shoreline near the ISFSI is protected by a seaward-sloping riprap berm that has protected Buhne Hill from coastal erosion since it was installed in the 1950s and upgraded in the 1980s (PG&E, 2005). The top of the bluff is set 21 m (70 ft) away from the ISFSI providing protective buffer from potential erosion.

The riprap berm at the base of the bluff was designed for storm wave erosion. PG&E performs periodic inspection and maintenance of the riprap berm, and this is an important ongoing effort to provide some defense against sea level rise and scour by distant tsunamis.

Continued periodic inspections and maintenance of the riprap berm along the shoreline base of Buhne Hill are important continuing actions by PG&E to provide protection of the slope against storm wave erosion and partial mitigation against possible future tsunami wave erosion.

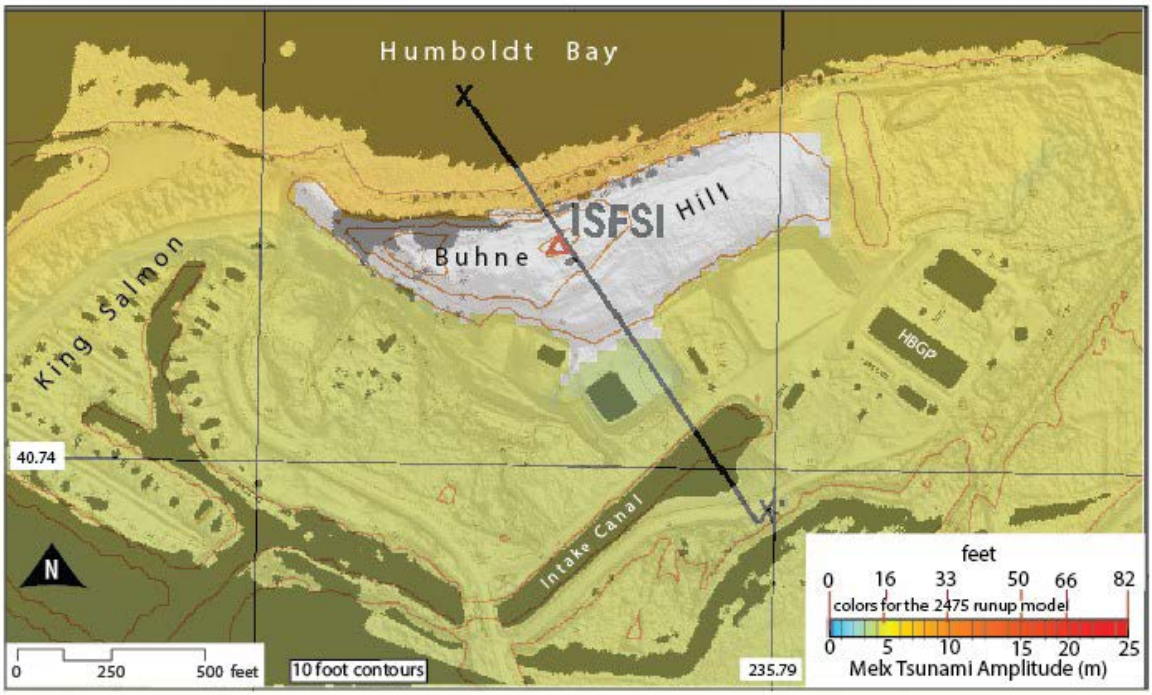

DEM of Buhne Hill Showing the 2475 Year Tsunami Inundation Levels

EXPLANATION

Qc	Colluvium
Qpm	Intertidal marsh, silt and peat
Qt	Marine terrace, Pleistocene 80 ka
Qh	Hookton Fm, Pleistocene marine siltstone

NOTES:

Two separate surveys are merged at the Buhne Hill coast line. NAVD88 is the reference datum for the onshore elevations at Buhne Hill. Sea levels, MSL, MLLW, MHW, measured at Fields Landing (Figure 1-5) are the data used for marine sea level data. In the Fields Landing data set NAVD88 is located 3.5 feet below MSL. To merge the two, NAVD88 is 3.5 feet below MSL. Therefore, 3.5 feet is added to the tsunami runup.

The Cross section shows the point tsunami elevation on the Buhne Hill bluff and on the leaward side west of the Intake Canal

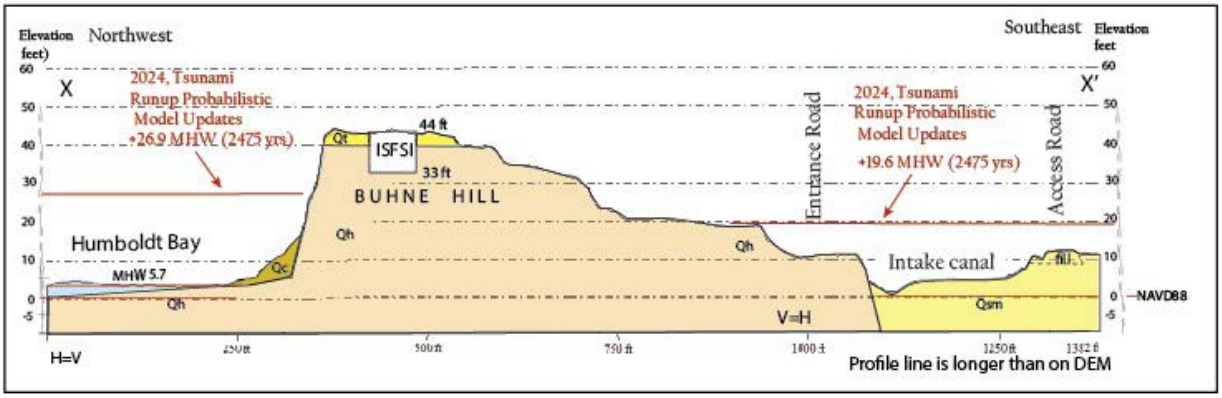

Figure 3-2. Probabilistic tsunami runup modeling results for Buhne Hill and vicinity. (Top) Map view, with lidar DEM as background, overlain by 2475-yr model runup heights in meters. (Bottom) Updated 2024 geologic cross section showing the estimated 2475-yr-model runup (in feet) at the bluff and leeward sides. These runups are based on the CGS (2021) models.

3.6 Continued Monitoring and Research

Because research on the CSZ and other potential tsunami sources is ongoing, and tsunami modeling continues to advance, PG&E regularly re-evaluates the most recently available information as part of its due diligence under the Long-Term Seismic Program (LTSP). This update addresses the new data and advances in modeling developed since 2015. Where appropriate, and as part of these updates, PG&E may also identify maintenance and/or monitoring activities for the purpose of assessing future potential changing conditions that could require the implementation of new defense-in-depth measures for the facility. Based on the results of the current update, which indicate that the ISFSI is not likely to be impacted by a tsunami generated by an earthquake on the CSZ or another near-source fault, tsunami mitigation actions are not deemed necessary and are thus not proposed herein.

4.0 REFERENCES

Abramson, H. F. (1998). Evidence for tsunamis and earthquakes during the last 3500 years from Lagoon Creek, a coastal freshwater marsh, northern California [Masters Thesis]. Humboldt State University.

Admire, A. R., Dengler, L. A., Crawford, G. B., Uslu, B. U., Borrero, J. C., Greer, S. D., & Wilson, R. I. (2014). Observed and Modeled Currents from the Tohoku-oki, Japan and other Recent Tsunamis in Northern California. Pure and Applied Geophysics, 171(12), 3385–3403. https://doi.org/10.1007/s00024-014-0797-8

Admire, A. R., Dengler, L., Crawford, G., Uslu, B., Montoya, J., & Wilson, R. (2011). Observed and Modeled Tsunami Currents on California's North Coast. AGU Fall Meeting Abstracts, 03.

Alhamid, A.K., Akiyama, M., Ishibashi, H., Aoki, K., Koshimura, S., and Frangopol, D.M., 2022, Framework for probabilistic tsunami hazard assessment considering the effects of sea-level rise due to climate change: Structural Safety, v. 94, p. 102152, doi:10.1016/j.strusafe.2021.102152.

American Society of Civil Engineers (ASCE), 2017. Minimum Design Loads and Associated Criteria for Buildings and Other Structures (7-16).

American Society of Civil Engineers (ASCE), 2023. Minimum Design Loads and Associated Criteria for Buildings and Other Structures (7-22).

Aslam, K.S., Thomas, A.M., and Melgar, D., 2021, The Effect of Fore-Arc Deformation on Shallow Earthquake Rupture Behavior in the Cascadia Subduction Zone: Geophysical Research Letters, v. 48, p. e2021GL093941, doi:10.1029/2021GL093941.

Atwater, B.F., 1987, Evidence for Great Holocene Earthquakes Along the Outer Coast of Washington State: Science, v. 236, p. 942–944, doi:10.1126/science.236.4804.942.

Atwater, B.F., and Hemphill-Haley, E., 1997, Recurrence Intervals for Great Earthquakes of the Past 3500 Years at Northeastern Willapa Bay, Washington: v. 1576, p. 108.

Atwater, B.F., Carson, B., Griggs, G.B., Johnson, H.P., and Salmi, M.S., 2014, Rethinking turbidite paleoseismology along the Cascadia subduction zone: Geology, v. 42, p. 827–830, doi:10.1130/G35902.1.

Atwater, B.F., Musumi-Rokkaku, S., Satake, K., Tsuji, Y., Ueda, K., and Yamaguchi, D.K., 2005, The orphan tsunami of 1700—Japanese clues to a parent earthquake in North America: Seattle, WA / Washington, D.C., University of Washington Press and U.S. Geological Survey Professional Paper 1707, 135 p., http://pubs.er.usgs.gov/publication/pp1707 (accessed May 2020).

Atwater, B.F., Tuttle, M.P., Schweig, E.S., Rubin, C.M., Yamaguchi, D.K., and Hemphill-Haley, E., 2003, Earthquake recurrence inferred from paleoseismology, in Developments in Quaternary Sciences, Elsevier, v. 1, p. 331–350, doi:10.1016/S1571-0866(03)01015-7.

Bahuguna, A., Nayak, S., & Roy, D. (2008). Impact of the tsunami and earthquake of 26th December 2004 on the vital coastal ecosystems of the Andaman and Nicobar Islands assessed using RESOURCESAT AWiFS data. International Journal of Applied Earth Observation and Geoinformation, 10(2), 229–237. https://doi.org/10.1016/j.jag.2008.02.010

Balster-Gee, A.F., Hill, J.C., and O'Brien, T.F., 2020b, Archive of boomer sub bottom data collected off shore Eureka, California during USGS field activity W-1-96-NC from 1996-06-29 to 1996-07-07: US Geological Survey Data Release, doi:https://doi.org/10.5066/ P950276G.

Balster-Gee, A.F., Kluesner, J.W., Watt, J.T., Hill, J.C., Brothers, D.S., Michalak, M.J., and O'Shea, D., 2020a, Multichannel minisparker seismic reflection data of USGS field activity 2018-658-FA

collected between Cape Blanco and the Mendocino Triple Junction from 2018-10-04 to 2018-10-18: US Geological Survey Data Release, doi:https://doi.org/10.5066/P9R3QM97.

Bartlow, N.M., 2020, A Long-Term View of Episodic Tremor and Slip in Cascadia: Geophysical Research Letters, v. 47, p. e2019GL085303, doi:10.1029/2019GL085303.

Beeson, J.W., Goldfinger, C., and Fortin, W.F., 2017, Large-scale modification of submarine geomorphic features on the Cascadia accretionary wedge caused by catastrophic flooding events: Geosphere, v. 13, p. 1713–1728, doi:10.1130/GES01388.1.

Bernard, E., Mader, C., Curtis G., and Satake, K., 1994, Tsunami inundation model study of Eureka and Crescent City, California, NOAA Technical Memorandum ERL PMEL-103, 80 pp.

Bilek, S.L., and Lay, T., 2018, Subduction zone megathrust earthquakes: Geosphere, v. 14, p. 1468–1500, doi:10.1130/GES01608.1.

Blackwell E, Shirzaei M, Ojha C, Werth S. Tracking California's sinking coast from space: Implications for relative sea-level rise. Sci Adv. 2020 Jul 31;6(31):eaba4551. doi: 10.1126/sciadv.aba4551

Blackwell, E., Shirzaei, M., Ojha, C., and Werth, S., 2020, Tracking California's sinking coast from space: Implications for relative sea-level rise: Science Advances, v. 6, p. eaba4551, doi:10.1126/sciadv.aba4551.

Bodmer, M., Toomey, D.R., Hooft, E.E.E., and Schmandt, B., 2018, Buoyant Asthenosphere Beneath Cascadia Influences Megathrust Segmentation: Geophysical Research Letters, v. 45, p. 6954–6962, doi:10.1029/2018GL078700.

Bold, S.E., and Michalak, M.J., 2022, Incision And Deformation Of The Yager Creek–Van Duzen River Fluvial Terraces From Qua- ternary Mapping And Geochronology: Triangle of Doom V.2 - Archeology, Stratigraphy, Tectonics, Geomorphology, and Geophysics in the Region of the Mendocino Triple Junction, p. 101–108.

Bombardier, M., Cassidy, J.F., Dosso, S.E., and Kao, H., 2024, Spatial Distribution of Tremor Episodes From Long-Term Monitoring in the Northern Cascadia Subduction Zone: Journal of Geophysical Research: Solid Earth, v. 129, p. e2024JB029159, doi:10.1029/2024JB029159.

Borrero, J. C., Lynett, P. J., & Kalligeris, N. (2015). Tsunami currents in ports. Philosophical Transactions of the Royal Society A: Mathematical, Physical and Engineering Sciences, 373(2053), 20140372. https://doi.org/10.1098/rsta.2014.0372

Brandsma, M., Divoky, D., & Hwang, L.S. (1979). Tsunami atlas for the coasts of the United States. U.S. Nuclear Regulatory Commission. Division of Reactor Safety Research.; NRC FIN no. B-3016, NUREG/CR-1106, TC-486, Tetra Tech, Inc.

Brudzinski, M.R., and Allen, R.M., 2007, Segmentation in episodic tremor and slip all along Cascadia: Geology, v. 35, p. 907, doi:10.1130/G23740A.1.

Burgette, R.J., Weldon, R.J., and Schmidt, D.A., 2009, Interseismic uplift rates for western Oregon and along-strike variation in locking on the Cascadia subduction zone: Journal of Geophysical Research: Solid Earth, v. 114, p. 2008JB005679, doi:10.1029/2008JB005679.

Burke, R.M., and Carver, G.A., (eds), 1992, A look at the southern end of the Cascadia subduction zone and the Mendocino triple junction: Guidebook for the Pacific Cell Friends of the Pleistocene Field Trip to Coastal Northern California: 256 p.

California Coastal Commission, 2015, California Coastal Commission Draft Sea-Level Rise Policy Guidance,

California Geological Survey. (2021). California Official Tsunami Inundation Maps. California Department of Conservation. https://www.conservation.ca.gov/cgs/tsunami/maps

Carbotte, S.M. et al., 2024, Subducting plate structure and megathrust morphology from deep seismic imaging linked to earthquake rupture segmentation at Cascadia: Science Advances, v. 10, p. eadl3198, doi:10.1126/sciadv.adl3198.

Carver, G. A., Abramson, H. A., Garrison-Laney, C. E., & Leroy, T. H. (1998). Investigation of paleotsunami evidence along the north coast of California (p. 238). prepared for Pacific Gas and Electric Company.

Carver, G.A., Abramson, H.A., Garrison-Laney, C.E., and Leroy, T., 1998, Paleotsunami evidence of subduction earthquakes for northern California: Final Report for Pacific Gas and Electric Co., 164 p., plus appendices. In URS, 2008.

Carver, G.A., and Plafker, G., 2008, Paleoseismicity and neotectonics of the Aleutian Subduction Zone—An overview, in Active Tectonics and Seismic Potential of Alaska, Washington, D.C., American Geophysical Union Geophysical Monograph Series, v. 179, p. 43–63, http://adsabs.harvard.edu/abs/2008GMS...179...43C (accessed June 2020).

Crawford, B., Hartshorn, E., Hemphill-Haley, M., and Michalak, M., 2022, A New Look at Coastal Uplift and Holocene Marine Terrace Formation South of Cape Mendocino, California, in p. 42–49.

Davies, G., Griffin, J., Løvholt, F., Glimsdal, S., Harbitz, C., Thio, H. K., Lorito, S., Basili, R., Selva, J., Geist, E., & Baptista, M. A. (2018). A global probabilistic tsunami hazard assessment from earthquake sources. Geological Society, London, Special Publications, 456(1), 219–244. https://doi.org/10.1144/SP456.5

De Risi, R., and Goda, K., 2016, Probabilistic Earthquake–Tsunami Multi-Hazard Analysis: Application to the Tohoku Region, Japan: Frontiers in Built Environment, v. 2, doi:10.3389/fbuil.2016.00025.

Dragert, H., Wang, K.-K., and James, T., 2001, Episodic Silent Slip: A New Aspect of Cascadia Megathrust Behaviour: AGU Fall Meeting Abstracts,.

Engelhart, S.E., Hemphill-Haley, E., Kelsey, H.M., and Padgett, J.S., 2016, Refined Estimates of Coseismic Subsidence along the Southern Cascadia Subduction Zone in Northern Humboldt Bay (Arcata Bay): Collaborative Research with University of Rhode Island and Humboldt State University: U.S. Geological Survey NERHP Final Technical Report G14AP00128, G14AP00129, 38 p.

Fan, J., and Zhao, D., 2021, Subslab heterogeneity and giant megathrust earthquakes: Nature Geoscience, v. 14, p. 349–353, doi:https://doi.org/10.1038/s41561-021-00728-x.

Feldens, P., Schwarzer, K., Szczuciński, W., Stattegger, K., Sakuna, D., & Somgpongchaiykul, P. (2009). Impact of 2004 Tsunami on Seafloor Morphology and Offshore Sediments, Pakarang Cape, Thailand. Polish Journal of Environmental Studies, 18(1), 63–68.

Frederikse, T. et al., 2020, The causes of sea-level rise since 1900: Nature, v. 584, p. 393–397, doi:10.1038/s41586-020-2591-3.

Freymueller, J.T., Haeussler, P.J., Wesson, R.L., and Ekström, G., 2013, Active Tectonics and Seismic Potential of Alaska: John Wiley & Sons, 850 p.

Gao, X., and Wang, K., 2017, Rheological separation of the megathrust seismogenic zone and episodic tremor and slip: Nature, v. 543, p. 416–419, doi:10.1038/nature21389.

Garrison-Laney, C. E. (1998). Diatom evidence for tsunami inundation from Lagoon Creek, a coastal freshwater pond, Del Norte County, California [Masters Thesis, Humboldt State University]. http://dspace.calstate.edu/handle/10211.3/140561

Goda, K., 2023, Probabilistic Tsunami Hazard Analysis for Vancouver Island Coast Using Stochastic Rupture Models for the Cascadia Subduction Earthquakes: GeoHazards, v. 4, p. 217–238, doi:10.3390/geohazards4030013.

Goda, K., 2023, Statistical characterization of full-margin rupture recurrence for Cascadia subduction zone using event time resampling and Gaussian mixture model: Geoscience Letters, v. 10, p. 52, doi:10.1186/s40562-023-00306-6.

Goldfinger, C. et al., 2012, Turbidite event history—Methods and implications for Holocene paleoseismicity of the Cascadia subduction zone: U.S. Geological Survey Professional Paper Professional Paper 1661-F, 170 p.

Goldfinger, C., Kulm, L.D., Yeats, R.S., McNeill, L., and Hummon, C., 1997, Oblique strike-slip faulting of the central Cascadia submarine forearc: Journal of Geophysical Research: Solid Earth, v. 102, p. 8217–8243, doi:10.1029/96JB02655.

Goldfinger, C., Morey, A.E., Black, B., Beeson, J., Nelson, C.H., and Patton, J., 2013, Spatially limited mud turbidites on the Cascadia margin: segmented earthquake ruptures? Natural Hazards and Earth System Sciences, v. 13, p. 2109–2146, doi:10.5194/nhess-13-2109-2013.

Goldfinger, C., Wong, I., Kulkarni, R., and Beeson, J., 2016, Reply to "Comment on 'Statistical Analyses of Great Earthquake Recurrence along the Cascadia Subduction Zone' by Ram Kulkarni, Ivan Wong, Judith Zachariasen, Chris Goldfinger, and Martin Lawrence" by Allan Goddard Lindh: Bulletin of the Seismological Society of America, v. 106, doi:10.1785/0120150282.

Gomberg, J., 2018, Cascadia Onshore-Offshore Site Response, Submarine Sediment Mobilization, and Earthquake Recurrence: Journal of Geophysical Research: Solid Earth, v. 123, p. 1381–1404, doi:10.1002/2017JB014985.

González, F. I., Geist, E. L., Jaffe, B., Kânoğlu, U., Mofjeld, H., Synolakis, C. E., Titov, V. V., Arcas, D., Bellomo, D., Carlton, D., Horning, T., Johnson, J., Newman, J., Parsons, T., Peters, R., Peterson, C., Priest, G., Venturato, A., Weber, J., … Yalciner, A. (2009). Probabilistic tsunami hazard assessment at Seaside, Oregon, for near- and far-field seismic sources. Journal of Geophysical Research: Oceans, 114(C11). https://doi.org/10.1029/2008JC005132

Graehl, N.A., Kelsey, H.M., Witter, R.C., Hemphill-Haley, E., and Engelhart, S.E., 2015, Stratigraphic and microfossil evidence for a 4500-year history of Cascadia subduction zone earthquakes and tsunamis at Yaquina River estuary, Oregon, USA: Geological Society of America Bulletin, v. 127, p. 211–226, doi:10.1130/B31074.1.

Hall, K., Houston, H., and Schmidt, D., 2018, Spatial Comparisons of Tremor and Slow Slip as a Constraint on Fault Strength in the Northern Cascadia Subduction Zone: Geochemistry, Geophysics, Geosystems, v. 19, p. 2706–2718, doi:10.1029/2018GC007694.

Harrichhausen, N., Morell, K.D., and Regalla, C., 2024, Forearc faults in northern Cascadia do not accommodate elastic strain driven by the megathrust seismic cycle: Seismica, v. 2, doi:10.26443/seismica.v2i4.1177.

Hartshorn, E., Crawford, B., Hemphill-Haley, M., and Michalak, M., 2022, An Abrupt Transition: Documenting Changes in Marine Terrace Morphology Across Cape Mendocino, California: Triangle of Doom V.2 - Archeology, Stratigraphy, Tectonics, Geomorphology, and Geophysics in the Region of the Mendocino Triple Junction - FOP Guidebook, p. 50–54.

Hayes, G.P., Moore, G.L., Portner, D.E., Hearne, M., Flamme, H., Furtney, M. & Smoczyk, G.M., 2018. Slab2, a comprehensive subduction zone geometry model. Science, 362, 58–61. doi:10.1126/science.aat4723

Hazarika, H., Kasama, K., Suetsugu, D., Kataoka, S., & Yasufuku, N. (2013). Damage to Geotechnical Structures in Waterfront Areas of Northern Tohoku Due to the March 11, 2011 Tsunami Disaster. Indian Geotechnical Journal, 43(2), 137–152. https://doi.org/10.1007/s40098-012-0021-7

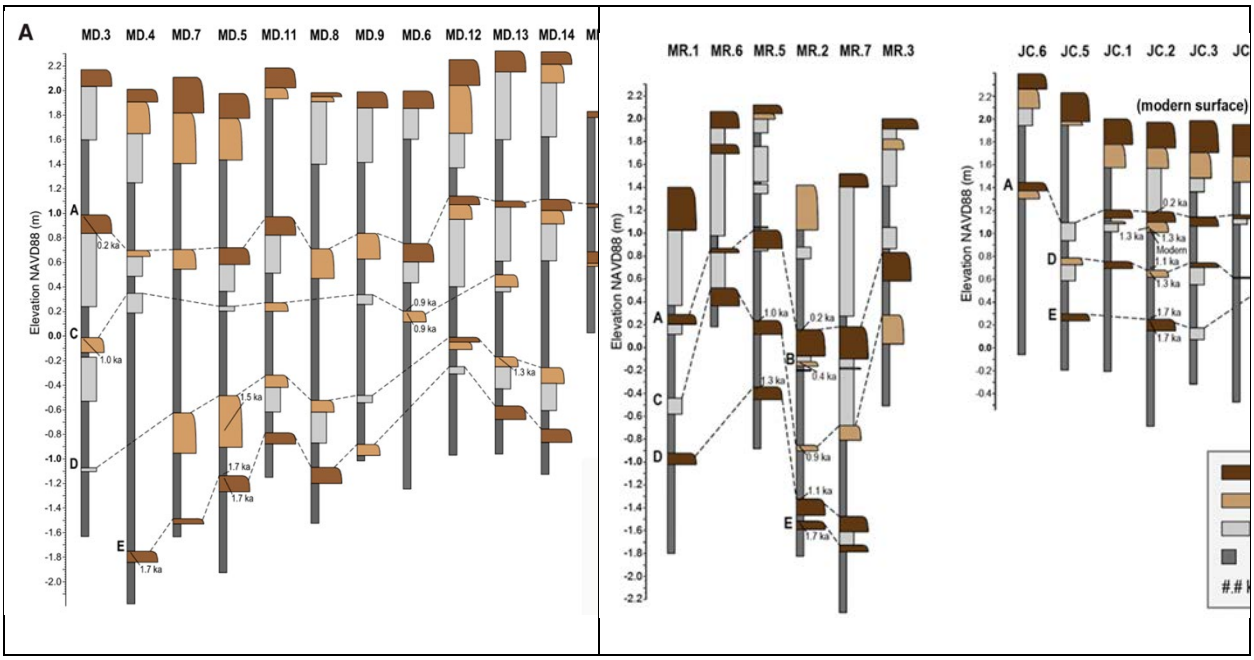

Figure 2-15. Core diagrams (from Padgett et al., 2021, 2022) showing multiple times in the past that areas of northern Humboldt Bay coseismically subsided and former marshes (indicated by the dark reddish brown to brown "peat" intervals) were buried by thick accumulations of intertidal mud (indicated by gray intervals). Following subsidence, the land builds back up over time to an elevation high enough to support marsh growth again, until the next great earthquake and subsequent burial.
MD = McDaniel Creek; MR = Mad River Slough; JC = Jacoby Creek.

2.3.1 Coseismic and Interseismic Uplift

As mentioned in Section 2.3 above, there is no direct evidence for coseismic uplift along the CSZ related to megathrust earthquakes, as all studied sites show evidence of coseismic subsidence (e.g., Nelson et al., 2006; Hutchinson and Clague, 2017). However, an uplift signal has been documented along the north coast of Humboldt County (Woodward-Clyde Consultants, 1980; Burke and Carver, 1992; Swan et al., 2002; McCrory, 2000), and uplift is also indicated from Humboldt Bay to northern Washington by a series of marine terraces at least 200,000 years old in the coastal hills above the coast. This permanent, long-term strain signal is interpreted as evidence that megathrust earthquakes do not completely release all interseismic elastic strain stored along the subduction zone (Stanton et al., 2024). At Humboldt Bay, these terraces are thought to record the progressive regional uplift of the accretionary sediments above the megathrust, while adjacent synclines (i.e., Arcata Bay – Freshwater Syncline and South Bay – South Bay Syncline) are absent of terraces, indicating that these low-lying areas do not record the regional uplift signal seen elsewhere in Humboldt Bay (Figure 2-16). An older record of uplift is noted in the separation of the base of Neogene sediments forming the cores of the folds where it is estimated that more than 3,400 m (~11,150 ft.) of separation exists across the Little Salmon and Table Bluff faults (Ogle, 1953; Kelsey and Carver, 1988; Swan et al., 2002; Vadurro, 2006). These terraces record a longer-term trend of tectonic uplift that has accumulated over many episodes of megathrust activity and not the interspersed, episodic coseismic events.

IPCC, 2019, Summary for Policymakers, In: IPCC Special Report on the Ocean and Cryosphere in a Changing Climate: Intergovernmental Panel on Climate Change.

IPCC, 2022, The Ocean and Cryosphere in a Changing Climate: Special Report of the Intergovernmental Panel on Climate Change: Intergovernmental Panel on Climate Change, doi:10.1017/9781009157964.

Jacoby, G.C., Carver, G.A., and Wagner, W., 1995, Trees and herbs killed by an earthquake ~300 yr ago at Humboldt Bay, California: Geology, v. 23, p. 77–80, doi:10.1130/0091-7613(1995)023<0077:TAHKBA>2.3.CO;2.

Kelsey, H.M., and Carver, G.A., 1988, Late Neogene and Quaternary tectonics associated with northward growth of the San Andreas Transform Fault, northern California: Journal of Geophysical Research: Solid Earth, v. 93, p. 4797–4819, doi:10.1029/JB093iB05p04797.

Kulkarni, R., Wong, I., Zachariasen, J., Goldfinger, C., and Lawrence, M., 2013, Statistical Analyses of Great Earthquake Recurrence along the Cascadia Subduction Zone: Bulletin of the Seismological Society of America, v. 103, p. 3205–3221, doi:10.1785/0120120105.

La Selle, S.M., Nelson, A.R., Witter, R.C., Jaffe, B.E., Gelfenbaum, G., and Padgett, J.S., 2024, Testing Megathrust Rupture Models Using Tsunami Deposits: Journal of Geophysical Research: Earth Surface, v. 129, p. e2023JF007444, doi:10.1029/2023JF007444.

Ladinsky, T., Kelsey, H., Michalak, M., Witter, R., and Bold, S., 2022a, A Paleoseismic and Geomorphic Investigation of the Central Segment of the Little Salmon Fault, Humboldt County, CA: Triangle of Doom V.2 - Archeology, Stratigraphy, Tectonics, Geomorphology, and Geophysics in the Region of the Mendocino Triple Junction - FOP Guidebook, p. 114–130.

Ladinsky, T., Kelsey, H., Michalak, M., Witter, R., and Bold, S., 2022b, A Paleoseismic Investigation of the Goose Lake Fault, Humboldt County, CA: Triangle of Doom V.2 - Archeology, Stratigraphy, Tectonics, Geomorphology, and Geophysics in the Region of the Mendocino Triple Junction, p. 108–113.

Lamberson, R.H., Grimes, S. and Scarr, D., 1998, A tsunami simulation and shoreline inundation model for Humboldt Bay, pilot study: Report to PG&E Geosciences Department, 43 p.

Lander, J. F., Lockridge, P. A., & Kozuch, M. J. (1993). Tsunamis Affecting the West Coast of the United States, 1806-1992 (No. 29; NGDC Key to Geophysical Records, p. 254). National Oceanic and Atmospheric Administration.

Ledeczi, A., Lucas, M., Tobin, H., Watt, J., and Miller, N., 2024, Late Quaternary Surface Displacements on Accretionary Wedge Splay Faults in the Cascadia Subduction Zone: Implications for Megathrust Rupture: Seismica, v. 2, doi:10.26443/seismica.v2i4.1158.

Leroy, T.H., 2006, Coastal sand dune stratigraphy and geomorphology of the North Spit of Humboldt Bay: Paper 3-2-C in Friends of the Pleistocene, Pacific Cell 2006, Signatures of Quaternary crustal deformation and landscape evolution in the Mendocino deformation zone, NW California: pp. 269-280. Lettis, W.R., and Thompson, S.C., 2020, Estimated 100-year Relative Sea-Level Change at Buhne Hill, Humboldt County, California:, 15 p.

Lettis, W.R., and Thompson, Steven C., 2020, Estimated 100-year Relative Sea-Level Change at Buhne Hill, Humboldt County, California, 15 p, prepared for PG&E.

Li, L., Switzer, A.D., Wang, Y., Chan, C.-H., Qiu, Q., and Weiss, R., 2018, A modest 0.5-m rise in sea level will double the tsunami hazard in Macau: Science Advances, v. 4, p. eaat1180, doi:10.1126/sciadv.aat1180.

Li, W.-H., 1992, Evidence for the late Holocene coseismic subsidence in the Lower Eel River valley, Humboldt county, Northern California: An application of foraminiferal zonation to indicate tectonic submergence [Masters Thesis]: Humboldt State University.

Lindh, A., 2016, Comment on “Statistical Analyses of Great Earthquake Recurrence along the Cascadia Subduction Zone” by Ram Kulkarni, Ivan Wong, Judith Zachariasen, Chris Goldfinger, and Martin Lawrence: Bulletin of the Seismological Society of America, v. 106, doi:10.1785/0120150069.

Luo, Y., and Liu, Z., 2019, Rate-and-State Model Casts New Insight into Episodic Tremor and Slow-slip Variability in Cascadia: Geophysical Research Letters, v. 46, p. 6352–6362, doi:10.1029/2019GL082694.

Lynett, Patrick, Hong Kie Thio, Michael Scott, Tom Murphy, Tom Shantz, Jian-Dzwan Shen, 2021. VALIDATION OF TSUNAMI DESIGN GUIDELINES FOR COASTAL BRIDGES, Final Report, PROJECT TPF 5(307) for Oregon Department of Transportation and Federal Highway Administration

Magoon, O. T. (1965). Structural Damage by Tsunamis. American Society of Civil Engineers Specialty Conference on Coastal Engineering, 35–68.

Materna, K., Murray, J., Pollitz, F., and Patton, J.R., 2022, Interseismic Fault Loading in California’s North Coast Constrained by Geodetic Data:Triangle of Doom V.2 - Archeology, Stratigraphy, Tectonics, Geomorphology, and Geophysics in the Region of the Mendocino Triple Junction - FOP Guidebook, p. 196-198.

McAdoo, B. G., Ah-Leong, J. S., Bell, L., Ifopo, P., Ward, J., Lovell, E., & Skelton, P. (2011). Coral reefs as buffers during the 2009 South Pacific tsunami, Upolu Island, Samoa. Earth-Science Reviews, 107(1), 147–155. https://doi.org/10.1016/j.earscirev.2010.11.005

McCrory, P.A., 2000, Upper plate contraction north of the migrating Mendocino triple junction, northern California: Implications for partitioning of strain: Tectonics, v. 19, p. 11441160.

McKenzie, K.A., and Furlong, K.P., 2021, Isolating non-subduction-driven tectonic processes in Cascadia: Geoscience Letters, v. 8, p. 10, doi:10.1186/s40562-021-00181-z.

McKenzie, K.A., Kelsey, H.M., Kirby, E., Rittenour, T.M., and Furlong, K.P., 2022, Differential coastal uplift quantified by luminescence dating of marine terraces, central Cascadia forearc, Oregon: Quaternary Science Reviews, v. 298, p. 107853, doi:10.1016/j.quascirev.2022.107853.

McPherson, R.C., Patton, J.R., and Hemphill-Haley, M., 2022, A Sequence of Earthquakes Beyond the Northern San Andreas and Their Connection to Singley Flat Terraces: Triangle of Doom V.2 - Archeology, Stratigraphy, Tectonics, Geomorphology, and Geophysics in the Region of the Mendocino Triple Junction - FOP Guidebook, p. 77–82.

Melgar, D., 2021, Was the January 26th, 1700 Cascadia Earthquake Part of a Rupture Sequence? Journal of Geophysical Research: Solid Earth, v. 126, p. e2021JB021822, doi:10.1029/2021JB021822.

Melgar, D., Williamson, A.L., and Salazar-Monroy, E.F., 2019, Differences between heterogenous and homogenous slip in regional tsunami hazards modelling: Geophysical Journal International, v. 219, p. 553–562, doi:10.1093/gji/ggz299.

Merritts, D.J., 1996, The Mendocino triple junction: Active faults, episodic coastal emergence, and rapid uplift: Journal of Geophysical Research: Solid Earth, v. 101, p. 6051–6070, doi:10.1029/95JB01816.

Michel, S., Gualandi, A., and Avouac, J.-P., 2019, Interseismic Coupling and Slow Slip Events on the Cascadia Megathrust: Pure and Applied Geophysics, v. 176, p. 3867–3891, doi:10.1007/s00024-018-1991-x.

Milker, Y., Nelson, A.R., Horton, B.P., Engelhart, S.E., Bradley, L.-A., and Witter, R.C., 2016, Differences in coastal subsidence in southern Oregon (USA) during at least six prehistoric megathrust

earthquakes: Quaternary Science Reviews, v. 142, p. 143–163, doi:10.1016/j.quascirev.2016.04.017.

Montillet, J.-P., Melbourne, T. I., & Szeliga, W. M. (2018). GPS vertical land motion corrections to sea-level rise estimates in the Pacific Northwest. Journal of Geophysical Research: Oceans, 123, 1196–1212. https://doi. org/10.1002/2017JC013257

Murray, M.H., Marshall, G.A., Lisowski, M., and Stein, R.S., 1996, The 1992 M=7 Cape Mendocino, California, earthquake: Coseismic deformation at the south end of the Cascadia megathrust: Journal of Geophysical Research: Solid Earth, v. 101, p. 17707–17725, doi:10.1029/95JB02623.

Nagai, R., Takabatake, T., Esteban, M., Ishii, H., and Shibayama, T., 2020, Tsunami risk hazard in Tokyo Bay: The challenge of future sea level rise: International Journal of Disaster Risk Reduction, v. 45, p. 101321, doi:10.1016/j.ijdrr.2019.101321.

National Research Council, 2012, Sea Level Rise for the Coasts of California, Oregon and Washington: Past Present and Future:, https://nap.nationalacademies.org/resource/13389/sea-level-rise-brief-final.pdf (accessed September 2024).

National Research Council, 2012, Sea Level Rise for the Coasts of California, Oregon and Washington: Past Present and Future, National Academy Press, Washington, D.C.,

Nelson, A.R., DuRoss, C.B., Witter, R.C., Kelsey, H.M., Engelhart, S.E., Mahan, S.A., Gray, H.J., Hawkes, A.D., Horton, B.P., and Padgett, J.S., 2021, A maximum rupture model for the central and southern Cascadia subduction zone—reassessing ages for coastal evidence of megathrust earthquakes and tsunamis: Quaternary Science Reviews, v. 261, p. 106922, doi:10.1016/j.quascirev.2021.106922.

Nelson, A.R., Hawkes, A.D., Sawai, Y., Horton, B.P., Witter, R.C., Bradley, L.-A., and Cahill, N., 2020, Minimal stratigraphic evidence for coseismic coastal subsidence during 2000 yr of megathrust earthquakes at the central Cascadia subduction zone: Geosphere, v. 17, p. 171–200, doi:10.1130/GES02254.1.

Nelson, A.R., Kelsey, H.M., and Witter, R.C., 2006, Great earthquakes of variable magnitude at the Cascadia subduction zone: Quaternary Research, v. 65, p. 354–365, doi:10.1016/j.yqres.2006.02.009.

Nicovich, S.R., Hemphill-Haley, M., and Leroy, T., 2024, Deformed Latest Pleistocene Fluvial Terraces Reveal Complex Active Faulting within Tectonic Transition Zone, Mendocino Triple Junction, Northern California: The Seismic Record, v. 4, p. 62–71, doi:10.1785/0320230043.

Nieminski, N.M., Sylvester, Z., Covault, J.A., Gomberg, J., Staisch, L., and McBrearty, I.W., 2024, Turbidite correlation for paleoseismology: Geological Society of America Bulletin, doi:10.1130/B37343.1.

Ocean Protection Council, 2024, California Sea Level Rise Guidance: 2024 Science and Policy Update: , p. 101.

Ogle, B.A., 1953, Geology of the Eel River Basin, Humboldt County, California: California Division of Mines Bulletin 164, 128 p., http://archives.datapages.com/data/bulletns/1953-56/data/pg/0037/0012/2750/2777.htm (accessed February 2020).

Padgett, J. S., Engelhart, S. E., Kelsey, H. M., Witter, R. C., & Cahill, N. (2022). Reproducibility and variability of earthquake subsidence estimates from saltmarshes of a Cascadia estuary. Journal of Quaternary Science, 37(7), 1294–1312. https://doi.org/10.1002/jqs.3446

Padgett, J., 2019, Cascadia subduction zone coseismic subsidence estimates from northern California and Washington: University of Rhode Island, doi:10.23860/diss-padgett-jason-2019.

Padgett, J.S., Engelhart, S.E., Kelsey, H.M., Witter, R.C., Cahill, N., and Hemphill-Haley, E., 2021, Timing and amount of southern Cascadia earthquake subsidence over the past 1700 years at northern Humboldt Bay, California, USA: GSA Bulletin, v. 133, p. 2137–2156, doi:10.1130/B35701.1.

Padgett, J.S., Kelsey, H.M., and Lamphear, D., 2019, Upper-plate deformation of Late Pleistocene marine terraces in the Trinidad, California, coastal area, southern Cascadia subduction zone: Geosphere, v. 15, p. 1323–1341, doi:10.1130/GES02032.1.

Page, W.D., 2005, Implications of long-term global warming and tectonic displacements at Buhne Hill, Humboldt County, California, report to the California Coastal Commission, 7/18/2005, 39 pp + figures. PG&E, 2005

Page, W.D., and Nishenko, S., 2015, Assessment of Potential Tsunami Runup at the Humboldt Bay Generating Station Site: PG&E Internal, 89 p.

Park, H., Cox, D.T., Alam, M.S., and Barbosa, A.R., 2017, Probabilistic Seismic and Tsunami Hazard Analysis Conditioned on a Megathrust Rupture of the Cascadia Subduction Zone: Frontiers in Built Environment, v. 3, doi:10.3389/fbuil.2017.00032.

Patton, J. and Dengler, L., 2006, Relative tsunami hazard mapping for Humboldt and Del Norte Counties, CA, in Proceedings 8th National Conference on Earthquake Engineering, Earthquake Engineering Research Institute, paper R1788.

Patton, J. R., Leroy, T. H., Williams, T., McPherson, R. C., Anderson, J. K., Burgette, R., Hemphill-Haley, M., Weldon, R., Carver, G., Kelsey, H.M., 2015 Mismatch between intcrseismic ground deformation and paleoseismic/paleogeodetic observations, Humboldt Bay, Northern California (abs) SSA Annual Meeting, Pasadena CA 15-485

Patton, J., Williams, T., Anderson, J., Hemphill-Haley, M., Burgette, R., Weldon Ii, R., McPherson, R., and Leroy, T., 2023b, 20th to 21st Century Relative Sea and Land Level Changes in Northern California:Tectonic Land Level Changes and their Contribution to Sea-Level Rise, Humboldt Bay Region, Northern California: Tektonika, v. 1, p. 17, doi:10.55575/tektonika2023.1.1.6.

Patton, J.R., 2004, Late Holocene coseismic subsidence and coincident tsunamis, southern Cascadia subduction zone, Hookton Slough, Wigi (Humboldt Bay), California: Humboldt State University, 76 p.

Patton, J.R., 2022, Tectonic Datums: Eel River Fluvial Terraces: Triangle of Doom V.2 - Archeology, Stratigraphy, Tectonics, Geomorphology, and Geophysics in the Region of the Mendocino Triple Junction - FOP Guidebook, p. 130–139.

Patton, J.R., Hemphill-Haley, M., McPherson, R.C., Micahalak, M.J., and Nicovich, S., 2022a, Triangle of Doom V2.0, Archeology, Stratigraphy, Tectonics, Geomorphology, and Geophysics in the Region of the Mendocino Triple Junction, in p. 235, https://www.fop.cascadiageo.org/pacific_cell/2022/2022_PAC_CEL_FOP_GUIDEBOOK.pdf (accessed September 2024).

Patton, J.R., Hemphill-Haley, M., Streig, A., and Leroy, T., 2022b, Tectonic Offset of Latest Pleistocene Fluvial Terrace Treads in Shively, Humboldt County, California: Triangle of Doom V.2 - Archeology, Stratigraphy, Tectonics, Geomorphology, and Geophysics in the Region of the Mendocino Triple Junction - FOP Guidebook, p. 140–148.

Patton, J.R., Leroy, T.H., Williams, T.B., Hemphill-Haley, M.A., McPherson, R., and Anderson, J.K., 2017, Perplexing records of coseismic subsidence; evaluation of sources for coseismic subsidence in the southern Cascadia subduction zone, Northern California: Geological Society of America, 2017 annual meeting & exposition, v. 49.

Patton, J.R., Williams, T.B., Anderson, J., and Heaton, T.H., 2017, Tectonic land level changes and their contribution to sea-level rise, Humboldt Bay region, Northern California: U.S. Fish and Wildlife Service Final Technical Report F11AC01092, 47 p.

Peterson, C. D., Carver, G. A., Cruikshank, K. M., Abramson, H. F., Garrison-Laney, C. E., & Dengler, L. A. (2011). Evaluation of the use of paleotsunami deposits to reconstruct inundation distance and runup heights associated with prehistoric inundation events, Crescent City, southern Cascadia margin. Earth Surface Processes and Landforms, 36(7), 967–980. https://doi.org/10.1002/esp.2126

PG&E, 2002, Seismic Hazard Assessment for the Humboldt Bay ISFSI Project: Technical Report TR-HBIP-2002-01 Rev 0, 417 p.

PG&E, 2003, Humboldt Bay ISFSI safety analysis report, December 2003: Pacific Gas and Electric Company report to the Nuclear Regulatory Commission, Washington D.C.

PG&E, 2010, Methodology for Probabilistic Tsunami Hazard Analysis: Trial Application for the Diablo Canyon Power Plant Site, in Berkeley, CA, p. 197.

PG&E, 2017, Humboldt Bay Independent Spent Fuel Storage Installation - Final Safety Analysis Report Update: NRC Docket No. 72-27, 765 p.

Plafker, G., 1969, Tectonics of the March 27, 1964 Alaska Earthquake, in Washington, D.C., U.S. Geological Survey Professional Paper 543-I, p. 74, https://pubs.usgs.gov/pp/0543i/ (accessed June 2020).

Plafker, G., 1972, Alaskan earthquake of 1964 and Chilean earthquake of 1960: Implications for arc tectonics: Journal of Geophysical Research (1896-1977), v. 77, p. 901–925, doi:10.1029/JB077i005p00901.

Plafker, G., 2002b, Review of empirical data on tsunami runup versus earthquake source parameters: Report to Pacific Gas and Electric Company, 18 p. plus figures.

Priest, G.R., Robert C. Witter, Y. Joseph Zhang, Kelin Wang, Chris Goldfinger, Laura L. Stimely, John T. English, Sean G. Pickner, Kaleena L.B. Hughes, Taylore E. Wille, and Rachel L. Smith, 2013. Tsunami Inundation Scenarios for Oregon, DOGAMI Open-File Report O-13-19.

Priest, G.R., Witter, R.C., Zhang, Y.J., Goldfinger, C., Wang, K., and Allan, J.C., 2017, New constraints on coseismic slip during southern Cascadia subduction zone earthquakes over the past 4600 years implied by tsunami deposits and marine turbidites: Natural Hazards, v. 88, p. 285–313, doi:10.1007/s11069-017-2864-9.

Priest, G.R., Zhang, Y., Witter, R.C., Wang, K., Goldfinger, C., and Stimely, L., 2014, Tsunami impact to Washington and northern Oregon from segment ruptures on the southern Cascadia subduction zone: Natural Hazards, v. 72, p. 849–870, doi:10.1007/s11069-014-1041-7.

Pritchard, C.J., 2004, Late Holocene relative sea-level changes, Arcata Bay, California : evaluation of freshwater syncline movement using coseismically buried soil horizons [Masters Thesis]: Humboldt State University, 63 p., http://dspace.calstate.edu/handle/2148/883 (accessed May 2020).

Robinson, M., Flanagan, S., and Hemphill-Haley, M., 2022, Terrace Formation in the Upper Headwater Region of the Mattole River Watershed Across the Mendocino Triple Junction, Northwest California, in Triangle of Doom V.2 - Archeology, Stratigraphy, Tectonics, Geomorphology, and Geophysics in the Region of the Mendocino Triple Junction - FOP Guidebook, p. 33–41.

Rogers, G., and Dragert, H., 2003, Episodic Tremor and Slip on the Cascadia Subduction Zone: The Chatter of Silent Slip: Science, v. 300, p. 1942–1943, doi:10.1126/science.1084783.

Rollins, J.C., and Stein, R.S., 2010, Coulomb stress interactions among M ≥ 5.9 earthquakes in the Gorda deformation zone and on the Mendocino Fault Zone, Cascadia subduction zone, and northern San Andreas Fault: Journal of Geophysical Research, v. 115, p. 1–19, doi:10.1029/2009JB007117.

Ryan, W.B.F. et al., 2009, Global Multi-Resolution Topography synthesis: Geochemistry, Geophysics, Geosystems, v. 10, doi:10.1029/2008GC002332.

SAFFR Tsunami Modeling Working Group. (2013). Modeling for the SAFRR Tsunami Scenario—Generation, Propagation, Inundation, and Currents in Ports and Harbors. In S. L. Ross & L. M. Jones (Eds.), The SAFRR (Science Application for Risk Reduction) Tsunami Scenario (p. 136). U.S. Geological Survey Open-file Report 2013-1170-D. https://pubs.usgs.gov/of/2013/1170/d/

Salaree, A., Huang, Y., Ramos, M.D., and Stein, S., 2021, Relative Tsunami Hazard From Segments of Cascadia Subduction Zone For M 7.5–9.2 Earthquakes: Geophysical Research Letters, v. 48, p. e2021GL094174, doi:10.1029/2021GL094174.

Satake, K, 1995, Linear and non-linear computations of the 1992 Nicaragua earthquake tsunami, Pure and Applied Geophysics, 144, 455.

Satake, K., Wang, K., and Atwater, B.F., 2003, Fault slip and seismic moment of the 1700 Cascadia earthquake inferred from Japanese tsunami descriptions, Jour. Geophys. Res., 108, 2535

Savage, J.C., Lisowski, M., and Prescott, W.H., 1991, Strain accumulation in western Washington: Journal of Geophysical Research: Solid Earth, v. 96, p. 14493–14507, doi:10.1029/91JB01274.

Sea-level Rise Leadership Team and Ocean Protection Council, 2022, State Agency Sea-Level Rise Action Plan for California: State and Federal Reports and Publications, 28 p.

Selva, J., Tonini, R., Molinari, I., Tiberti, M.M., Romano, F., Grezio, A., Melini, D., Piatanesi, A., Basili, R., and Lorito, S., 2016, Quantification of source uncertainties in Seismic Probabilistic Tsunami Hazard Analysis (SPTHA): Geophysical Journal International, v. 205, p. 1780–1803, doi:10.1093/gji/ggw107.

Sepúlveda, I., Haase, J.S., Liu, P.L. -F., Grigoriu, M., and Winckler, P., 2021, Non-Stationary Probabilistic Tsunami Hazard Assessments Incorporating Climate-Change-Driven Sea Level Rise: Earth's Future, v. 9, p. e2021EF002007, doi:10.1029/2021EF002007.

Shelly, D.R., Goldberg, D.E., Materna, K.Z., Skoumal, R.J., Hardebeck, J.L., Yoon, C.E., Yeck, W.L., and Earle, P.S., 2024, Subduction intraslab-interface fault interactions in the 2022 M w 6.4 Ferndale, California, earthquake sequence: Science Advances, v. 10, p. eadl1226, doi:10.1126/sciadv.adl1226.

Shennan, I., and Hamilton, S., 2006, Coseismic and pre-seismic subsidence associated with great earthquakes in Alaska: Quaternary Science Reviews, v. 25, p. 1–8, doi:10.1016/j.quascirev.2005.09.002.

Shennan, I., Barlow, N., Carver, G., Davies, F., Garrett, E., and Hocking, E., 2014, Great tsunamigenic earthquakes during the past 1000 yr on the Alaska megathrust: Geology, v. 42, p. 687–690, doi:10.1130/G35797.1.

Small, D.T., and Melgar, D., 2021, Geodetic Coupling Models as Constraints on Stochastic Earthquake Ruptures: An Example Application to PTHA in Cascadia: Journal of Geophysical Research: Solid Earth, v. 126, p. e2020JB021149, doi:10.1029/2020JB021149.

Smith, J.A., Moschetti, M.P., and Thompson, E.M., 2024, Comparing subduction ground-motion models to observations for Cascadia: Earthquake Spectra, v. 40, p. 1787–1817, doi:10.1177/87552930241256673.

Son, S., Lynett, P., & Ayca, A. (2020). Modelling scour and deposition in harbours due to complex tsunami-induced currents. Earth Surface Processes and Landforms, 45(4), 978–998. https://doi.org/10.1002/esp.4791

Staisch, L., 2024, Sensitivity Testing of Marine Turbidite Age Estimates along the Cascadia Subduction Zone: Bulletin of the Seismological Society of America, v. 114, p. 1739–1753, doi:10.1785/0120230252.

Stanton, K.M., Crider, J.G., Kelsey, H.M., and Feathers, J.K., 2024, The signature of accumulated permanent uplift, northern Cascadia subduction zone: Quaternary Research, v. 117, p. 98–118, doi:10.1017/qua.2023.59.

State of California, 2021. Tsunami Hazard Area Map, Humboldt County; produced by the California Geological Survey and the California Governor's Office of Emergency Services; dated 2021, displayed at multiple scales.

State of California. (2020). Humboldt County tsunami hazard map—South Bay [Tsunami hazard map]. California Geological Survey and California Governor's Office of Emergency Services. https://rctwg.humboldt.edu/sites/default/files/tsunamibrochures_humboldtcounty_october2020.pdf

State of California. (2021). Tsunami hazard area map, Humboldt county—Base map [Map]. California Geological Survey and California Governor's Office of Emergency Services.

Stone, I., Vidale, J.E., Han, S., and Roland, E., 2018, Catalog of Offshore Seismicity in Cascadia: Insights Into the Regional Distribution of Microseismicity and its Relation to Subduction Processes: Journal of Geophysical Research: Solid Earth, v. 123, p. 641–652, doi:10.1002/2017JB014966.

Swan, F.H., Carver, G.A., McLaren, M., and Page, W.D., 2002, Seismic Hazard Assessment for the Humboldt Bay ISFSI Project: Regional Geology and Seismology: Pacific Gas and Electric Company Technical Report TR-HBIP-2002-01, Section 3, 83 p.

Sweet, W.V. et al., 2022, Global and Regional Sea Level Rise Scenarios for the United States: updated Mean Projections and Extreme Water Level Probabilities Along U.S. Coastlines: NOAA Technical Report NOS 01, 111 p., https://oceanservice.noaa.gov/hazards/sealevelrise/noaa-nos-techrpt01-global-regional-SLR-scenarios-US.pdf.

Sypus et al. (2024). Development of the probabilistic tsunami source model for Cascadia. Report to DOGAMI, in prep.

Tappin, D.R., Watts, P., and Grilli, S.T., 2008, The Papua New Guinea tsunami of 17 July 1998: anatomy of a catastrophic event: Nat. Hazards Earth Syst. Sci., 8, 243–266, 2008 www.nat-hazards-earth-syst-sci.net/8/243/2008/

Thio, H. K. (2019). Probabilistic Tsunami Hazard Maps for the State of California (Phase 2) (p. 168) [Technical Report]. AECOM.

Thio, H. K., Somerville, P., and Polet, J., 2010, Probabilistic Tsunami Hazard in California, PEER Report 2010/108, at http://peer.berkeley.edu/tsunami/publications/

Thio, H.K., Wei, Y., Chock, G. & Li, W., 2017. Development of Offshore Probabilistic Tsunami Exceedance Amplitudes for ASCE 7-16, Word Document presented at the Sixteenth World Conference on Earthquake Engineering.

Tréhu, A.M., Blakely, R.J., and Williams, M.C., 2012, Subducted seamounts and recent earthquakes beneath the central Cascadia forearc: Geology, v. 40, p. 103–106, doi:10.1130/G32460.1.

Udo, K., Takeda, Y., & Tanaka, H. (2016). Coastal morphology change before and after 2011 off the Pacific Coast of Tohoku earthquake tsunami at Rikuzen-Takata coast. Coastal Engineering Journal, 58(4), 1640016-1-1640016–16. https://doi.org/10.1142/S0578563416400167

Uslu, B., 2008, Deterministic and Probabilistic Tsunami Studies in California from Near and Farfield Sources, PhD Thesis, University of Southern California, 194 pp.

Vadurro, G.A., 2006, Amount and rate of deformation across the Little Salmon fault and Table Bluff anticline within the onland portion of the Southern Cascadia Subduction Zone fold and thrust belt, NW California, in Signatures of Quaternary crustal deformation and landscape evolution in the Mendocino deformation zone, NW California, M. Hemphill-Haley, T. Leroy, B. McPherson, J. Patton, J. Stallman, D. Sutherland and T. Williams, Friends of the Pleistocene eds., Pacific Cell, p. 113–120.

Valentine, D.W., 1992, Late Holocene Stratigraphy, Humboldt Bay, California: Evidence for Late Holocene Paleoseismicity of the Southern Cascadia Subduction Zone [Masters Thesis]: Humboldt State University, https://escholarship.org/uc/item/7328g533 (accessed May 2020).

Valentine, D.W., Keller, E.A., Carver, G., Li, W.-H., Manhart, C., and Simms, A.R., 2012, Paleoseismicity of the Southern End of the Cascadia Subduction Zone, Northwestern California: Bulletin of the Seismological Society of America, v. 102, p. 1059–1078, doi:10.1785/0120110103.

Vermeer and Hemphill-Haley, 2022).

Vermeer, J., and Hemphill-Haley, M., 2022, Interseismic Lithospheric Response of the Southern End of the Cascadia Subduction Zone Since the 1992 Cape Mendocino M 7.1 Earthquake: Triangle of Doom V.2 - Archeology, Stratigraphy, Tectonics, Geomorphology, and Geophysics in the Region of the Mendocino Triple Junction - FOP Guidebook, p. 202–208.

Vick, G., 1988, Late Holocene Paleoseismicity and relative vertical crustal movements [Masters Thesis]: Humboldt State University, 96 p.

Walsh, T.J., Combellick, R.A., and Black, G.L., 1995, Liquefaction Features from a Subduction Zone Earthquake:Preserved Examples from the 1964 Alaska Earthquake: Washington State Department of Natural Resources, Division of Geology and Earth Resources Report Investigations 32, 90 p.

Walton, M.A.L. et al., 2021, Toward an Integrative Geological and Geophysical View of Cascadia Subduction Zone Earthquakes: Annual Review of Earth and Planetary Sciences, v. 49, p. 367–398, doi:10.1146/annurev-earth-071620-065605.

Wang, K., and Tréhu, A.M., 2016, Invited review paper: Some outstanding issues in the study of great megathrust earthquakes—The Cascadia example: Journal of Geodynamics, v. 98, p. 1–18, doi:10.1016/j.jog.2016.03.010.

Wang, K., Wells, R.E., Mazzotti, S., Hyndman, R.D., and Sagiya, T., 2003, A revised dislocation model of interseismic deformation of the Cascadia subduction zone: Journal of Geophysical Research B: Solid Earth, v. 108, doi:10.1029/2001JB001227.

Wang, P.-L., Engelhart, S.E., Wang, K., Hawkes, A.D., Horton, B.P., Nelson, A.R., and Witter, R.C., 2013, Heterogeneous rupture in the great Cascadia earthquake of 1700 inferred from coastal subsidence estimates: Journal of Geophysical Research: Solid Earth, v. 118, p. 2460–2473, doi:10.1002/jgrb.50101.

Watt, J.T., and Brothers, D.S., 2020, Systematic characterization of morphotectonic variability along the Cascadia convergent margin: Implications for shallow megathrust behavior and tsunami hazards: Geosphere, v. 17, p. 95–117.

Wells, R.E., Blakely, R.J., Sugiyama, Y., Scholl, D.W., and Dinterman, P.A., 2003, Basin-centered asperities in great subduction zone earthquakes: A link between slip, subsidence, and subduction erosion? Journal of Geophysical Research: Solid Earth, v. 108, doi:10.1029/2002JB002072.

Wells, R.E., Blakely, R.J., Wech, A.G., McCrory, P.A., and Michael, A., 2017, Cascadia subduction tremor muted by crustal faults: Geology, v. 45, p. 515–518, doi:10.1130/G38835.1.

Whitmore, P. M., 1993, Expected tsunami amplitudes and currents along the North American coast for Cascadia subduction zone earthquakes: Natural Hazards, v. 8, p. 59-73.

Wiegel, R. (1965). Protection of Crescent City, California from Tsunami Waves for the Redevelopment Agency of the City of Crescent (No. M–4825; p. 111).

Wilson, A., and Ma, S., 2021, Wedge Plasticity and Fully Coupled Simulations of Dynamic Rupture and Tsunami in the Cascadia Subduction Zone: Journal of Geophysical Research: Solid Earth, v. 126, p. e2020JB021627, doi:10.1029/2020JB021627.

Wilson, R., Davenport, C., & Jaffe, B. (2012). Sediment scour and deposition within harbors in California (USA), caused by the March 11, 2011 Tohoku-oki tsunami. Sedimentary Geology, 282, 228–240. https://doi.org/10.1016/j.sedgeo.2012.06.001

Witter, R.C., Kelsey, H.M., and Hemphill-Haley, E., 2003, Great Cascadia earthquakes and tsunamis of the past 6700 years, Coquille River estuary, southern coastal Oregon: Geological Society of America Bulletin, v. 115, p. 1289–1306.

Witter, R.C., Patton, J.R., Carver, G.A., Kelsey, H.M., Garrison, C., Koehler, R.D., and Hemphill-Haley, E., 2001, Upper-plate earthquakes on the western Little Salmon fault and contemporaneous subsidence of southern Humboldt Bay over the past 3,600 years, northwestern California: U.S. Geological Survey, National Earthquake Hazards Reduction Program (NEHRP) Final Technical Report 01HQGR0125, 47 p.

Witter, R.C., Zhang, Y., Wang, K., Goldfinger, C., Priest, G.R., and Allan, J.C., 2012, Coseismic slip on the southern Cascadia megathrust implied by tsunami deposits in an Oregon lake and earthquake-triggered marine turbidites: Journal of Geophysical Research: Solid Earth, v. 117, doi:10.1029/2012JB009404.

Woodward-Clyde Consultants, 1980, Evaluation of the potential for resolving the geologic and seismic issues at the HBPP Unit No. 3: Summary to Pacific Gas and Electric company, San Francisco, CA:, 74, plus appendix p.

Yeck, W.L., Shelly, D.R., Materna, K.Z., Goldberg, D.E., and Earle, P.S., 2023, Dense geophysical observations reveal a triggered, concurrent multi-fault rupture at the Mendocino Triple Junction: Communications Earth & Environment, v. 4, p. 94, doi:10.1038/s43247-023-00752-2.

Yoon, C.E., and Shelly, D.R., 2024, Distinct Yet Adjacent Earthquake Sequences near the Mendocino Triple Junction: 20 December 2021 Mw 6.1 and 6.0 Petrolia, and 20 December 2022 Mw 6.4 Ferndale: The Seismic Record, v. 4, p. 81–92, doi:10.1785/0320230053.

Zong, Y., Shennan, I., Combellick, R.A., Hamilton, S.L., and Rutherford, M.M., 2003, Microfossil evidence for land movements associated with the AD 1964 Alaska earthquake: The Holocene, v. 13, p. 7–20, doi:10.1191/0959683603hl590rp.